Novel radiological approaches for diagnosis and treatment of diseases in the pelvic region. Applications in the uterus and the prostate.

Bengtsson, Johan

2024

Document Version:
Publisher's PDF, also known as Version of record

Novel radiological approaches for diagnosis and treatment of diseases in the pelvic region

Applications in the uterus and the prostate

JOHAN BENGTSSON, M.D.
DEPARTMENT OF CLINICAL SCIENCES, LUND | FACULTY OF MEDICINE | LUND UNIVERSITY

Novel radiological approaches for diagnosis and treatment of diseases in the pelvic region

Applications in the uterus and the prostate

Johan Bengtsson, M.D.

LUND
UNIVERSITY

DOCTORAL DISSERTATION

Doctoral dissertation for the degree of Doctor of Philosophy (PhD) at the Faculty of Medicine at Lund University to be publicly defended on 14th of June 2024 at 09.00 in Segerfalksalen, BMC, Lund

Faculty opponent
Associate Professor Henrik Leonhardt; University of Gothenburg

Organization: LUND UNIVERSITY
Faculty of Medicine
Department of Clinial Sciences, Lund
Department of Diagnostic Radiology, Lund

Date of issue 14-06-24
Document name: Doctoral Dissertation
Sponsoring organization:

Author(s): Johan Bengtsson

Title and subtitle: Novel radiological approaches for diagnosis and treatment of diseases in the pelvic region. Applications in the uterus and the prostate.

Abstract:

Background: Continuous advancements in interventional and diagnostic radiological techniques are mandatory to meet the increasing demands of patients and health care professionals. This thesis aims to contribute to the development of more effective interventional and diagnostic radiological methods for pelvic diseases. Ultimately, these advancements can lead to improved patient outcomes, optimised treatment strategies, and enhanced precision in diagnosing and managing conditions affecting the uterus and prostate.

Aim: The overarching aim of this thesis is to investigate both interventional and diagnostic radiological methods for pelvic diseases, and specifically for the uterus and the prostate. Specifically, we aim to address the feasibility, usability and effectiveness of a new degradable starch microsphere (DSM) intended for use in transarterial embolisation of the uterus and prostate (papers I and II), and prostate MRI features with applications on estimations of tumour aggressiveness and prostate volume (papers III and IV).

Methods: The experimental trial of papers I and II was performed on sheep that underwent transarterial uterine artery embolisation with either a DSM or a permanent commercially available permanent sphere, trisacryl gelatine microspheres (TGMS) in a blinded randomised controlled trial. Two weeks after embolisation, a follow-up angiogram was performed to assess recanalisation, and thereafter the animals were euthanised, and organs were collected for histopathology. The primary outcome measures were the occurrence of recanalisation of the embolised arteries and the presence of ischaemic changes in the embolised organs. Papers III and IV were retrospective cohort studies of men diagnosed with prostate cancer who had an MRI prior to prostatectomy. In paper III, we evaluated the correlation of absolute tumour apparent diffusion coefficient (ADC) and ADC ratios with pathology-based tumour aggressiveness in terms of ISUP grade group according to the International Society of Urological Pathology five-grade scale. Two experienced radiologists, independently from each other, measured the ADC values of 98 men that met the inclusion criteria. In paper IV, 124 men from the same main cohort as in paper III were included. Different MRI-based and ultrasound-based methods, including one machine learning MRI-based method for prostate volume, were compared to two different gold standards: weight volume from pathology and volume from manual planimetry, by an experienced radiologist on MRI.

Results: The ischaemic effect according to histopathology of the DSM in papers I and II was comparable with the commercially available market-leading equivalent. A significantly higher number of recanalised vessels were found in the DSM group as well as less vasculitis of the embolised arteries and a similar ischaemic effect of the embolised organs. In paper III, no correlation was seen between ADC and ISUP grade and no benefit of using ADC ratio over absolute ADC was found. The interrater reliability was substantial to almost perfect for all variables analysed. In paper IV we found that the machine learning software was more stringent than manual methods in calculating prostate volume, and no systematic error was found.

Conclusion: Our study showcases the efficacy of embolisation using the new DSM, offering potential for recanalisation and blood flow restoration. Moreover, embolisation with DSM demonstrates comparable tissue effects to TGMS with less vascular inflammation and enhanced recanalisation. Our findings also challenge previous assumptions by revealing no correlation between ADC metrics and ISUP grade, while affirming the reliability of deep learning algorithms for prostate volume assessment. These insights underscore the evolving landscape of interventional procedures and imaging techniques that will shape future clinical practices.

Key words: Embolization, uterine fibroid, benign prostate hyperplaisa, magnetic resonance imaging, prostate neoplasms, deep learning, diffusion weighted imaging

Supplementary bibliographical information

Language English **Number of pages**: 105

ISSN and key title: 1652-8220 Lund University, Faculty of Medicine Doctoral Dissertation Series 2024:82

ISBN: 978-91-8021-577-0

Recipient's notes Price Security classification

Signature Date 2024-04-22

Novel radiological approaches for diagnosis and treatment of diseases in the pelvic region

Applications in the uterus and the prostate

Johan Bengtsson, M.D.

LUND
UNIVERSITY

Faculty of Medicine Department
Department of Clinical Sciences Lund
Department of Diagnostic Radiology
Lund University, Sweden

ISBN 978-91-8021-577-0
ISSN 1652-8220
Lund University, Faculty of Medicine Doctoral Dissertation Series 2024:82

Printed in Sweden by Media-Tryck, Lund University
Lund 2024

Kommer tid, kommer råd!

Table of Contents

Abstract **8**

Populärvetenskaplig sammanfattning **10**

List of papers 12

Papers not included in the thesis 13

Thesis at a glance **14**

Abbreviations 15

Introduction and aims **16**

The specific aims of the studies presented in the papers 17

Transarterial embolisation **18**

History 18

Embolisation materials 20

Histological and immunological effects 23

Uterine fibroma and treatment 26

Benign prostate hyperplasia 33

Prostate cancer **39**

The prostate 39

Epidemiology and risk factors 40

Diagnostics of prostate cancer 43

Magnetic resonance imaging **47**

Background and routine use of MRI 47

Sequences 48

The role of MRI in the diagnosis of prostate cancer 53

Artificial intelligence and prostate MRI **57**

Machine learning 58

Neural network 58

AI in radiology 59

Material and methods **64**
Statistical methods used in the papers. 64
Cohorts and study design 67
Ethics 71
Results **74**
Paper I 74
Paper II 76
Paper III 79
Paper IV 81
Discussion **82**
Papers I and II 82
Paper III 84
Paper IV 85
Conclusions **87**
Future perspectives **88**
Acknowledgements **90**
References **94**

Abstract

Background

Continuous advancements in interventional and diagnostic radiological techniques are mandatory to meet the increasing demands of patients and health care professionals. This thesis aims to contribute to the development of more effective interventional and diagnostic radiological methods for pelvic diseases. Ultimately, these advancements can lead to improved patient outcomes, optimised treatment strategies, and enhanced precision in diagnosing and managing conditions affecting the uterus and prostate.

Aim

The overarching aim of this thesis is to investigate both interventional and diagnostic radiological methods for pelvic diseases, and specifically for the uterus and the prostate. Specifically, we aim to address the feasibility, usability, and effectiveness of a new degradable starch microsphere intended for use in transarterial embolisation of the uterus and prostate (papers I and II), and prostate MRI features with applications on estimations of tumour aggressiveness and prostate volume (papers III and IV).

Methods

The experimental trial of papers I and II was performed on sheep that underwent transarterial uterine artery embolisation with either a degradable starch microsphere (DSM) or a permanent commercially available permanent sphere, trisacryl gelatine microspheres (TGMS) in a blinded randomised controlled trial. Two weeks after embolisation, a follow-up angiogram was performed to assess recanalisation, and thereafter the animals were euthanised, and organs were collected for histopathology. The primary outcome measures were the occurrence of recanalisation of the embolised arteries and the presence of ischaemic changes in the embolised organs. Papers III and IV were retrospective cohort studies of men diagnosed with prostate cancer who had an MRI prior to prostatectomy. In paper III, we evaluated the correlation of absolute tumour apparent diffusion coefficient (ADC) and ADC ratios with pathology-based tumour aggressiveness in terms of

ISUP grade group according to the International Society of Urological Pathology five-grade scale. Two experienced radiologists, independently from each other, measured the ADC values of 98 men that met the inclusion criteria.

In paper IV, 124 men from the same main cohort as in paper III were included. Different MRI-based and ultrasound-based methods, including one machine learning MRI-based method for prostate volume, were compared to two different gold standards: weight volume from pathology and volume from manual planimetry, by an experienced radiologist on MRI.

Results

The ischaemic effect according to histopathology of the DSM in papers I and II was comparable with the commercially available market-leading equivalent. A significantly higher number of recanalised vessels were found in the DSM group as well as less vasculitis of the embolised arteries and a similar ischaemic effect of the embolised organs.

In paper III, no correlation was seen between ADC and ISUP grade and no benefit of using ADC ratio over absolute ADC was found. The interrater reliability was substantial to almost perfect for all variables analysed.

In paper IV we found that the machine learning software was more stringent than manual methods in calculating prostate volume, and no systematic error was found.

Conclusions

In conclusion, our study showcases the efficacy of embolisation using the new DSM, offering potential for recanalisation and blood flow restoration. Moreover, embolisation with DSM demonstrates comparable tissue effects to TGMS with less vascular inflammation and enhanced recanalisation. Our findings also challenge previous assumptions by revealing no correlation between ADC metrics and ISUP grade, while affirming the reliability of deep learning algorithms for prostate volume assessment. These insights underscore the evolving landscape of interventional procedures and imaging techniques that will shape future clinical practices.

Populärvetenskaplig sammanfattning

Med radiologi, dvs olika bilddiagnostiska metoder som vanlig röntgen, datortomografi, magnetkameraundersökning (MR) och ultraljud kan vi diagnosticera en mängd olika tillstånd. Alla metoder har sina fördelar och nackdelar och vi inom radiologin strävar hela tiden att förbättra metoderna och hur vi tolkar bilderna. Vårt mål är att hitta sjukdomar tidigt och sätta rätt diagnos för att kunna erbjuda tidig behandling som kan innebära bot eller lindring. Däremot vill vi inte hitta onödiga fynd i bilderna som kan orsaka onödiga och felaktiga behandlingar. Fynd och misstolkning av harmlösa tillstånd leder ofta till oro för patienterna och eventuellt onödiga ytterligare undersökningar och provtagningar och i värsta fall behandlingar som i sig är förenade med risker.

Vi kan även använda röntgenteknik till att guida behandling av olika tillstånd, så kallad interventionell radiologi. Med hjälp av katetrar, som vi för in i blodkärl kan vi med ledning av röntgen leta oss fram till olika organ i kroppen, till exempel hjärna, hjärta, lungor, lever, njurar, livmoder och prostata. Här kan vi göra olika behandlingar som annars skulle innebära att man behövde operera. Dessa ingrepp kan ersätta många större operationer och ofta kan patienten gå hem redan samma dag med endast ett plåster på huden där vi förde in katetern. Dessa behandlingar kallar vi för minimalinvasiva.

I arbete I och II undersökte vi en ny typ av sfär, dvs en sorts kula, mindre än 1 millimeter stor som kan sprutas in i kroppen via kateter för att behandla olika tillstånd i kroppen. Ett exempel kan vara muskelknutor i livmodern, så kallade myom. Dessa är mycket vanliga och kan ibland orsaka problem, speciellt om de blir stora eller väldigt många. Dessa kan opereras men kan även behandlas med interventionell radiologi då de små sfärerna vi sprutar in täpper till blodkärlen till muskelknutorna som blir utan blod och syre och därmed dör och krymper ihop. Vanligtvis använder man sig av sfärer av plast som stannar kvar i kroppen resten av livet. Vi tror att sfärer som bryts ner efter några dagar är väl så bra för ändamålet. Vem vill ha kvar sfärerna när de väl har fullgjort sitt syfte? Vi har därför testat att jämföra sfärerna på får (tackor) som vi behandlat med antingen de nedbrytbara sfärerna eller plastsfärer. Vi kunde konstatera att båda sfärerna åstadkom ungefär samma effekt men att de nedbrytbara sfärerna till största delen hade försvunnit efter två veckor. Alla undersökningar gjorde vi på tackorna medan de var sövda och de fick gott om smärtlindrande mediciner. De hade tillsyn av djurvårdare och veterinär.

Vi tror att dessa sfärer kan användas även för behandling i människor, vilket kan visas i framtida forskning.

Arbetena III och IV handlar om diagnostik med MR för prostatacancer. Det finns olika sätt att ta reda på om en patient har prostatacancer. Ett av dessa innebär att man tar ett vävnadsprov då man sticker i prostatan via ändtarmen. Detta kan ge svar på frågan om cancer finns, men cancern kan också missas och förbli oupptäckt. För att lyckas bättre tar man många vävnadsprover. Detta kan i vissa fall ge oönskade sidoeffekter som blödningar eller blodförgiftning. På senare år görs i stället MR-undersökning och om man hittar en misstänkt cancer gör man vävnadsprov, annars låter man bli. På så vis behöver färre män genomgå vävnadsprov och således undvika riskerna med provtagningen. Dessutom vet man var i prostata man skall sticka.

Detta ställer dock höga krav på MR-undersökningen och vår tolkning av bilderna. Vi vill ju inte hitta förnedringar i prostata som kanske inte är cancer och som man sticker i onödan, å andra sidan vill vi inte misstolka något för en snäll förändring som i själva verket är cancer. I arbete III och IV jämför vi olika MR-bilder på män som genomgått MR av prostata och sedan opererat bort prostatan på grund av cancer. Vi gör olika mätningar på MR-bilderna och jämför med vad patologen hittat vid mikroskopisk undersökning av den utopererade prostatan. Vi har även undersökt om artificiell intelligens (AI) kan hjälpa till i bedömningen av bilderna genom att räkna ut hur stor volym prostatan har genom analys av MR-bilderna. Det har vi sedan jämfört med resultaten som röntgenläkaren kommit fram till och hur stor prostatan i själva verket var när den opererats ut. Det visar sig att AI var minst lika bra som vi röntgenläkare på detta. Och betydligt snabbare.

Förhoppningsvis kan resultaten i avhandlingen hjälpa till att föra forskningen framåt både inom interventionell och diagnostisk radiologi.

Johan Bengtsson

Dalby 2024-04-22

List of papers

Paper I

Bengtsson J, Cwikiel W, Sundgren PC, Karlstam E, Gavier-Widen D, Keussen I. The effects of uterine artery embolization with a new degradable microsphere in an experimental study. Acta Radiologica. 2017;58(11):1334-41.

Paper II

Keussen I, **Bengtsson J**, Gavier-Widen D, Karlstam E. Uterine artery embolization in a sheep model: biodegradable versus non-degradable microspheres. Acta Radiologica. 2018;59(10):1210-7.

Paper III

Bengtsson J, Thimansson E, Baubeta E, Zackrisson S, Sundgren PC, Bjartell A, Flondell-Site D. Correlation between ADC, ADC ratio, and Gleason Grade group in prostate cancer patients undergoing radical prostatectomy: Retrospective multicenter study with different MRI scanners. Front Oncol. 2023; 13:1079040.

Paper IV

Thimansson E**, Bengtsson J**, Baubeta E, Engman J, Flondell-Site D, Bjartell A, Zackrisson S. Publisher Correction: Deep learning algorithm performs similarly to radiologists in the assessment of prostate volume on MRI. Eur Radiol. 2023;33(4):3004.

Papers not included in the thesis

Alterbeck M, Thimansson E, **Bengtsson J**, Baubeta E, Zackrisson S, Bolejko A, et al. A pilot study of an organised population-based testing programme for prostate cancer. BJU Int. 2024;133(1):87-95.

Eriksson S, **Bengtsson J**, Torén W, Lätt J, Andersson R, Sturesson C. Changes in apparent diffusion coefficient and pathological response in colorectal liver metastases after preoperative chemotherapy. Acta Radiologica. 2023;64(1):51-7.

Alterbeck M, Jarbur E, Thimansson E, Wallstrom J, **Bengtsson J**, Bjork-Eriksson T, et al. Designing and Implementing a Population-based Organised Prostate Cancer Testing Programme. Eur Urol Focus. 2022;8(6):1568-74.

Asp M, Malander S, **Bengtsson J**, Sartor H, Kannisto P. Prognostic value of peritoneal cancer index after complete Cytoreductive surgery in advanced ovarian cancer. Anticancer research. 2022;42(5):2541-51.

Asp M, Malander S, Wallengren N-O, Pudaric S, **Bengtsson J**, Sartor H, Kannisto P. The role of computed tomography in the assessment of tumour extent and the risk of residual disease after upfront surgery in advanced ovarian cancer (AOC). Archives of Gynecology and Obstetrics. 2022;306(4):1235-43.

Grigoriadis A, Imeen Ringe K, **Bengtsson J**, Baubeta E, Forsman C, Korsavidou-Hult N, et al. Development of a prognostic MRCP-score (DiStrict) for individuals with large-duct primary sclerosing cholangitis. JHEP Rep. 2022;4(12):100595.

Thesis at a glance

Study	Question	Method	Results and Conclusions
I	Can a new degradable starch microsphere (DSM) be used for transarterial embolisation? Will it be degraded in vivo, and will it cause intended ischaemia?	Uterine artery embolisation with DSM was performed on 6 ewes. Follow-up angiography and histopathological evaluation were performed.	Five successful embolisations were performed. Ischaemic changes of the embolised organs were observed, histologically and macroscopically. DSM was partly degraded.
II	How does the DSM perform compared to the market-leading permanent sphere (TGMS) in terms of manageability, local tissue effect, side effects and recanalisation of the embolised vessels.	Blinded study. 22 ewes were embolised with DSM or TGMS. 2 week-follow-up with angiography, blood samples, clinical data, degree of recanalisation, macroscopical and histological evaluation.	Successful procedures in all animals. Significantly more recanalisation in the DSM group. Similar effect on tissue. Fewer vascular changes in the DSM group.
III	Is there a correlation between apparent diffusion coefficient (ADC), ADC ratio, and Gleason Grade group in prostate cancer patients undergoing radical prostatectomy?	Retrospective cohort study evaluating the correlation between ADC metrics and histopathological results on patients operated with prostatectomy for prostate cancer.	In contrast to previously published single-centre studies, no correlation between ADC, ADC ratio and tumour aggressiveness was found in this multicentre study.
IV	Can a commercially available AI model assess the prostate volume from MRI on a par with today´s gold standard radiologist dependent method using a clinical dataset?	Retrospective agreement study comparing radiologist ellipsoid formula with AI model. Expert manual radiologist planimetry and specimen weight volume as reference standards.	The AI model demonstrates comparable performance to radiologists in evaluating prostate volume on MR imaging. This has the potential to free up radiologists for more intricate tasks.

Abbreviations

ADC	Apparent Diffusion Coefficient
BPH	Benign Prostate Hyperplasia
CT	Computerized Tomography
CZ	Central Zone
DRE	Digital Rectal Examination
DHT	Dihydrotestosterone
DSM	Degradable Starch Microsphere
DWI	Diffusion Weighted Imaging
HCC	Hepatocellular Carcinoma
ISUP	International Society of Urological Pathology
LUTS	Lower Urinary Tract Symptoms
MRI	Magnetic Resonance Imaging
PCa/csPCa	Prostate Cancer/clinically significant PCa
PES	Post Embolization Syndrome
PI-RADS	Prostate Imaging Reporting & Data System
PSA	Prostate Specific Antigen
PSAD	Prostate Specific Antigen Density
PVA	Polyvinyl Alcohol
PZ	Peripheral Zone
RALP	Robot Assisted Laparoscopic Prostatectomy
TACE	Transarterial Chemoembolization
TARE	Transarterial Radiotherapy
TGMS	Trisacryl Gelatine Microspheres
TRUS	Transrectal Ultrasound
TURP	Transurethral resection of the prostate
TZ	Transitional Zone
UFE/UAE	Uterine Fibroid Embolization/Uterine Artery Embolization

Introduction and aims

The relationship between interventional radiology and diagnostic radiology has been a cornerstone in the evolution of modern medical imaging and interventions. The two disciplines have developed hand in hand, each driving the advancements of the other. Both the diagnostic and interventional branches offer minimally invasive procedures to achieve their respective goals. Before the discovery of X-rays, magnetic resonance imaging (MRI), and ultrasound, all diagnostics were associated with more invasive and less accurate methods. The same goes for interventional procedures, where the alternative would be open surgery. The advancement of both disciplines continues, and new landmarks can be achieved, further facilitated by machine learning. In the future, radiology might be able to offer precise non-invasive histology and treatments for more complex conditions with the use of catheters.

This relationship is reflected in this thesis, which consists of two parts. Papers I and II deal with interventional radiology and the development of a new biocompatible degradable microsphere for interventional procedures. The intention was to use the product for embolisation of benign and malignant tumours in the liver, uterus, and prostate.

The second part of the thesis deals with MRI diagnostics of prostate cancer. The modern approach in a prostate cancer workup, MRI first, means that the result of the MRI determines whether to perform biopsies or not. Prostate cancer can be indolent and harmless, and detection of these tumours yields anxiety, high costs for the health system, and unnecessary biopsies with potential life-threatening side effects. On the other hand, tumours can be aggressive and early metastasising. Early detection is crucial to be able to treat the tumour in time and to offer a possible cure. Hence, we must balance overdiagnosis with underdiagnosis. More powerful MRI sequences are being developed to increase specificity. Machine learning and radiomics have further improved diagnostics. Papers III and IV in this thesis investigate different diagnostic aspects of prostate MRI.

The overarching aim of this thesis is to investigate both interventional and diagnostic radiological approaches for pelvic diseases, and specifically for the uterus and the prostate.

The specific aims of the studies presented in the papers were:

I. To evaluate *in vivo* degradation, local tissue effects, and possible recanalisation following intra-arterial deposition of a new, degradable starch microsphere (DSM), in a short-term experimental pilot study.

II. To compare the local tissue effects, possible side effects, and extent of recanalisation following uterine artery embolisation, using either degradable or non-degradable microspheres in a sheep model.

III. To investigate the correlation between ADC and ADC ratio compared to tumour aggressiveness determined by a histopathological examination after radical prostatectomy.

IV. To assess whether a deep learning algorithm can replace manual methods for calculating prostate volume.

Transarterial embolisation

History

One of the most important landmarks in the history of interventional radiology was the introduction of the *Seldinger technique* by the Swedish radiologist, Dr. Sven-Ingvar Seldinger. Dr Seldinger was born in Mora, Dalecaria, Sweden 1921. In 1950, he was working as a substitute physician in the radiology department of the new Karolinska Hospital in Solna, Sweden. He was assisting Dr. Åke Lindbom with angiographic procedures for his thesis[1]. He realised that there was a need for an improved method for percutaneous access. Dr. Seldinger´s family had run a mechanical workshop for generations and were considered technical geniuses. With his interest in fine mechanics, he made several attempts to find a more precise and less harmful procedure for vascular access. After several failures, he had a Eureka moment when he found himself sitting, disappointed with a needle, a wire, and a catheter. He suddenly realised how to use these objects!

> Needle in – wire in – needle off – catheter on wire – catheter in – catheter advance – wire off (Fig. 1).

This moment was later described by Dr. Seldinger as “a severe attack of common sense”. It was presented at the Congress of the Northern Association of Medical Radiology in Helsinki in 1952 and published in Acta Radiologica in 1953[2].

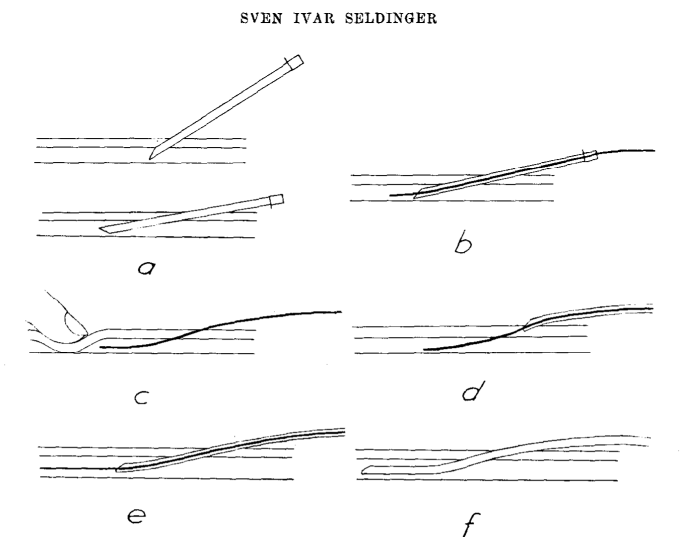

Figure 1
Dr Seldinger´s drawing explaining stepwise the Seldinger Technique. From the original publication 1953[2]. With permission from Sage.

A decade later, the man known as the father of interventional radiology, Dr. Charles Dotter, took the use of catheters beyond diagnostics when he started using the catheters for treatments. He described a procedure for treating patients with lower extremity claudication. Under fluoroscopic control, a 0.1-inch tapered Teflon dilatation catheter was slipped over a guidewire and advanced to enlarge the lumen of a stenosis in the femoral or popliteal artery. Eleven patients were treated with the procedure, later called the percutaneous transluminal angioplasty technique (PTA) or the Dotter technique. Half of the patients improved markedly, and four amputations were avoided[3].

Dr. Andreas Gruentzig in Zürich invented the first PTA balloon catheter, a rigid, sausage-shaped device which he and his wife Michaela manufactured on their kitchen table. The first patient was treated with the device in 1974 for intermittent claudication caused by superficial femoral artery stenosis. Eventually, a modified PTA catheter was used for the coronary arteries in 1975[4, 5].

The first endovascular treatment for haemorrhage was performed by Dr. Josef Rösch and Dr. Charles Dotter on a 43-year-old woman with diabetes, chronic alcoholism, and liver failure. She presented with a bleeding peptic ulcer which was confirmed with angiography. Selective epinephrine injection through the diagnostic catheter gained only temporary haemostasis. However, with a 2-cc autologous blood clot injected through the catheter, a permanent 4 cm thrombus was formed and hence, complete haemostasis was achieved[6]. This procedure, called Transarterial

Embolisation (TAE), has since undergone refinement in terms of techniques and materials and is now used to treat a wide range of conditions such as bleeding, varices, and benign or malignant tumours.

Interventional radiology is a branch speciality of medical radiology. The European Society of Cardiovascular Radiology and Interventional Radiology (ESCVIR) and the European College of Angiography (ECA) were both founded in 1976. In 1985, these two societies were merged, and the Cardiovascular and Interventional Radiological Society of Europe (CIRSE) was formed[7]. It now has 4200 members organised in 24 national societies. CIRCE is the largest of the subspeciality radiological societies in Europe. The Swedish Society for Interventional Radiology is called the Seldinger Society of Vascular and Interventional Radiology (Seldingersällskapet) to honour Dr. Sven-Ingvar Seldinger.

Embolisation materials

Various embolisation materials are currently available, all used for a common purpose: the obstruction of blood flow. These materials are categorised based on their specific properties, intended applications, and mechanisms of action, falling into classifications as medical devices, medicinal products, or combination products. The European Medicines Agency (EMA), a decentralised agency within the European Union, assumes responsibility for the scientific evaluation, supervision, and safety monitoring of both medicines and medical devices. In the United States, the equivalent regulatory authority is the Food and Drug Administration (FDA).

The categorisation of a product hinges on its mode of action. If the product primarily exerts its effect through physical means, such as the blockage of an artery, it is likely to be classified as a medical device. Conversely, if the action involves a pharmacological effect, it falls into the category of medicinal products. Within Europe, medical devices are stratified into four main classes (Classes I, IIa, IIb, III) based on risk level, ranging from low to high. The majority of embolisation materials align with Classes IIa to III. The delineation of these classifications is outlined in the European Union's Medical Devices Regulation (MDR).

Types of embolisation materials

Particles

A broad spectrum of embolisation particles is commercially available, each designed for specific therapeutic applications. The particles can be natural, i.e. gelatine particles, or synthetic. They can have irregular shapes with a wide size range or can be precisely calibrated in both shape and size[8]. The smaller the particle,

the more peripheral occlusion and more pronounced ischaemia will be achieved. Most particles are used for embolisation only, while others can be loaded with cytotoxic drugs which will be eluted from the particles at the target. The beads can also be loaded with radioactivity for similar targeted tumour delivery[9]. While most particles must be mixed with contrast media to be visible on fluoroscopy, some particles are inherently radiopaque. Temporary particles can be used when re-intervention in the same vessel is anticipated or when only a short period of ischaemia is needed[10-12].

PVA (polyvinyl alcohol) particles were first used in household sponges, and the material is biocompatible. It has been used for embolisation of gastrointestinal bleeding, and embolisation of uterine fibroids and of arteriovenous malformations These particles are available in sizes ranging from 100 μm to 1100 μm. Upon injection, these particles aggregate and adhere to the intima of the vessel wall, leading to the formation of a thrombus. This process induces inflammation and necrosis of the vessel wall. Despite the permanent nature of the material, recanalisation can occur either through angiogenesis within the thrombus[13] or through transarterial exclusion of the material from the vessel lumen[14]. PVA tends to aggregate in the delivery catheters, which may occlude. The unpredictable size of the aggregates may cause an unpredictable level of embolisation in terms of the size of the occluded vessel. The use of PVA is therefore associated with a relatively high rate of complication and failure[15-17].

Gelatine sponge (Gelfoam, Pfizer) particles are extracted from porcine skin. Gelfoam is also available as sheets which can be cut into smaller pieces and mixed with contrast and saline to form an injectable slurry solution. Gelatine sponge induces a clotting reaction, and a thrombus is formed. It is considered a temporary material; however, it causes a very strong inflammatory reaction and a subsequent proliferation of the intimal tissue with narrowing and eventually permanent occlusion. Gelfoam is used for gastrointestinal haemorrhage control and preoperative embolisation. It used to be the most used material for uterine fibroid embolisation (UFE).

Calibrated microspheres have been developed to achieve a more controlled level of occlusion. The spheres are available in different sizes, ranging from 50 μm to 1300 μm (figure 2). They have uniform physical properties such as size, buoyancy and rigidity and elastic recovery[11]. Tris-acryl gelatine microspheres (TGMS) and Polyzene-F coated hydrogel particles are commonly used permanent spheres often used for embolisation of benign prostate hyperplasia (BPH) and UFE. Degradable calibrated spheres are also available. 50 μm starch microspheres degrade within an hour and are used for embolisation of hepatocellular carcinoma (HCC). Hydrophobic poly(lactic-co-glycolic acid) (PLGA) spheres, coated with collagen, have a degradation time extending over several months[18, 19].

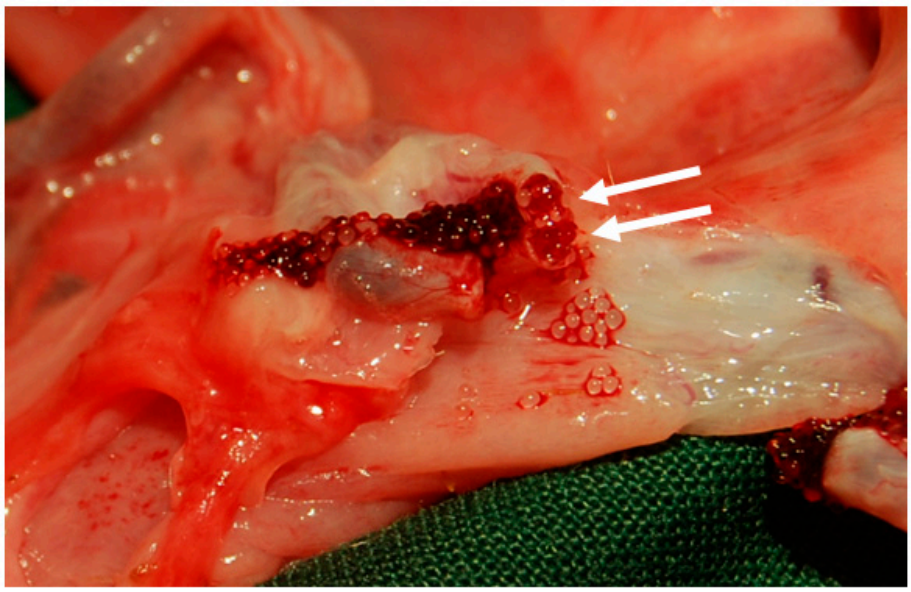

Figure 2
Degradable Starch Microspheres (DSM) 500-700 µm, 19 hours after uterine artery embolisation. No macroscopic evidence of degradation. The uterine artery is cut open (white arrows). Source: Author.

Coils

In contrast to embolisation agents which allow peripheral embolisation, like particles or liquids, coils are mainly used in medium- to large-sized arteries. Constructed from diverse metal alloys, coils can be either bare or coated with various materials, such as wool strands or hydrogel, aiming to enhance packing density and improve occlusion effectiveness. The primary utility of coils lies in the treatment of aneurysms and haemorrhage injuries[20].

Liquids

Other embolisation materials depend on the patient's own coagulation system, while liquid materials are inherently occlusive. Some of these materials can also reach very peripheral areas, beyond the reach of catheters[20, 21]. When the material is injected, it undergoes various reactions, such as polymerisation[22], to solidify. The most common agent is ethanol, which quickly denatures proteins, destroys the endothelium, and leads to permanent vessel occlusion. Ethanol can be used for the treatment of kidney cancer and arteriovenous malformations[23, 24]. Embolisation with acrylic glue has many applications, but it polymerises quickly and may therefore be difficult to control, carrying a risk of attachment to the catheter. Several modern adhesive-like materials are more easily manageable.

Other devices

Balloons can be used for temporary occlusion of larger vessels. Plugs of various kinds are used for the occlusion of larger vessels and can have a diameter of up to a few centimetres.

The optimal embolisation device

Since the first embolisation with autologous blood in the early 1970s, there has been an accelerating development of various embolisation materials. In 2007, Laurant delineated characteristics an ideal embolisation sphere should possess[12]. A parallel depiction of the optimal embolisation material was presented by Dr. Wang et al. in 2020[20]. The product should be made of bioengineered material and be non-toxic, capable of being injected through any catheter without preparation. After achieving its embolisation effect, the material should degrade to avoid undesired chronic inflammation and allow repeated intervention in the same vessel. The material should be visible under fluoroscopy as well as on computed tomography (CT) and MRI. Additionally, the material should be able to be loaded with various drugs for local effect[19]. These features inspired the writing of the first two papers in the thesis.

Histological and immunological effects

The desired outcome of most interventions involving embolisation is to achieve a temporary or permanent cessation of blood flow in the target organ or tissue, subsequently, resulting in ischaemia. This will inevitably initiate tissue reactions. The body responds to the event by attempting to restore blood flow and heal the incurred damage. In addition to the effects on the embolised target organ, the vessel containing the embolisation material is also affected[10, 14]. Acute and chronic reactions arise here as well, with the purpose of restoring conditions to normal[14].

Vascular changes

Certain embolisation materials induce more vascular tissue reactions than others. Among these are alcohol, where the damage that arises is the desired reaction leading to vessel occlusion. Gelatine sponge also produces a significant local vascular reaction. However, the local vascular reaction is considerably milder when using calibrated microspheres, such as TGMS, for embolisation.

The acute reaction that occurs involves inflammation with infiltration of neutrophilic granulocytes and macrophages in and around the vascular wall. Both the induced inflammation and the response to the embolisation material itself cause damage to the endothelium, with subsequent degeneration or necrosis of the vascular wall. Depending on whether the embolisation material is degradable or not,

subacute to chronic changes occur. Subacute changes manifest with the initiation of subintimal deposition of loose connective tissue, resulting in narrowing of the vascular lumen (figure 3A). Non-degradable/long-lasting material also initiates a foreign body reaction in the vessel wall (figure 3B)[10]. The inflammatory response plays a central role in the subsequent remodelling of the vessels, mediated by metalloproteinases (MMPs) and cytokines (TNF-alpha, IL-2, and IL-6)[25].

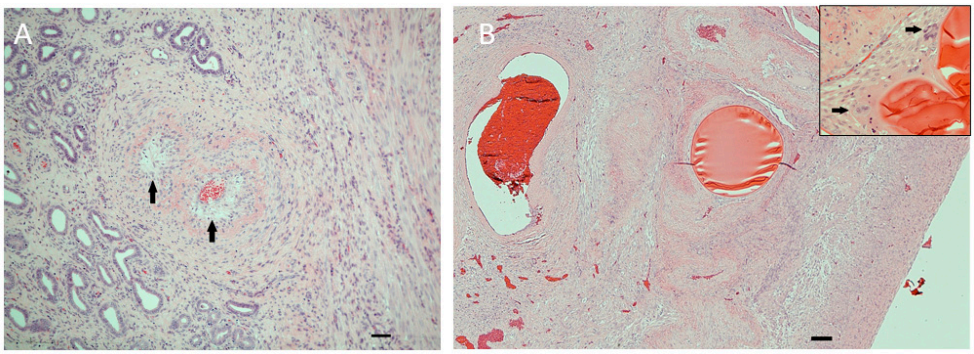

Figure 3
(A). Histological photograph of the uterus of a sheep embolised with degradable starch microsphere. The artery in the endometrium shows subintimal deposition of loose connective tissues (arrows), with mild to moderate narrowing of the arterial lumen. Haematoxylin and eosin staining. Bar 100 µm. **(B)** Histological photograph of the uterus of a sheep embolised with TGMS. Spherules in the lumen of arteries of the myometrium, associated vascular lesions characterised by infiltration of macrophages and multinucleated giant cells of foreign body type (arrows), ingrowth of fibroblasts/fibrosis around intra-arterial spherules. Spherules and the surrounding inflammatory reaction completely obstruct the arterial lumina. Haematoxylin and eosin staining. Bar 120 µm. Inset: higher magnification of vascular lesions. Source: Author.

In cases where permanent or more long-lasting embolisation materials have been used, such as PVA particles, new, thin, and tortuous vessels can form to partially restore blood flow[13]. This process, known as angiogenesis or neovascularisation, is stimulated by various angiogenic cytokines, such as Vascular Endothelial Growth Factor (VEGF), which can be expressed by endothelial cells, smooth muscle cells in the vessels, and macrophages[26].

In a long-term animal study, sheep underwent uterine artery embolisation with TGMS or PVA. Approximately two years after the embolisation, a majority of the embolisation material had exited the vascular lumen and migrated entirely or partially (transvascularly) through the vascular wall. The larger aggregates of the embolisation material were predominantly located in the intima and media, while the smaller ones were also found outside the vessel. Persistent damage to the internal and external elastic lamina of the vessel wall was evident. The embolisation material remained relatively intact but sometimes had become calcified. A chronic inflammatory reaction, with fibrosis and infiltration of multinucleated foreign body

cells, was present in close association with the aggregated embolisation material. The vessels were partially re-canalised but clearly exhibited luminal narrowing[14].

Tissue effects

Different tissues and organs respond differently to ischaemia. Tissues also have varying abilities to tolerate ischaemia and restore blood flow, thereby preserving function. This variability is influenced, for example, by the tissue's dependence on oxygen or how rapidly collateral blood flow can be recruited. The liver, for instance, can tolerate nearly complete loss of arterial blood flow due to the presence of a parallel portal flow that immediately compensates for the loss. The uterus demonstrates a good ability to recruit collateral vessels from the ovaries and adjacent organs if blood flow through the uterine arteries ceases. Skeletal muscle at rest can withstand several hours of ischaemia, while the brain and cardiac muscle sustain damage within minutes.

Within minutes of ischaemia, cardiac muscle cells and cell membranes begin to be damaged. Consequently, cells swell, and contractability diminishes. After a few hours, inflammatory cells start to accumulate, and if ischaemia persists, cell death occurs. Similar effects, albeit not as rapid, occur in other organs.

One of the body's fastest and most effective ways to restore blood flow is by recruiting new vessels from nearby vascular territories. This occurs, for example, in the brain during acute stroke[27], and if the blood flow to the spleen is cut off, blood can reach the spleen through vessels in the stomach wall. These rapid changes are stimulated by decreased post-stenotic pressure and a decrease in oxygen levels.

Chronic inflammation and angiogenesis are interconnected phenomena that frequently coexist. Hypoxia serves as a common trigger for both processes[26]. Hypoxic conditions prompt the accumulation of macrophages and other immune cells, which produce cascades of cytokines (MMP and VEGF) that stimulate the formation of new blood vessels (figure 4)[26]. This function is particularly effective in tumours, whose growth partly relies on angiogenesis and overexpression of proangiogenic factors[28]. In the context of tumour embolisation, following transarterial chemoembolisation (TACE) of HCC, rapidly growing and new tortuous vessels develop as a response to the sudden ischaemia.

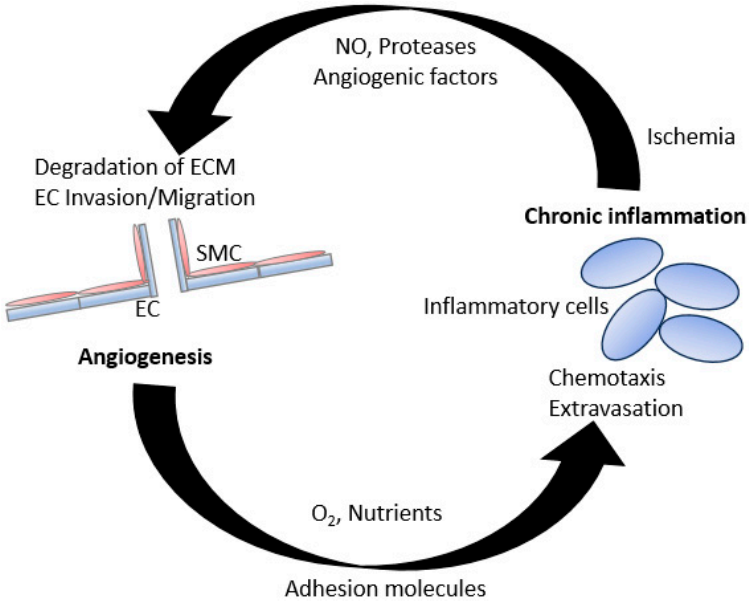

Figure 4
Cross-link between chronic inflammation and angiogenesis. Growth, factors, cytokines and proteases are secreted by the inflammatory cells. Degradation of the extracellular matrix (ECM) and growth of endothelial cells (EC) are induced. The inflammation is enhanced by angiogenesis which provides cytokines, nutrients and oxygen and enables chemotaxis of inflammatory cells. The loop further enhances both angiogenesis and inflammation[26]. SMC – smooth muscle cell. Source: Author.

Finally, it is important to point out that angiogenesis is not only a phenomenon involved in pathology but also in the growing organism and in regeneration of tissues[29].

Uterine fibroma and treatment

Background

Uterine leiomyoma or uterine fibroma is the most common tumour type in gynaecological organs. The prevalence is high but challenging to study as most uterine fibroids remain asymptomatic. The prevalence increases with age. Various numbers are reported, ranging from 40% in women aged over 40 years[30] to 80% in women aged 50 years[31]. A study using ultrasound in premenopausal women reported a prevalence of 62%[32]. In contrast, only 5.4% of 335 Swedish women were found to have fibroids on ultrasound[33]. In a study involving 95,061 premenopausal nurses in the USA, a higher annual incidence was observed for black women compared to white women, with rates of 30.9 per 1000 and 8.9 per 1000, respectively[34].

The mortality of uterine fibroids is nearly negligible, while the morbidity is obvious. Different figures are reported here as well, with 20-40% of women experiencing symptoms from their uterine fibroids[35]. Uterine fibroids are the most common cause of hysterectomy worldwide and the second most common gynaecological surgery after caesarean section[36, 37].

The most significant and widely reported risk factor for developing fibroids is race, with black women having a significantly higher risk. In general, both oestrogen and progesterone are risk factors for the development of fibroids[38]. This means, for example, that fibroids grow in the early stages of pregnancy, and their growth halts after menopause. Other risk factors include advanced age, heredity, hypertension, nulliparity, early menarche, late menopause, overweight, vitamin D deficiency, and exposure to various chemicals, including alcohol and tobacco. Injectable contraceptives containing medroxyprogesterone acetate (MPA), a synthetic progestin, have a protective effect. Oral contraceptive pills in younger years increase the risk of developing fibroids, while the use of oral contraceptives later in life decreases the risk[38, 39].

The clinical symptoms depend on the size and location of the fibroids. The most common symptom is pain. Abnormal bleeding and unusually heavy or prolonged menstruation (menorrhagia) as well as bleeding between regular menstrual periods (metrorrhagia) can also occur. Other symptoms may be related to pregnancy, such as implantation issues, premature delivery, and miscarriage. Difficulties during childbirth and urinary incontinence may also occur[40, 41].

The role of uterine fibroids in infertility is a subject of debate. When other causes of infertility are ruled out, fibroids are found in 1-2% of women. However, meta-analyses suggest that fibroids do indeed have an impact on fertility, with the primary cause believed to be their effect on uterine contractility and, consequently, embryo migration. In particular, submucosal fibroids have a negative impact on implantation, pregnancy, and the incidence of miscarriages[42]. Intramural fibroids have a significantly lesser effect, and all studies indicate that subserosal fibroids do not affect fertility at all[43], unless they are large and located near the fallopian tubes. Although the extent of fibroid impact on fertility is not fully established, fibroids are often treated with the aim of increasing the chances of a successful pregnancy[38].

Classification

Uterine fibroids are monoclonal tumours that arise from smooth muscle, such as the myometrium. They are often well-defined and can occur at various locations in the uterus, including the cervix and parametrium. Fibroids are classified based on their location (figure 5). Subserosal and submucosal fibroids may also be pedunculated. Intramural fibroids can have more or less contact with the endometrium and are classified accordingly.

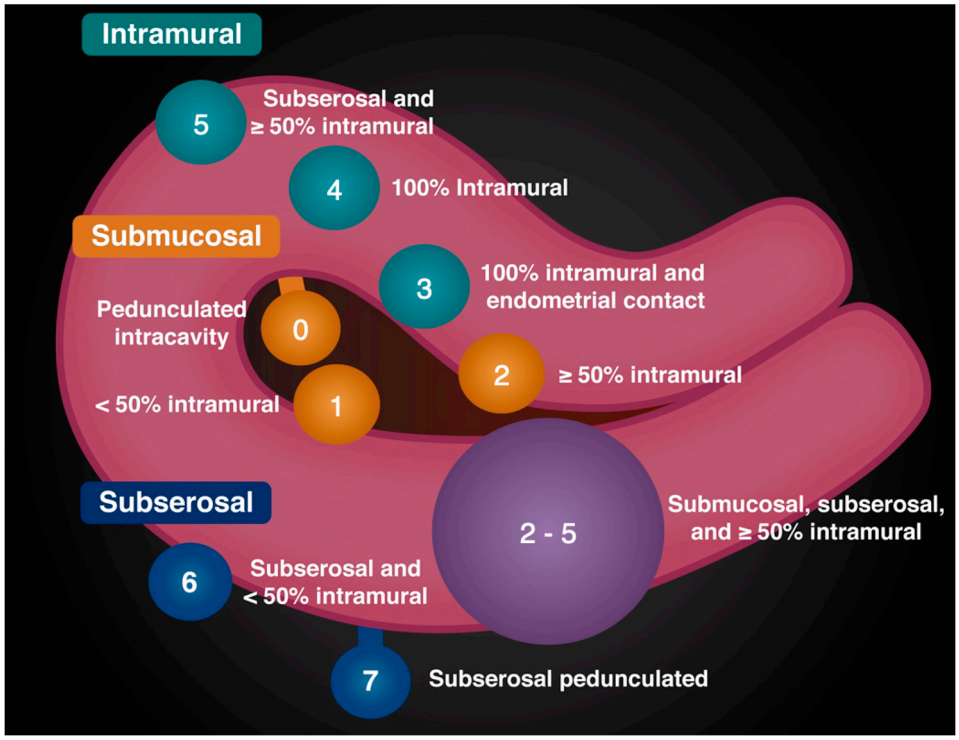

Figure 5
Diagram describing the uterine fibroid classification system. Organised according to the location between the submucosal (0 – 2), intramural (3 – 5), and subserosal (6 – 7) layers of the uterus. Subtype '8' is not illustrated and denotes 'other' location e.g. cervical fibroid. Image courtesy of Sachi Hapugoda, Radiopaedia.org, rID: 62908

Treatment options

Various treatment options are available for uterine fibroids. The choice of treatment is dependent on the number and the location of the fibroids, as well as the woman's desire to conceive. Surgical treatment is by far the most common approach, as indicated by a dataset from the United States based on insurance claims. Hysterectomy was the predominant treatment, accounting for 82.2%, followed by myomectomy at 14.7%. Only 3.1% underwent uterine fibroid embolisation[44].

Surgery

The definitive cure for fibroids is hysterectomy, with the clear consequence that future pregnancy is precluded. Other surgical methods include uterus-preserving myomectomy, which can be performed either hysteroscopically, laparoscopically, or through open surgery (laparotomy). During myomectomy, the tumours are

enucleated. Hysteroscopic myomectomy is best suited for intramural fibroids, while subserosal fibroids require abdominal surgery. Like all surgeries, these procedures carry risks of complications such as bleeding, infections, and scar tissue formation (synechiae or adhesions). Injuries to adjacent organs such as the bladder, bowel, and ureters can also occur. Laparoscopic myomectomy reported 9.1% minor and 2% major complications[45].

The cumulative five-year recurrence risk after resection of multiple fibroids was 74%, compared to only 11% after resection of a single fibroid[38].

Pharmacological therapy

Pharmacological treatment of fibroids focuses on the inhibition of female sex hormones, primarily progesterone. The treatment is not curative but can sometimes alleviate symptoms and improve quality of life. Often, pharmacological treatment serves as a palliative measure until surgery becomes a consideration. In cases of bleeding issues, tranexamic acid or hormonal intrauterine devices may be used. Newer treatments targeting genetic and receptor levels are under development[36, 39].

High-intensity focused ultrasound

HIFU is sometimes used with MRI guidance and hence referred to as MRgFUS. Local treatment with high-frequency ultrasound can be applied to smaller fibroids. It is considered suitable for women who wish to preserve fertility. Highlighted advantages include the ability to perform the treatment on an outpatient basis and its association with very few complications[46]. HIFU appears to be more effective than myomectomy in terms of quality of life (QoL). In a meta-study, symptom recurrence was lower compared to myomectomy, but the re-intervention rate was slightly higher[47, 48].

Uterine artery embolisation

Uterine artery embolisation (UAE) or Uterine fibroid embolisation (UFE) are synonymous terms for the same treatment.

Embolisation is a uterus-preserving alternative to surgery in the treatment of symptomatic fibroids. Its best effect is observed in reducing menorrhagia, where over 90% experience a reduction in bleeding. While the desire for pregnancy is not an absolute contraindication, many consider myomectomy to be a better treatment option for women who want this. There is an increased risk of miscarriage, premature birth, and lower birth weight after embolisation. However, several studies report completely normal pregnancies.

Gynaecological examination, including ultrasound, should be conducted before treatment to exclude other causes for the symptoms. Any signs of malignancy, such as sarcomas, should result in further investigation and use of a treatment other than embolisation. Pedunculated and very large fibroids are better suited for surgery[49, 50]. However, a very large uterus with a significant number of smaller fibroids may be suitable for embolisation. MRI should be performed before and after the embolisation[51]. Absolute contraindications for UFE are pregnancy and suspicion of malignancy, while renal failure, coagulopathy, and contrast allergy are relative contraindications. Vascular mapping with CT or MRI prior to the intervention is not routinely performed.

Vascular anatomy of the uterus

The uterine artery is a branch of the anterior division of the internal iliac artery. It turns medially across the pelvic floor at the base of the broad ligament towards the uterine cervix. It crosses the ureter anteriorly, then ascends along the side of the uterus. At the superolateral angle of the uterus, it turns laterally and runs along the uterine tube and terminates by dividing into two branches, the tubal branch, and the ovarian branch. Those terminal branches will anastomose with two corresponding arteries from the ovarian artery. The branches will supply the tube and ovary respectively. Branches from the ovarian and uterine artery will form the periovarian arcade from which numeral arterial twigs will enter the mesovarium forming a plexus in the ovarium medulla (figure 6A).

The first branch from the uterine artery is the ureteral branch (not shown in the figure). Close to the cervix and the lateral fornix of the vagina, the vaginal and the vaginal branches arise. Along the side of the uterus body, the uterine artery gives off arcade branches which run transversely on the anterior and posterior surfaces of the uterus and anastomoses with their contralateral counterparts along the midline. At the superolateral angle of the uterus, branches to the fundus arise (figure 6A).

The ovarian arteries often arise from the abdominal aorta, below the renal arteries. They have a typical corkscrew appearance[51].

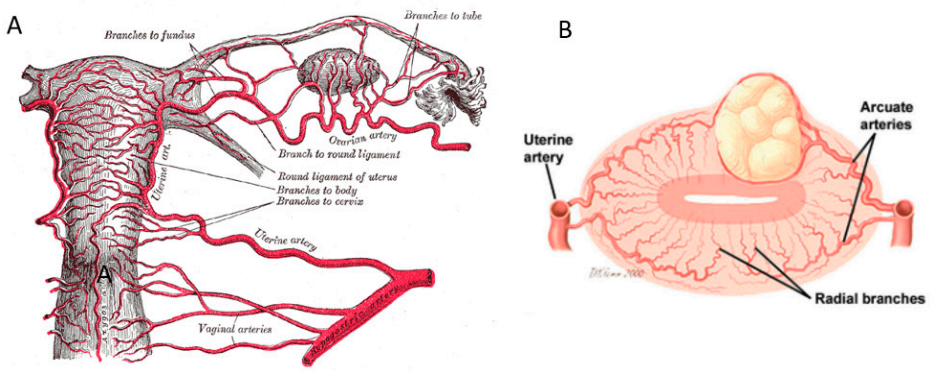

Figure 6
(A) Anatomy of the arterial supply of the uterus, cervix and ovaries. **(B)** A transverse section of the uterus including a uterine fibroma. Large bilateral feeding arteries supply the fibroma, however without the same network of radial branches as the normal tissue which makes the fibroma more vulnerable to ischaemia. (A) The image is in the public domain. (B) Reprinted with permission from Radiographics[51].

Several variations of the vasculature have been described in the literature and must be taken into account during the procedure[52, 53]. Awareness of the anastomoses described above is important to optimise the result and to minimise adverse side effects and complications. The utero-ovarian anastomoses are identified in 10-30%[52, 54]. The diameter of the anastomoses is usually less than 500 µm.

The fibroids are often supplied from both sides and usually with enlarged feeding vessels. However, compared to the normal uterine tissue, the fibroids have a more primitive vascularisation and are supplied by small centripetal arteries (figure 6B). Therefore, the fibroids are more vulnerable to ischaemia. In some cases, especially in women with prior pelvic surgery, fibroids can be supplied from the ovarian arteries[52].

Embolic material

For a successful outcome in both the short and long term, the most crucial factor is achieving total ischaemia of the fibroid. Recurrence growth occurs from the non-infarcted parts of the fibroid[55]. Fibroids embolised with particles reach more peripheral areas than coils and glue, resulting in better infarction. No differences have been observed when using smaller particles (<500µm) or larger particles (500-700µm) in randomised controlled trials. Although smaller particles are theoretically more effective, they pose greater risks as they can more easily pass into other organs and cause ischaemic damage, of non-target embolisation, such as the ovaries. If angiography reveals anastomoses to the ovaries, larger spheres should be used (700 – 900 µm). In most of the studies comparing the effectiveness of TGMS and PVA particles, no difference was seen in the short or long-term results[56-60]; however, a systematic review by Jiang et al. found an overall better outcome for TGMS at six

and twelve months post-embolisation for quality of life, symptom relief, fibroid and uterus volume as well as infarction rate[60]. The most common material for UFE in Sweden today is PVA particles (350-500µm) and TGMS (500-700µm)[61].

Procedure

Preprocedural consultation with an anaesthesiologist for adequate analgesia is recommended. Typically, the procedure can be performed under local anaesthesia, but in some cases, epidural anaesthesia or sedation may be considered. Antiemetics and mild sedation are recommended.

Transarterial access is obtained through retrograde puncture of the common femoral artery. Subsequently, a catheter is advanced over the aortic bifurcation to the contralateral common iliac artery. After catheterising the internal iliac artery, a subtraction angiography is performed as a roadmap for further catheterisation. The uterine artery has a typical U-shaped appearance. Usually, a co-axial microcatheter is required for further selective catheterisation. It is preferable to position the tip of the catheter peripherally to the origin of the ureteral and cervical branches unless there are fibroids in the cervix that need treatment. The treatment can now be initiated at this site. Care should be taken to ensure that the microcatheter is not occluded, and it should be regularly flushed with saline. As the flow stops due to embolisation, additional attention to reflux is required, as it may inadvertently cause undesired embolisation to other locations. After achieving stagnant flow, a few minutes should be allowed, followed by a careful angiography with hand injection to potentially replenish with more particles. Once the procedure is completed, the same procedure is performed on the other side, either through the same femoral access and ipsilateral approach or with a new puncture on the other side. An alternative is simultaneous treatment from both sides using two access sites, which can reduce the amount of ionising radiation. After completing the procedure, the catheters and introducers are removed[61, 62].

Post-procedural management

Pain relief with oral analgesics is usually sufficient, however, sometimes an epidural anaesthesia is required. Post-embolisation syndrome (PES) may occur and may require additional treatment, such as antibiotics. PES is a frequently observed phenomenon, occurring in approximately 40% of patients within the initial week following UFE for the treatment of leiomyomas. PES is characterised by the manifestation of pelvic pain, low-grade fever, nausea, vomiting, reduced appetite, and general discomfort during the early stages of post-procedural recovery. Although the exact underlying causes of PES remain largely unknown, it is believed to stem from an inflammatory response caused by the ischaemia and necrosis of the tumour and uterine tissues[63].

Complications

Large intracavitary or intramural fibroids with submucosal contact can be expelled. This typically occurs between three weeks to six months after the treatment and manifests as severe menstrual-like cramps and bleeding or discharge. Other possible complications include infection, pulmonary embolism, mis-embolisation, injury to the myometrium, or loss of ovarian function[62].

Results

Both menorrhagia and bulk symptoms improve in 80-95% of patients. Re-intervention is needed in approximately 5-10% of cases within a year due to the lack of effect. Long-term results show similar results as surgery[64]. For women desiring pregnancy, most indications suggest that myomectomy is a better treatment, at least during the first two years[65].

Benign prostate hyperplasia

Background

With increasing age, the formation of small benign adenomas occurs within the transition zone of the prostate. These adenomas consist of glandular epithelial tissue, smooth muscle, and connective tissue; therefore, the term "stromo-glandular hyperplasia" is used. The adenomas can proliferate and result in BPH. This process may commence in certain individuals as early as in their thirties. By the time the eighties are reached, approximately 90% of all men exhibit microscopic hyperplasia. As the prostate gland enlarges, it can cause obstructive symptoms. The affected individual then experiences the characteristic manifestations of BPH, known as lower urinary tract symptoms (LUTS). The growth of glandular cells is dependent upon functioning testes where the androgens, including testosterone, are produced by the Leydig cells. It is released into the bloodstream and enters the cells by diffusion. Testosterone is converted within the prostate by the enzyme 5-alpha reductase to dihydrotestosterone (DHT), which exhibits much higher affinity to the androgen receptor in the prostate compared to testosterone. DHT attaches to the androgen receptors and stimulates the growth of cells in the transition zone of the prostate. This process is necessary for normal gland development as well as the growth which leads to hyperplasia. In hyperplasia development, there is an imbalance; the rate of formation of new cells is faster than the rate of cell death. Consequently, prostate hyperplasia is characterised by a dysfunction in apoptosis, wherein cells do not undergo normal programmed cell death at the expected rate. Regarding testosterone, it is a well-known fact that eunuchs and men castrated before puberty have an atrophic prostate and do not develop BPH[66].

Genetic factors may play a role in BPH development as well as obesity. BPH is more commonly seen in certain ethnic groups, such as African Americans. A sedentary lifestyle and type 2 diabetes also contribute to an increased risk of BPH[67].

LUTS and BPH are highly prevalent. A Swedish population study revealed that over 30% of more than 2,000 randomly selected men from across the country had an international prostate symptom score (IPSS) of 8 or higher, while over 10% had an IPSS of 15 or higher. One-third of men with LUTS reported a significant negative impact on their quality of life[68].

There are different methods for diagnosing BPH and LUTS, such as patient history and basic examination, which includes palpation of the prostate, a urine dipstick, and checks of prostate-specific antigen (PSA), and creatinine levels. The urologist usually performs a transrectal ultrasound of the prostate. The International Prostate Symptom Score is the most used tool. It is a validated, self-administered questionnaire. The output is a score between 0 and 35 where 0 is asymptomatic and 35 is severely symptomatic[66]. Further evaluation may include uroflowmetry and post-void residual. MRI is usually not a part of the workup unless suspicion of cancer.

Treatment

The American Urological Association describes a wide range of treatment options. Depending on the severity of the symptoms and associated symptoms and conditions, different options are recommended[66].

Medical therapy is often the first line option regardless of severity. Monotherapy or combination of drugs. If the cause of LUTS is a prostate gland size over 40 ml, 5-alpha reductase inhibitors can reduce gland size and decrease symptoms. Alpha-receptor blockers relax smooth muscle in the prostate gland and the bladder neck, thereby increasing urine flow. The advantages of alpha-receptor blockers lie in their prompt efficacy, evident within a few days, irrespective of prostate size. Anticholinergics/muscarinic receptor inhibitors may be considered for storage symptoms. The risk of urinary retention caused by anticholinergic treatment is exaggerated but not entirely negligible. In such cases, selective beta-3-adrenoceptor agonists can be tested. They enhance the storage phase of the bladder with an equivalent clinical effect to anticholinergic treatment, yet with a somewhat more favourable side effect profile. Phosphodiesterase type 5 (PDE5) inhibitors, commonly known as Sildenafil, lead to increased levels of cGMP, which exerts a relaxing effect on smooth muscle, including the prostate. For patients with combined LUTS and erectile dysfunction, this may serve as an alternative[66].

Surgery is indicated for patients with impaired renal function, urinary retention, gross haematuria due to BPH or recurrence of bladder stones. Total prostatectomy should only be performed on very large glands. Transurethral resection of the prostate (TURP) or transurethral incision of the prostate (TUIP) are smaller

interventions. TURP is the most common surgery for BPH. Prostatic urethral lift[69] or adenoma enucleation are other options. Several other local, often transurethral therapies, using laser, heat, ultrasound, microwave, water vapour[70] and stenting can be effective alternatives.

Most surgery must be performed under general anaesthesia and requires postoperative hospitalisation. Side effects of surgical interventions range from acute events related to the surgery itself, i.e. bleeding or infection. After prostatectomy, there is a risk of incontinence and sexual dysfunction. Retrograde ejaculation is common after TURP.

A relatively new treatment option is Prostate Artery Embolisation (PAE)[66, 71].

Prostate artery embolisation

In 1976, Mitchell et al. treated four men with severe haematuria from the bladder or prostate with bilateral embolisation of the internal iliac arteries[72]. The benefit of PAE was first described by DeMeritt in 2000[73]. He performed a unilateral embolisation of the inferior vesical artery with PVA (150-250µm) for treating haematuria due to BPH. One year later the IPSS score was improved from 24 to 13 and the volume of the gland was reduced by 40%. Carnevale et al. successfully treated two men with acute BPH-related urinary obstruction with PAE in 2010. The embolisation was performed with calibrated microspheres, TGMS (300-500µm)[74] with symptom relief at the six-month follow-up. A year later, Pisco et al.[75] presented a case series of 15 patients who underwent PAE. Significant improvement was achieved in most patients, however one patient required surgical resection of the urinary bladder because of ischaemia[75]. Over the years, PAE has now become a treatment option for BPH worldwide.

Several papers, including review articles, have been published on the topic. PAE is often compared to TURP. Carnevale concluded that TURP and PAE yield similar symptom improvement. However, TURP has better urodynamics but more adverse events[76]. Similar results were found in a Cochrane review by Jung et al. in 2023[77]. The same article did not find any significant differences in major or minor adverse events or differences in QoL/IPSS between the two groups. However, PAE has a shorter hospital stay after the treatment and a lower frequency of ejaculatory disorders but a higher re-treatment rate than TURP. The UK-ROPE trial was performed by the British Society of Interventional Radiologists and by the British Association of Urological Surgeons. The results indicated that PAE provided a clinically and statistically significant improvement in symptoms and QoL, although some of these improvements were greater in the TURP arm. The safety profile and quicker return to normal life were advantages for the PAE group[78].

Low rates of side effects and complications after PAE are reported. Most post-procedural events are temporary and include dysuria, haematuria, rectal bleeding,

hematospermia, urinary retention and infection. Inflammation after embolisation secondary to ischaemia is an expected side effect. PES may require additional treatment with antibiotics or percutaneous drainage in the case of abscess formation. There is a risk, however low, for urethral stricture secondary to ischaemia. Non-target embolisation of the rectum, urinary bladder, seminal vesicles, and penis have been described[79, 80].

Prostate artery embolisation

Preprocedural CT angiography is performed to map the arterial anatomy, especially the origin of the inferior vesical artery (IVA) (prostate artery), and to identify troublesome anastomoses. MRI angiography is an alternative for mapping but is not as good as CT angiography. MRI is better for assessing the prostate gland and can be used to detect malignancy and for volumetry. Usually, CT, MRI and ultrasound are performed prior to the treatment. As the procedure progresses, Cone Beam CT (CBCT) should be performed to evaluate the anatomy and treatment.

Anatomy

Similar to the uterine artery, the IVA arises from the anterior division of the internal iliac artery (figure 7). The branches arising from the common trunk of the iliac artery are (internal **p**udendal, middle **r**ectal, **o**bturator, **i**nferior **v**esical, **s**uperior vesical). The acronym PROVISO (O for ipsilateral **o**blique view) is used to memorise the branches. However, there are many anatomical variants. In the figure below the inferior and superior vesical arteries originate from a common trunk (figure 7B).

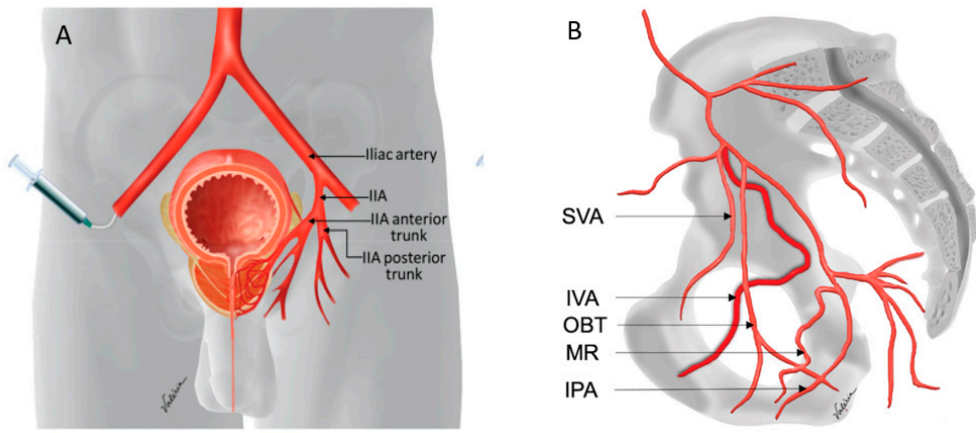

Figure 7
(A, B) Arterial anatomy of the prostate gland. **(A)** shows a coronal view with the access for the intervention from the contralateral side. **(B)** shows an ipsilateral oblique view of the internal iliac artery branches. In this case, the inferior and superior vesical arteries originate from a common trunk which is an anatomic variant. IIA – internal iliac artery, SVA – superior vesical artery. IVA – inferior vesical artery, OBT – obturator artery, MR – middle rectal artery, IPA – internal pudendal artery. Reprinted with permission from Radiographics[79]

Embolisation procedure

In a similar manner to UAE, the iliac internal artery is catheterised. The PERFECTED technique (proximal embolisation first, then embolise distal) should be used. When the microcatheter has been placed in the proximal IVA and a vasodilator has been injected through the catheter, it is further advanced distal to the collateral branches supplying nearby organs. After another aliquot of vasodilator, the embolisation commences with a diluted solution of calibrated microspheres. The size of the spheres is important. Smaller spheres penetrate more distally and yield a better ischaemia but have a greater risk of non-target embolisation. Spheres of different sizes can also be combined. Usually, spheres sized 100-300µm or 300-500µm are used.

When stasis has been achieved and verified with angiography the microcatheter is advanced into the intraprostatic branches for additional embolisation. Another 30-100% of spheres can usually be delivered. After a final angiography, the procedure is repeated on the contralateral side. Catheters and wires are removed. A haemostatic device can be used. Usually, the patient can be discharged on the same day. Postoperative pain management is provided with oral analgesics[79].

Tumour embolisation

Tumour embolisation is often performed in the liver but can also be carried out in other organs, such as the kidneys and lungs. The embolisation material may be loaded with cytostatic drugs in chemoembolisation (TACE) or with radioactive isotopes in radioembolisation (TARE). In TACE, the ischaemic effect is combined with the effect of the active substance. When only the embolic material is used, the procedure is referred to as transarterial embolisation or bland embolisation. The therapy's usual purpose is palliation, but it is sometimes employed as a bridge to transplantation or partial liver resection.

The liver has a parallel blood supply, with approximately 2/3 of the normal liver parenchyma being supplied by the portal system and the rest by the arterial system, while tumours are entirely supplied by the arterial system. This means tumours are more vulnerable to embolisation of the hepatic artery. A prerequisite for treating the liver with TACE is that the portal system is patent; otherwise, ischaemia would severely affect the healthy liver parenchyma, especially with non-selective treatment[81]. In the case of TARE, the ischaemic effect is less pronounced, and this procedure can be performed also when the portal vein is non-patent.

Since TAE and TACE are performed to induce ischaemia, they work best on hypervascular tumours, i.e., tumours with high perfusion and a high demand for oxygen. In the liver, this primarily involves HCC and metastases from neuroendocrine tumours, such as carcinoids, which often produce multiple large liver metastases. Treatment often occurs non-selectively, treating an entire liver lobe

at a time rather than the individual metastasis selectively. However, the trend is now towards a more selective approach. Before embolisation begins, any shunts to the venous system must be mapped and avoided. If the tumour load is extensive, the treatment can be painful and may require general anaesthesia, but in most cases, it can be performed with sedation and intravenous pain relief. In the case of carcinoid metastases, the treatment may induce a hormone release from metastases, leading to a so-called carcinoid crisis. Therefore, premedication, including somatostatin analogues, is required. TAE is performed with small particles, such as PVA 45-150 µm, but other materials such as starch spheres or Lipiodol emulsions may be used. Serious complications occur in 10% of cases, including acute liver and kidney failure, carcinoid crisis, and bleeding ulcers. Sepsis and liver abscesses may also occur. PES occurs in 90% of cases[61].

The most common indication for embolisation of the liver is HCC. HCC is often hypervascular and can be treated with TACE as well as TAE.

TACE can be performed as conventional TACE (cTACE) with Lipiodol emulsion as the carrier of the active drug, or as DEB-TACE with drug-eluted beads as the carrier. For HCC, doxorubicin is the active drug[82]. TACE can also be performed for colorectal metastases, using irinotecan as the active substance[83]. These metastases are usually hypovascular and the embolisation effect itself is not sufficient and must be combined with an active drug. The practical procedure is more or less the same as described above. However, a more selective approach is usually adopted, reducing the risk of liver damage. Since selective treatment minimises the effect on the normal liver parenchyma, portal vein thrombosis is not an absolute contraindication. Subsequent PES and systematic reactions to cytostatic drugs may occur.

In recent years, a few studies have been published on PAE for the treatment of prostate cancer[84]. DEB-PACE of the prostate was described in 2022 by Guan, Wang and Zhang. Epirubicin-loaded beads showed promising results in treating advanced prostate cancer. No further conclusions could be drawn from this small study[85]. The role of PAE and PACE regarding oncological outcomes must be assessed further.

Prostate cancer

The prostate

The prostate gland is a walnut-sized, fibromuscular accessory glandular organ that surrounds the prostatic urethra. The base of the prostate is located at the neck of the bladder. Its apex rests on the urogenital diaphragm. The anterior surface is separated from the symphysis by retropubic fat, and the posterior surface lies adjacent to the rectum and Denonvilliers', a part of the mesorectal fascia. The inferolateral part is close to the levator ani. The two seminal vesicles are located posterolaterally and connect with the vas deferens, forming the ejaculatory ducts that pass through the prostate and join the urethra at the verumontanum, also known as the seminal colliculus. The seminal vesicles produce most of the seminal fluid, containing substances such as fructose and enzymes.

The external sphincter is located below the apex and consists of an outer layer of horseshoe-shaped striated muscle and an inner circular layer of smooth muscle surrounding the urethra. The prostate consists of four histologically distinct zones (figure 8).

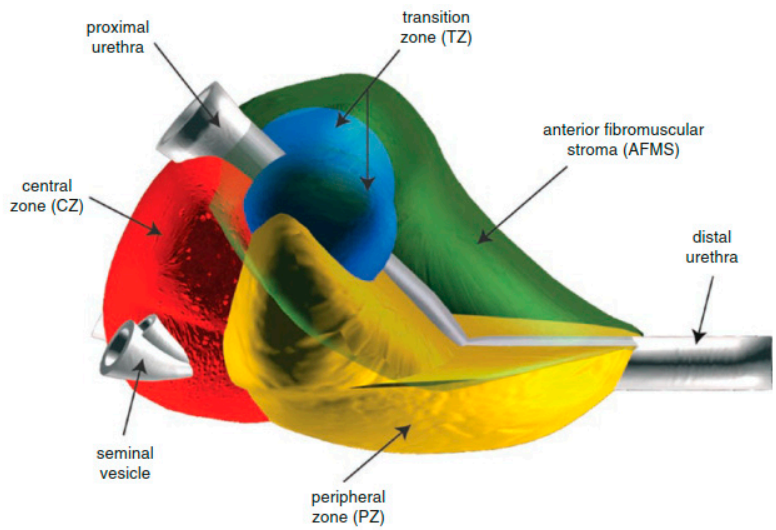

Figure 8.
Gross anatomy of the prostate and its lobes. In benign prostate hyperplasia, the transition zone becomes enlarged at the expense of the other zones. Reprinted with permission from Springer Verlag[86].

The *transition zone* (TZ) constitutes approximately 5% of a young boy's prostate and consists of paired lobes on either side of the proximal urethra. The TZ is located between the other three zones and is separated from them by the so-called surgical capsule. It is the TZ that undergoes growth in cases of benign prostatic hyperplasia and can, in extreme cases, account for almost 100% of the prostate, reaching volumes of 200-300 ml. 10-20% of malignancies arise in the TZ.

The *central zone* (CZ) comprises about a quarter of the prostate's volume. It is pyramid-shaped, situated dorsally, and surrounds the ejaculatory ducts. The CZ narrows downward. Pathology in the CZ is uncommon, with approximately 5% of malignancies originating here.

The *peripheral zone* (PZ) constitutes 70% of the prostate's volume, but as the TZ grows with age, the proportion decreases. The PZ is located dorsally, laterally, and apically. Ventral and cranial, it transitions into the anterior fibromuscular stroma. About 70% of malignancies have their origin in the PZ. The PZ has a close relationship with the dorsolateral neurovascular pedicles, which can be early sites of invasion by cancer from the PZ.

Finally, there is the *anterior fibromuscular stroma* (AFMS), which makes up one-third of the prostate but contains no glandular tissue. Basally, it transitions into the detrusor muscle and internal sphincter. Apically, it transitions into striated muscle in the external sphincter.

Epidemiology and risk factors

Prostate cancer is the most common form of cancer in men, with its incidence varying worldwide. It is highest among Afro-Americans in the United States and the Caribbean, followed by Caucasians in the United States and Scandinavia, while it is lowest in Southeast Asia. In French Guadeloupe, the prevalence is 184 per 100,000 men, whereas the corresponding figure in Sweden is 100 per 100,000 men[87].

In Sweden, the number of newly diagnosed cases doubled between 1990 and 2024 (figure 9). This increase is attributed to the introduction of PSA testing and other diagnostic procedures, leading to the detection of more low-grade and indolent tumours. One in five Swedish men is diagnosed with prostate cancer during his lifetime[88]. The age-standardised incidence trends are depicted in figure 9.

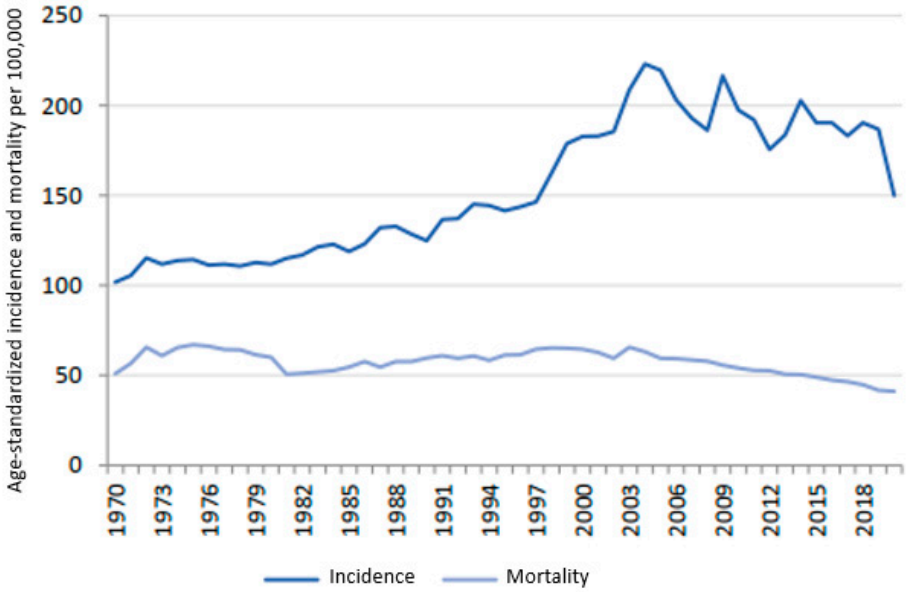

Figure 9.
Age-standardised incidence and mortality per 100,000 men in Sweden, 1970-2020. Age-standardised according to the age distribution in the NORDCAN population in the year 2000[88].

Prostate cancer is strongly age dependent. The disease rarely occurs before the age of 50 and almost never before the age of 40. Increased diagnostic activity has resulted in a decrease in the median age at diagnosis from 74 to 69 years during the period 1995-2005.

Prostate cancer is the most common cause of cancer-related death among Swedish men. In 2018, 5.3% of men died of prostate cancer (PCa). Half of those who die from PCa are over 82 years old, and 75% are over 75 years old.

A clear downward trend is observed in all age groups, with a 50% reduction in men under 75 years of age over the past 15 years (figure 10). However, the number of Swedish men dying from the disease has remained relatively unchanged over the past 10 years, as the population of elderly men has increased (figure 9).

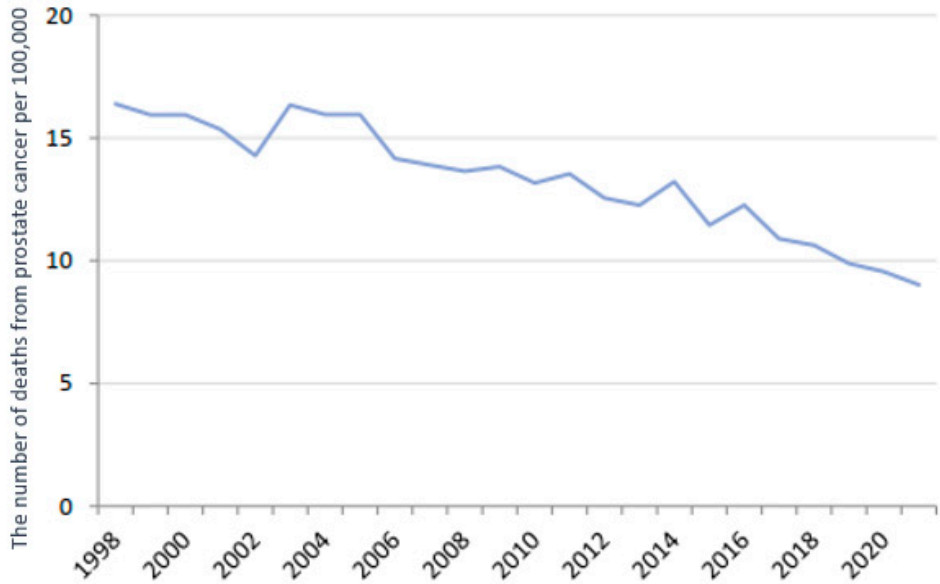

Figure 10.
The number of deaths from prostate cancer per 100,000 among men younger than 75 years in Sweden during the years 1998-2021[88].

In the year 2021, approximately 125,000 men in Sweden were living with diagnosed prostate cancer[89-91], which is three times more than 20 years ago (figure 11). This increase can be attributed partly to the growing population of elderly men, partly to earlier diagnosis of prostate cancer in comparison to previous years, and partly to improved treatment enabling men with advanced prostate cancer to live longer.

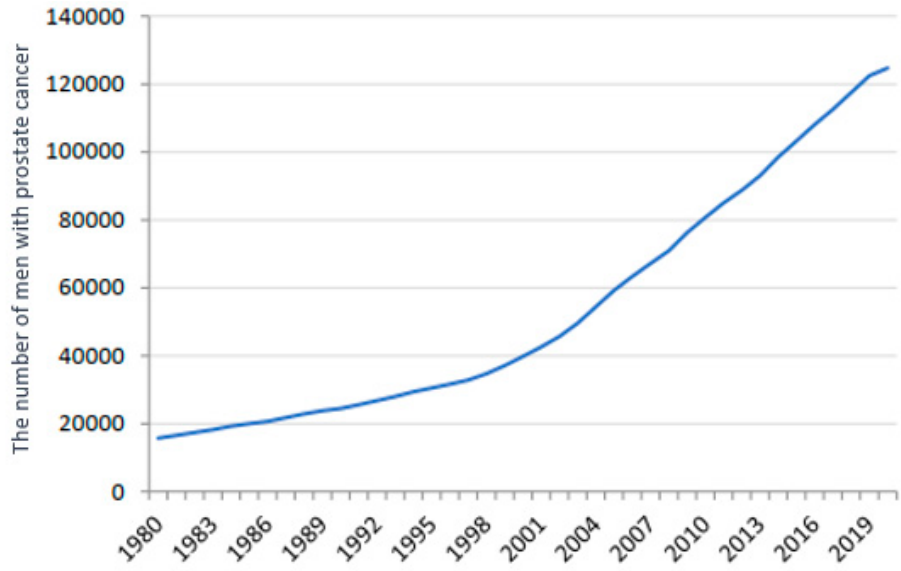

Figure 11.
The number of men living with a diagnosis of prostate cancer per year from 1980 to 2020. (NVP)

The Western lifestyle, including obesity and a high consumption of dairy products, may increase the risk of prostate cancer[91, 92]. Chronic inflammation and tobacco smoking may also play a role in the development of the disease[93]. Heredity is another significant factor, with sons and brothers of individuals with prostate cancer having higher risks, particularly if multiple family members are affected. Two genes, BRCA2 and HOXB13, have been identified as increasing the risk of prostate cancer[94, 95].

Diagnostics of prostate cancer

Prostate-specific antigen

Prostate-specific antigen is an enzyme produced in the glandular epithelium of the prostate and is secreted in high concentrations into seminal fluid, where it liquefies the gel surrounding sperm[96, 97]. PSA is predominantly produced in the prostate, and its production is stimulated by testosterone and DHT. The normal level of PSA in the blood is <3 µg/L, but it is age-dependent. The concentration is approximately one millionth of the concentration in seminal fluid. PSA in the blood leaks from prostate cells, and leakage increases when there is damage to cell membranes, as seen in conditions such as prostate cancer, inflammation, BPH, urinary retention, renal failure, and mechanical stimulation such as palpation. Other factors affecting

PSA levels in the blood include medications, such as 5-alpha-reductase inhibitors, and consideration of these factors is essential in the assessment.

Prostate cancer cells produce less PSA per cell than normal prostate cells, and PSA production decreases with dedifferentiation. Therefore, a poorly differentiated prostate cancer may be locally advanced and metastatic even with low PSA values.

In the blood, PSA exists both in a free form and bound to alpha-1-antichymotrypsin and alpha-2-macroglobulin, the latter of which is not detected in routine blood tests. The ratio between free and total PSA in the blood can provide additional information. A low ratio suggests malignancy, while a high ratio suggests BPH. Since PSA values are largely related to the amount of prostate tissue and thus the number of prostate cells, even healthy cells in a large, benign prostate with BPH can result in a high value. Therefore, PSA density is a more valuable measure than absolute PSA. To calculate density, knowledge of the prostate's volume is required. Different treatment plans use different threshold values, often set at 0.1 $\mu g/L/cm^3$. Another factor to consider is the change in PSA value over time, where a rapid change raises the suspicion of cancer[96-101].

Digital rectal examination

The digital rectal examination (DRE) is always included in the examination of men with LUTS or elevated PSA levels. Since only the dorsal parts of the prostate can be palpated, the majority of the prostate cannot be assessed, leading to a significant proportion of cancers being overlooked. The combination of DRE with PSA and biopsy has a specificity and sensitivity of less than 60%[101].

Transrectal ultrasound and biopsy

Transrectal ultrasound (TRUS) is routinely performed by urologists. TRUS is a valuable diagnostic tool in urology, providing detailed images of the prostate gland and surrounding structures to aid in the diagnosis and management of various prostate-related conditions. It is used to calculate the volume of the gland and to detect pathology. TRUS also serves as a guide for biopsies (figure 13A). Biopsies can be targeted towards a specific lesion (targeted) or conducted on 10-12 standardised locations (systematic). In systematic biopsies, the focus is primarily on sampling the dorsal parts of the prostate. To enhance the precision of targeted biopsies, various fusion techniques, such as with MRI, can be employed. Cognitive fusion means the urologist localising the lesion on MRI and then, based on this information, determining approximately where the biopsy should be taken. Other more resource-intensive biopsy techniques include transperineal biopsies or MRI-guided biopsies, so-called in-bore biopsies. While these techniques have their advantages, they have not proven to be superior to simpler methods[102].

Magnetic resonance tomography

MRI is now a cornerstone in PCa diagnosis. It will be described more thoroughly separately in the thesis.

Histology

The Gleason grading system was developed by Donald F. Gleason in 1966[103] and is still used in a modified form for grading prostatic adenocarcinoma[104]. Gleason identified five different histological patterns, grades 1 to 5 (well-differentiated to anaplastic/poorly differentiated) (figure 12). Previously, the two most common patterns were indicated as a sum, ranging from 2 to 10. Since 2005, the score is reported by first specifying the most prevalent pattern followed by the pattern with the highest grade, possibly 3+4.

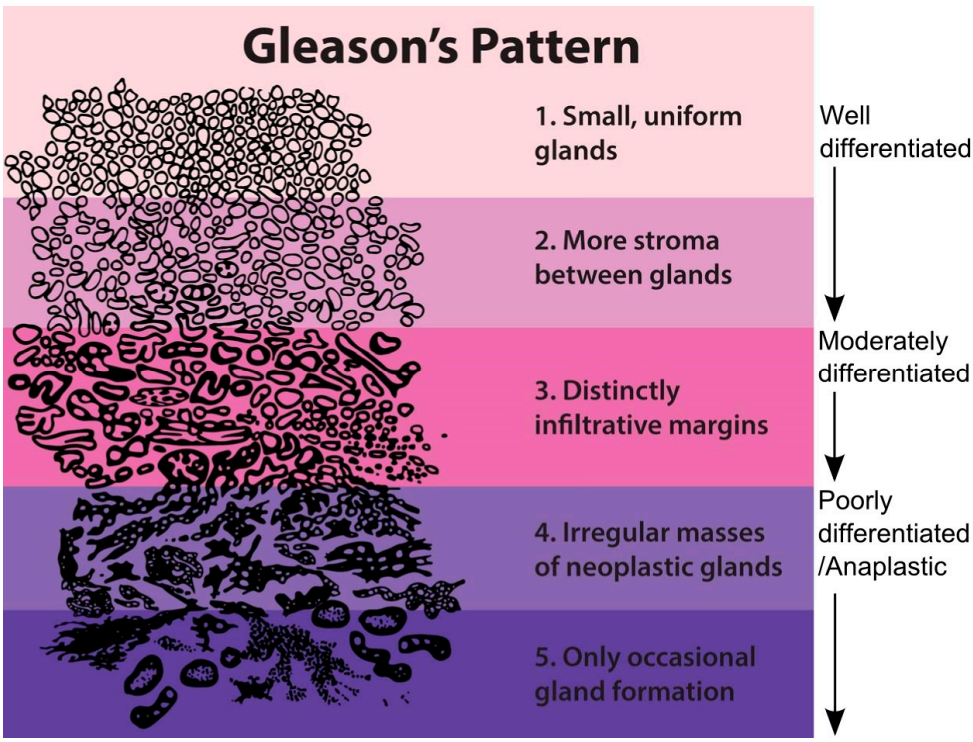

Figure 12
The Gleason grading system. Public Domain, https://commons.wikimedia.org/w/index.php?curid=440437

There is significant interobserver variability among pathologists[105, 106], which is troublesome as it affects risk assessment and treatment decisions. In 2014, the International Society of Urological Pathology (ISUP) agreed on a new grading system based on the Gleason Scores[107]. The different Gleason score combinations were grouped into five ISUP groups to provide a more straightforward and clinically relevant classification of cancer aggressiveness (table 1). The system helps patients and clinicians understand the severity of the disease and make informed treatment decisions.

Table 1
The International Society of Urological Pathology (ISUP) grade groups

ISUP Grade group	Gleason Score	Gleason Pattern
1	<6	<3+3
2	7	3+4
3	7	4+3
4	8	4+4, 3+5, 5+3
5	9 or 10	4+5, 5+4, 5+5

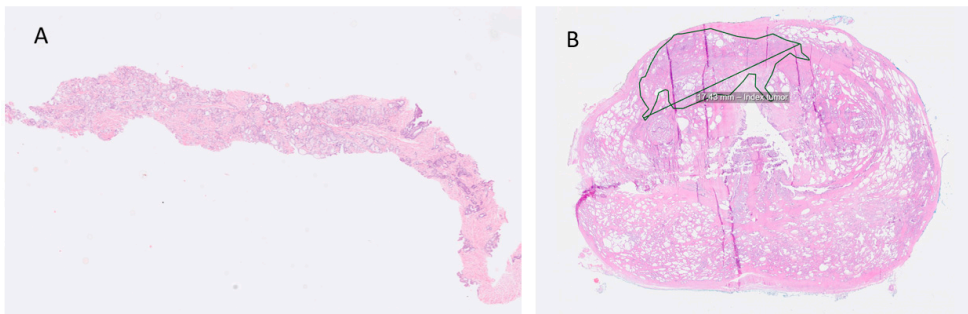

Figure 13
(A) TRUS 18G biopsy from the right anterior aspect of the TZ, Gleason 4+3 (ISUP 3). **(B)**. Whole mount surgical specimen from the same patient. Image courtesy Kevin Sandeman, Skåne University Hospital, Malmö. Department of Clinical Pathology.

Risk groups and treatment

The risk groups are divided into four categories: very low risk, low risk, intermediate risk, and high risk. These groups are based on PSA level, Gleason score, and cT stage. The cT stage is determined by the DRE according to the TNM 8 classification[88]. The choice of treatment depends on the risk group, possible metastases, patient wishes, symptoms, and remaining life expectancy. In short, treatment options include active surveillance, hormonal therapy, chemotherapy, radiotherapy, surgery, or combinations of these.

Magnetic resonance imaging

Background and routine use of MRI

In 1973, Paul L. Lauterbur and Sir Peter Mansfield were awarded the Nobel Prize for their discoveries in the field of magnetic resonance. The first MRI of the prostate was demonstrated and published by Steyn and Smith in 1982 (figure 14). Twenty-five patients were examined on a prototype 0.04-T scanner. They concluded that the images were comparable to first-generation CT scans[108].

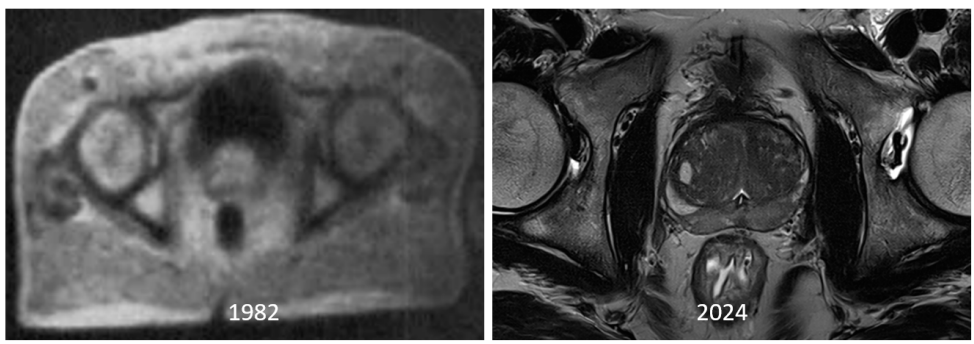

Figure 14.
The first MRI of a prostate from a 0.04T scanner from 1982[108]. Reprinted with permission from Wiley compared to a modern 3T T2W image from our clinical routine.

In addition to field strength, the image quality depends on the receiver coil. A review article in 2002 stated that endorectal coils improved staging performance[109]. Endorectal coils have been widely used, however, nowadays MRI is performed with external phased array body coils. Another passing trend was the use of MRI spectroscopy, a technique for chemical analysis and evaluation of the concentration of different metabolites such as citrate and choline[110]. The added value and specificity were low, and the technique has been abandoned in standard MRI imaging.

Today, there is a wide consensus about how to perform an MRI prostate examination. Imaging guidelines are based on prostate imaging reporting and data system (PI-RADS) version 2.1, developed by the American College of Radiology.

Multiparametric MRI (mpMRI) consist of T2-weighted (T2W), diffusion-weighted imaging (DWI), and dynamic T1-weighted sequences (DCE)[111].

An increasingly popular approach is to perform the examination without the use of a contrast agent, referred to as biparametric MRI (bpMRI), and it is now the predominant protocol in Sweden[88]. In addition to avoiding the administration of contrast, which requires intravenous access and elevates the risk of side effects, this approach significantly shortens the scan time and lowers the costs. Contrast-enhanced sequences are therefore reserved for specific circumstances, such as follow-up after focal therapy, where diffusion-weighted sequences cannot be performed, or in the presence of artefacts from metal, typically hip prostheses.

Sequences

T1-weighted imaging

T1-weighted imaging (T1W) is a term used in MRI to describe an imaging technique that provides contrast based on differences in the T1 relaxation time of tissues. The T1 relaxation time is related to the time it takes for the hydrogen protons connected to water in a tissue to realign with the external magnetic field after being disturbed. In prostate imaging, T1-weighted images are used to detect haemorrhage and delineate the borders of the prostate. The T1 property of the tissue can be enhanced by intravenous injection of a contrast medium, i.e. Gadolinium, and the procedure is then referred to as dynamic contrast enhancement (DCE). T1-weighted sequences are usually only obtained in the axial plane in prostate imaging.

T2-weighted imaging

T2-weighted imaging provides contrast based on the differences in the T2 relaxation time of tissues. The T2 relaxation time is related to the time it takes for the protons in a tissue to lose the transverse magnetisation component after being perturbed. Fluid has a high signal on T2-weighted imaging, hence, urine and cysts appear bright on these sequences. The PZ of a young man's prostate has a high density of glandular structures and is therefore also relatively bright on T2. In contrast, a prostate tumour is usually dark. In routine clinical prostate imaging, the sequence is obtained in at least two planes. It is used for detecting tumours in the TZ and for discerning the zonal anatomy, as well as to evaluate extraprostatic tumour growth (EPE) and seminal vesicle involvement (SVI).

Diffusion-weighted imaging

DWI imaging is a particularly important sequence in Prostatic MRI. Hence, it will be described in more detail in the following section.

Principles of diffusion

DWI exploits the random motion of water molecules. In a completely free environment, molecules move freely and randomly, which is known as Brownian motion or free diffusion. This phenomenon was named after the botanist Robert Brown, who observed the movement of plant spores immersed in water. In 1905 Einstein used the model when he tried to prove the existence of the atom[112, 113]

Within tissue, water molecules are influenced by various components such as cell membranes and organelles (figure 15A). Depending on tissue properties, such as cell density, this affects water molecules to varying extents. Tissues exhibiting this characteristic impeded diffusion, occurring in conditions such as tumours, abscesses, fibrosis, lymphatic tissue, and cytotoxic oedema[114].

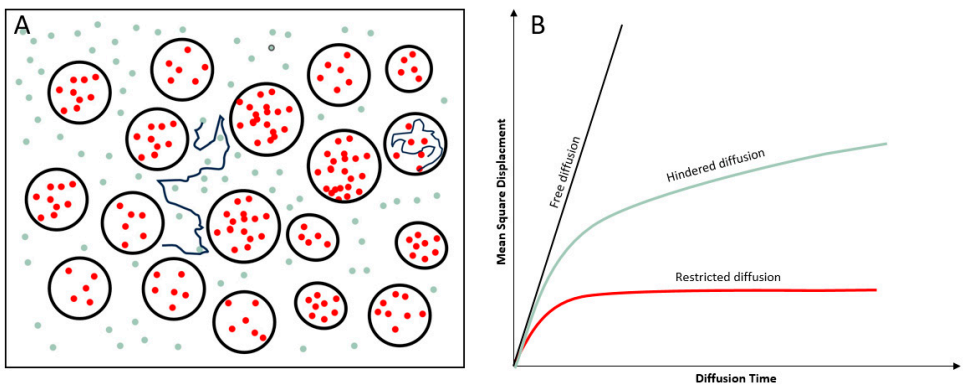

Figure. 15
(A) The image shows water molecules inside cells (red dots) and between cells (green dots). The movements of two molecules in respective locations are represented by the black traces. The water molecules between cells can travel far but are slowed down by obstacles; this is referred to as hindered diffusion. Water molecules that are trapped inside cells have a limited range of motion, hence, this is called restricted diffusion. Standard diffusion imaging cannot distinguish the two from each other, but both kinds are related to a lower apparent diffusion coefficient (ADC) compared to free diffusion. **(B)** Mean square displacement of particles that experience free diffusion (black line), hindered diffusion (blue line) and restricted diffusion (red line). Note that the lines are parallel at short diffusion times.

The mobility of water molecules can be described in the graph above (figure 15B). Initially, all water molecules move with equal ease, but after a few milliseconds, the surroundings exert varying degrees of influence.

Measurement of diffusion-weighted imaging

The most common DWI sequence is a spin echo with echo-planar imaging (EPI) readout. The spin echo is created by a 90° radiofrequency (RF) excitation pulse followed by a 180° RF refocusing pulse. The diffusion encoding is usually performed with two identical pulsed field gradients applied on either side of the refocusing pulse (figure 16).

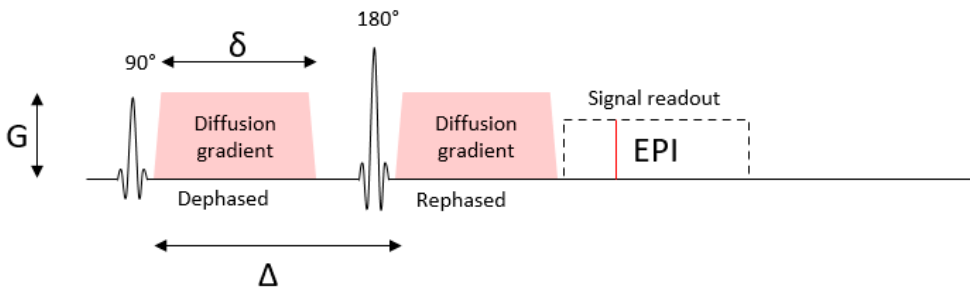

Figure 16.
The Diffusion Weighted Imaging (DWI) pulse sequence consists of two gradient pulses with a magnitude (G) and duration (δ) separated by a time (Δ). The gyromagnetic ratio (γ) varies by atomic species. For ^{1}H it is 42.58. The b-value can be calculated as $b = \gamma^2 G^2 \delta^2 (\Delta - \delta/3)$. Adapted from Szczepankiewicz, Filip[115].

The first gradient pulse induces a position-dependent phase shift for all spins within a voxel, and the second pulse restores the phase change. For stationary particles, the second gradient perfectly rewinds the phase shift created by the first gradient and the signal loss is minimal. This is the scenario, for instance, in a densely packed cellular environment with restricted diffusion. Conversely, in a tissue with relatively free diffusion, water molecules move a considerable distance during and between the two gradients, and the phase is not restored, i.e., not rephased. This results in signal attenuation that is proportional to the diffusivity of water molecules.

b-value

The b-value describes the strength of the diffusion weighting and is calculated from the gradient amplitude, duration, and time between gradients. The most common way to vary the b-value is by adjusting the gradient amplitude (figure 17).

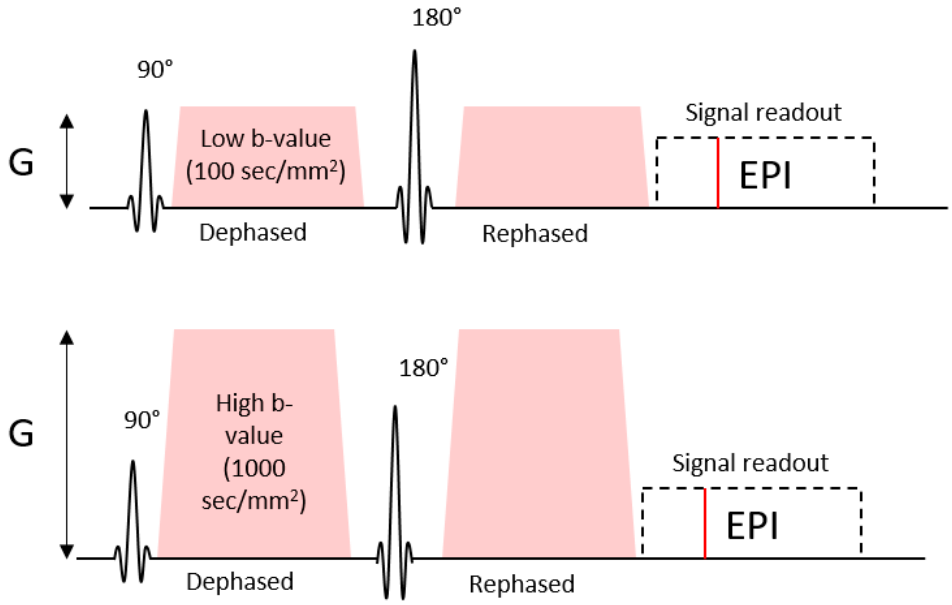

Figure. 17

Pulse sequences with high (top) and low (bottom) b-value. In this case, modulated by changing the amplitude of the diffusion gradient (G) and keeping the rest of the parameters unchanged. Adapted from Filip Szczepankiewicz[115].

A b-value of 0, indicates no gradient applied, and the image is a fat-saturated T2-weighted image, similar to magnetic resonance cholangiopancreatography. Since the movement of water molecules is restricted in dense cellular tissues, the signal loss will be less than the signal loss for water molecules in a tissue that allows more mobility. Thus, the signal loss will be lower for dense cellular tissues at high b-values compared to cell-poor tissues. However, it is important to note that there is always some signal loss at high b-values, but its magnitude varies depending on the extent of disruption caused by the gradient compared to the amount that has been restored by the second gradient.

Quantification of apparent diffusion coefficient

Diffusion-weighted imaging can be used to quantify the apparent diffusion coefficient (ADC). This is done by measuring the signal at multiple b-values and fitting an exponential function to the signal. This fit serves to estimate the non-diffusion-weighted signal as well as the diffusivity. To visualise how this works, we can plot the logarithm of the signal as a function of the b-value, in which the slope of the line will represent the diffusivity (Fig 18).

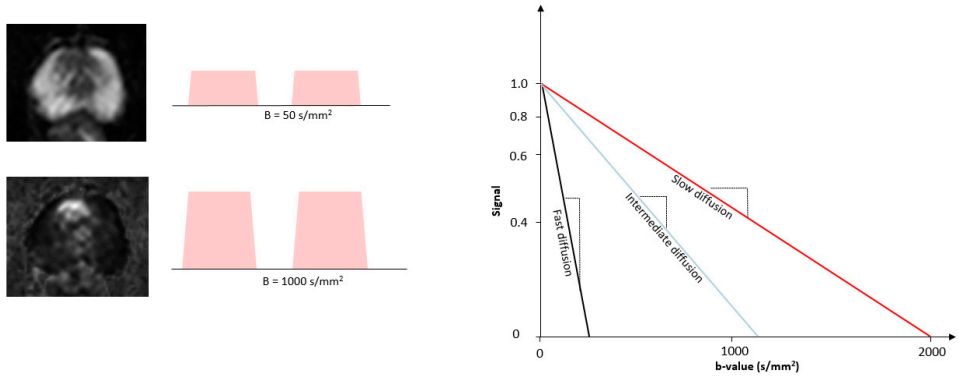

Figure 18
The slope of the curve represents the diffusivity (D) or apparent diffusion coefficient (ADC). This depends on how freely water molecules can move within the tissue. The maximum diffusivity at body temperature is 3000 μm²/s, and values close to this may be present in urine. Normal tissue in the prostate peripheral zone (PZ) ranges between 1300-1800 μm²/s, while a tumour in the PZ may have a diffusivity of 500-1000 μm²/s.

T2 shine through

In a tissue with long T2 in a T2W image, such as a cyst, the signal may be relatively high even at high b-values, despite the signal loss from diffusion gradients. One might be misled into thinking that the high signal indicates restricted diffusion. By comparing the signal at high and low b-values and calculating the ADC, a cyst will exhibit a high ADC, whereas a tumour would have a low ADC.

Which b-values should be used, and which should not

To calculate the ADC, a minimum of two unique b-values are required. To obtain representative values, these points should be widely spaced, for example, at b=100 s/mm² and b=800 s/mm². Additional intermediate b-values can be used, but they extend the examination time.

At low b-values, approximately b < 200 s/mm², there is interference from the motion of blood in the capillaries. The motion of capillary blood causes a fast reduction of the signal which can be mistaken for fast diffusion or cause an overestimation of the ADC. To avoid this, b-values less than 200 s/mm2 are not recommended. This phenomenon is known as Intravoxel Incoherent Motion (IVIM)[116] and can be exploited in situations where perfusion estimation in a tissue is desired (figure 19A).

At higher b-values, the diffusion-weighted signal is largely suppressed, leaving mostly noise in the signal. This noise is thereby relatively high compared to the remaining true signal. As noise becomes more prominent compared to the signal, the signal-to-noise ratio (SNR) decreases, in other words, there is low precision in the signal. Close to the noise floor, the accuracy of the signal deteriorates. A lower

SNR can affect the accuracy and reliability of ADC measurements, leading to increased variability in the calculated ADC values. This positive signal bias leads to an inaccurate, low ADC (figure 19b).

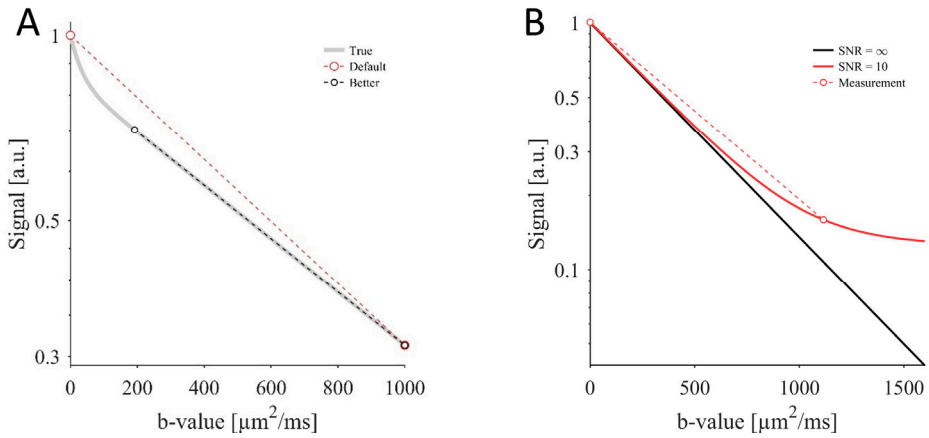

Figure 19
(A) The contribution of perfusion which gives an incorrect apparent diffusion coefficient (ADC) when using a b-value of zero. **(B)**The bias of using a high b-value. Courtesy of Filip Szczepankiewicz.

The role of MRI in the diagnosis of prostate cancer

Prostate cancer exhibits a spectrum ranging from benign, asymptomatic, low-grade tumours to highly aggressive ones. It is crucial, therefore, that diagnostic methods can accurately identify the tumours. Overdiagnosis of harmless tumours leads to unnecessary anxiety, investigations, treatments, and consequently, resource wastage. On the other hand, underdiagnosis results in the failure to detect and treat dangerous tumours in a timely manner. Therefore, diagnostic approaches need to be as specific as possible. This contrasts with many other tumour types, where early detection is generally beneficial.

In addition to previously discussed methods, more complex analyses, such as the Stockholm 3 test, have been introduced. This test combines biomarkers, genetic factors, and clinical variables with the aim of increasing specificity[117]. The traditional diagnostic pathway involved PSA, DRE, and subsequent biopsies. This approach led to both over- and under-diagnosis, especially as the ventral parts of the prostate could not be adequately examined. A more modern approach is the MRI pathway or MRI first strategy. In this approach, patients with suspected prostate cancer, often based on symptoms or elevated PSA levels, undergo an initial MRI. The results of this MRI, combined with other information, determine the subsequent

diagnostic pathway. The procedure, when presented in the PRECISION study[118] demonstrated the detection of more significant tumours and fewer insignificant tumours, with a reduction in the number of biopsies performed. Similar results were reported in a Cochrane review in 2019[119]. The findings from these and several other studies form the basis for current guidelines, both nationally and internationally, such as EAU-ESUR[88, 120].

PI-RADS

The requirements for a structured assessment of prostate MRI have increased. A structured system for the assessment and reporting of MRI has been developed by the American College of Radiology (ACR). The Prostate Imaging – Reporting and Data System (PI-RADS), first version, was published in 2012, and the latest version, PI-RADS 2.1, was published in 2019[111]. The document provides detailed guidelines on how the examination should be conducted, interpreted, and reported.

The assessment, resulting in a score between 1 and 5, indicates the likelihood of clinically significant cancer, i.e., cancer that potentially requires treatment (table 2).

Table 2.
PI-RADS v.2.1 Assessment Categories[111]

PI-RADS score	Likelihood	Description
PI-RADS 1	Very low	Clinically significant cancer is highly unlikely to be present
PI-RADS 2	Low	Clinically significant cancer is unlikely to be present
PI-RADS 3	Intermediate	The presence of clinically significant cancer is equivocal
PI-RADS 4	High	Clinically significant cancer is likely to be present
PI-RADS 5	Very high	Clinically significant cancer is highly likely to be present

Depending on whether the assessment pertains to a lesion in the PZ or TZ different parameters are weighted differently. In the PZ, DWI/ADC is crucial, while T2-weighted imaging is the most significant sequence in the TZ. The DWI/ADC scores are described in table 3. The description of DWI/ADC is subjective, and terms like ‘hyperintense’ or ‘markedly hyperintense’ are used without further specification. This poses the risk of individual and progressively shifting assessments.

Table 3
The role of DWI/ADC in the interpretation of Prostate MRI, ver. PI-RADS 2.1[111]

Score	Description
1	No abnormality (i.e., normal) on ADC and high b-value DWI
2	Linear/wedge-shaped hypointense on ADC and/or linear/wedge-shaped hyperintense on high b-value DWI
3	Focal (discrete and different from the background) hypointense on ADC and/or focal hyperintense on high b-value DWI; may be markedly hypointense on ADC or markedly hyperintense on high b-value DWI, but not both.
4	Focal markedly hypointense on ADC and markedly hyperintense on high b-value DWI; <1.5cm in greatest dimension
5	Same as 4 but ≥1.5cm in greatest dimension or definite extraprostatic extension/invasive behaviour

ADC threshold and ADC ratio

Based on knowledge of diffusion and ADC, it is understood that cell-dense tissues exhibit lower ADC values. Often, a more malignant tumour is denser in cellular composition than a less malignant one. This relationship is utilised in various contexts. In studies on liver metastases before and after neoadjuvant therapy, an increase in ADC value is considered a sign of tumour response. Cui et al. found a relationship between tumor response by size with increase in ADC[121] and Donati et al. found a linear correlation between tumour regression grade and ADC[122]. However, in a multicenter study, Eriksson et al. did not find any significant correlation between TRG and ADC[123].

In prostate diagnostics, ADC values are employed to differentiate between PI-RADS 3 and PI-RADS 4/5. Many radiologists have developed an intuitive sense for when a value is pathological on their scanner.

Several studies in the field have attempted to identify a threshold value, and although consensus is lacking, ACR in PI-RADS version 2.1 suggests 750-900 μm²/sec for lesions in the PZ. It is noted, however, that there is a significant overlap with other conditions. In a review based on 1633 patients, the pooled mean was 1100 μm²/sec for Gleason 5 and 6 (ISUP 1) and 860 μm²/sec for Gleason ≥7. They proposed 750 μm²/sec as a threshold for significant cancer[124].

Several technical factors influence the ADC value, such as the b-values used, the method for calculating ADC, scanner field strength, and patient characteristics[125]. When examining images from different centres, it is evident that ADC varies considerably between different scanners and hospitals. However, a Danish study on ADC values in phantoms on different scanners showed robust ADC values[126].

In an attempt to normalise potential differences between various conditions that might affect the ADC value, different types of ratios have been used. Calculating the ratio of ADC values between lesions and adjacent tissues could yield a more comparable value. Several studies suggest that this is better than absolute ADC values, while

others show the opposite. However, Woo et al. suggest that errors are added rather than normalised[127]. For example, they state that even healthy prostate tissue can vary among individuals, especially due to age, and hence, is an unreliable dominator in the equation. DeCobelli et al. are on a similar track, suggesting that seemingly healthy prostate tissue may be influenced by tumour infiltration and fibrosis[128].

In Paper III of this thesis, we investigate these relationships in a study that includes MRI scanners from different vendors, different field strengths, and different protocols[125].

PSA density and prostate volume

The PSA level in blood is proportional to the volume of the prostate. A benign enlarged prostate produces more PSA than a benign small prostate. Hence, an elevated PSA does not always mean malignancy. To overcome this, the PSA density (PSAD) is used. It is calculated as a ratio between PSA (µg/l) and the prostate volume (mm^3)[88, 129]. Different cut-offs are used, usually 0.10 or 0.15 ng/mL^2. A higher value raises the suspicion of cancer.

The volume of the prostate can be obtained by different methods. From TRUS or MRI three orthogonal diameters can be measured. The ellipsoid formula is calculated by multiplication of length x width x depth x π/6. This method comes with a high degree of variation. It is challenging to find the correct positions of the measurements, especially in the apex which can be difficult to delineate. The method does not consider an asymmetry of the gland and there is no consensus on how to include the median lobe in volume. A more accurate but much more time-consuming method is manual planimetry (segmentation), used primarily for radiotherapy planning and for targeted fusion biopsies[130]. The border of the prostate is delineated on transverse MRI images, every 3-5 mm. Software reformats the areas to a 3D volume (figure 20). In recent years, more automated AI-assisted software has become available for the purpose. Paper IV in this thesis evaluates a deep learning-based system for volume assessment of prostate volume on MRI[131].

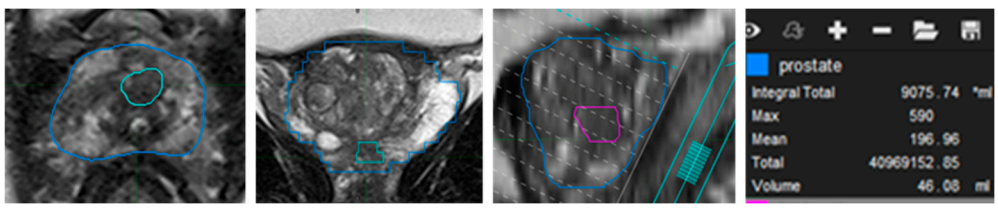

Fig 20.
The borders of the prostate are contoured manually on axial images (blue), in this case, a suspicious tumour is also contoured (turquoise). The software builds a coronal and a sagittal as well as a 3D reconstruction (not shown). These can be used for targeted fusion biopsies. The volume is also presented by the software. Image courtesy of Kjartan Thorarinsson, Skåne University Hospital, Malmö, Sweden.

Artificial intelligence and prostate MRI

Artificial means not natural, i.e., it is not biological. A fundamental aspect of intelligence is the ability to learn from experience and thereby develop one's thinking. In essence, AI is a constructed system that takes in information, identifies it, makes decisions, and learns from experience.

A way to visualise the mutual relationship and hierarchy of different fields of AI is presented in figure 21 and will be discussed further in this chapter.

A typical computer program processes information based on rules programmed by humans. A regular computer program solves the task but does not gain experience. AI constructs its own rules based on the information it handles and can improve its results by adjusting the rules. This is achieved through machine learning.

Previously, different systems were specific to each task, but this is changing with neural networks. A distinction arises when AI can transfer knowledge from one task to another.

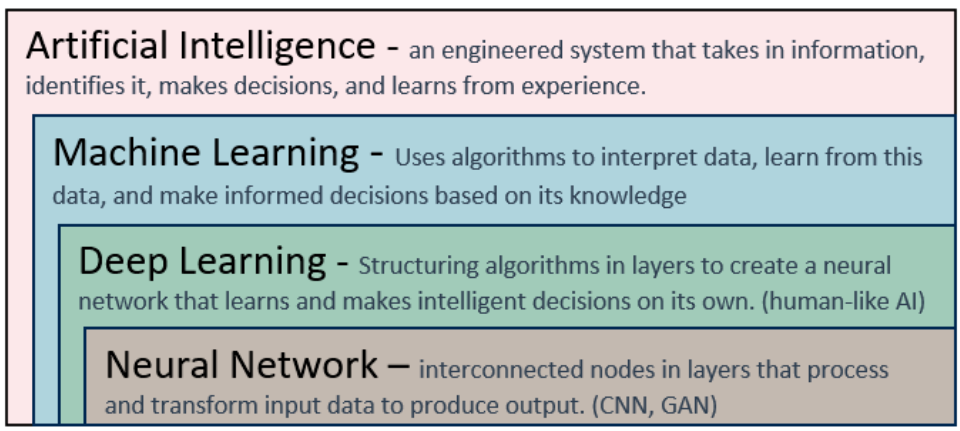

Figure 21
The relationship of the main concepts in AI. Source: Author.

Machine learning

Machine learning is divided into three main categories: supervised, unsupervised and reinforcement learning[132]. Supervised learning is the most common type in medical imaging research, humans act as guides, teaching the algorithm what conclusions it should reach. Data needs to be labelled with ground truth from human experts. Unsupervised learning is what one might call classical AI. The concept relates to computer learning on its own without human guidance. An example of this is generative learning. The third category, reinforcement learning involves the system learning through feedback from humans, with correct conclusions being reinforced while incorrect ones are suppressed[130, 133].

Neural network

The old self-regulating AI systems were long considered superior to neural networks, and it was believed that the idea of networks worked best in theory. However, thanks to new algorithms, larger volumes of training data, and more computational power, neural networks have taken the lead. Just like the neurons in the brain, the smallest components of the neural network handle a simple function, but when interconnected with billions of other neurons, it can manage highly complex tasks. Neural networks, like other AI systems, create their own rules through machine learning. What is revolutionary about neural networks is not only their ability to handle even more complex information than previous AI systems but also that the same system can be trained for various tasks.

A neural network consists of three layers: an input layer, a hidden layer, and an output layer. A deep neural network consists of two or more hidden layers (figure 22). The more layers, the higher the capability to handle complex tasks. A neural network is usually referred to as a black box; we observe how information flows, but we do not comprehend what is happening inside the box. However, we can discern the relationship between the information the network receives and what it produces. A common application of deep neural networks is pattern recognition, employed, for example, in radiology. The key to the system's high performance is its ability to break down complex patterns into a series of simpler patterns.

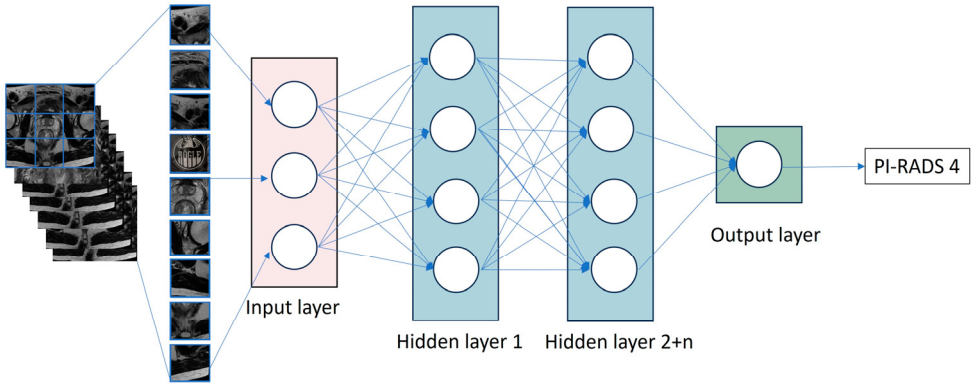

Figure. 22
A deep neural network consists of two or more hidden layers. The more layers, the higher the ability to handle complex tasks. Source: Author.

AI in radiology

In radiology and deep learning, primarily two types of networks are used: Convolutional neural networks (CNN) and generative adversarial networks (GAN) (figure 21). The structures of the two are different, and so are their applications. To some extent, they go hand in hand. GAN consists of two neural networks that can be based on different architectures. Understanding the nuanced differences between CNNs and GANs is crucial for leveraging their combined potential effectively in radiology applications.

Convolutional neural networks

Convolution is a mathematical operation that involves combining two functions to create a third. In this context, it means applying filters on the input data to extract various patterns from the image or data. These filters are used to identify features that may be useful for solving the current problem, such as edges, shapes, or textures in an image. Examples of applications include image classification, object detection, and segmentation.

Analysing an MRI image of the prostate to assign a PI-RADS score is a step-by-step process that is a typical application for CNNs, as described in figure 23. The process involves, in brief, preprocessing the images from the MRI scanner (orange part) so that desired images are available and spatially consistent with each other. This step also includes segmenting the prostate from the rest of the image. The segmented area then undergoes further analysis. Next, processing occurs in the CNN (turquoise part). First, a candidate heatmap is generated, representing what the

network perceives as abnormal, which may also include false positive changes. This can serve as initial guidance for the radiologist to identify potential pathology areas. Then, in the subsequent step, a sub-volume-based false positive reduction network operates by eliminating false positives. Finally, another sub-volume-based scoring network assigns the PI-RADS categories.

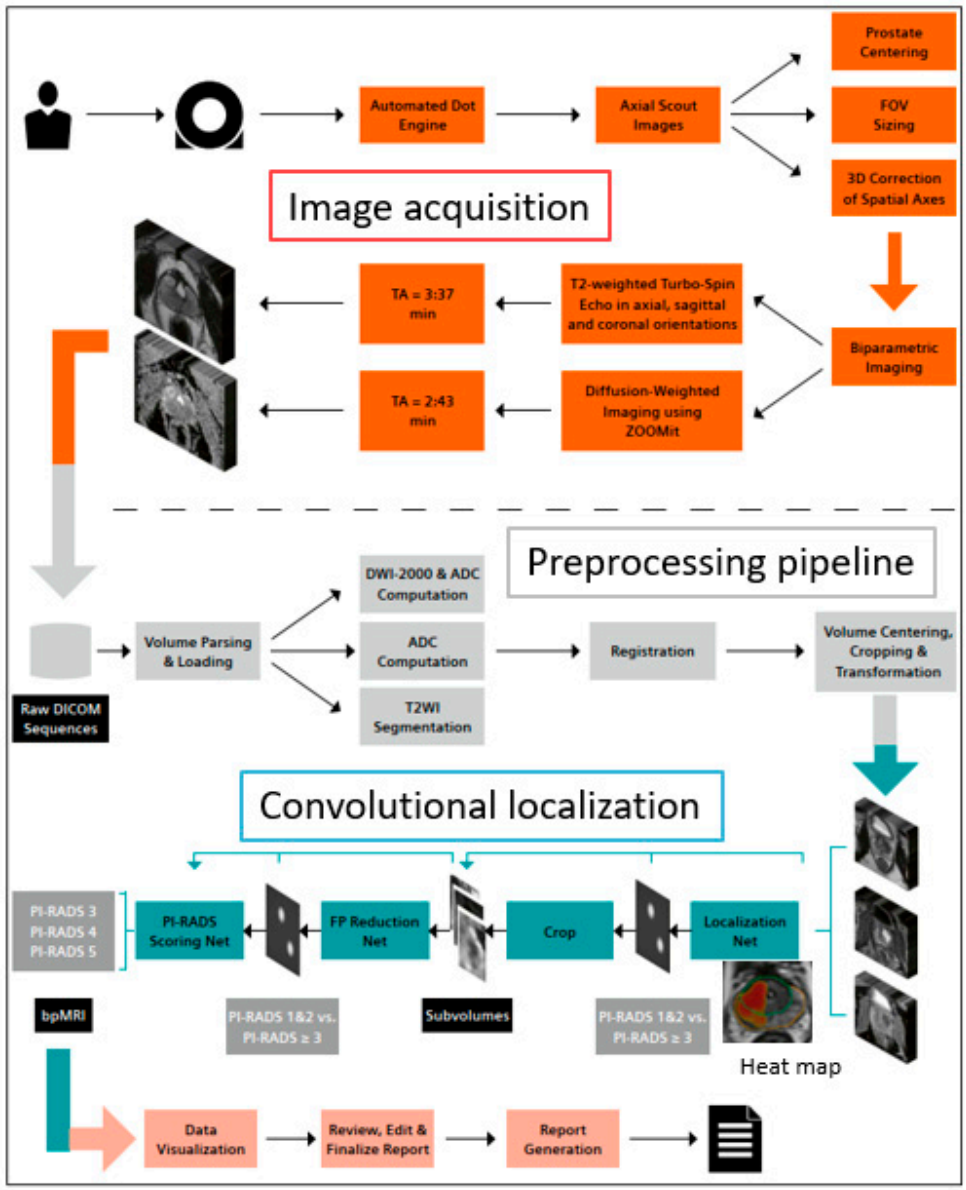

Figure 23.
The workflow from image acquisition to generated report. Adapted from Siemens Healthcare[134].

Generative adversarial networks

GAN consists of two neural networks that are trained by competing against each other. In radiology, GAN is used for various purposes, including image enhancement, such as improving contrast or reducing noise in images. Thanks to GAN, lower radiation doses can be used in CT scans, and MRI scan times can be shortened. GAN can also generate images that can be used to train CNNs.

GAN consists of two components, or neural networks: a generator, which generates an image that resembles a real image, and a discriminator, which receives images from the generator as well as real images from reality. The generator aims to create as realistic images as possible to deceive the discriminator, which in turn strives to become better and better by learning to classify each image as either real or created by the generator. During training, the two networks compete against each other (adversarial) and thus push each other to improve. Eventually, when GAN has been trained for a sufficient period, the generator can produce data that is so realistic that it is difficult to distinguish it from real data[135]. This process can be likened to a counterfeiting operation becoming more skilled as the police become better at distinguishing counterfeit bills from genuine ones.

Training and validation of machine learning

For AI to perform well, neural networks must be trained for specific tasks. During training, the CNN model is fed with a large number of examples of data along with their corresponding labels or classifications. The model adjusts its internal parameters gradually. The more varied and representative training data used, the better the model becomes at generalising and handling new, unseen data correctly.

Training data should be representative of the conditions the model is expected to encounter during usage, and it is important that it covers the relevant domain for the problem the model is intended to solve. If the training data lacks diversity of examples, the algorithm may become biased.

Developers of AI algorithms therefore strive to obtain quality-controlled datasets, which can be obtained from medical databases, open datasets, or through collaboration with clinical institutions. When validating an algorithm, it is crucial that the training data is separated from the test data. Otherwise, there is a risk that the algorithm will “memorise” the specific test cases, leading to an overestimation of its performance.

Most commercial AI models are locked once they have been trained by the developer and reach the market, but some models use continuous feedback systems to continually improve. This can occur through user feedback, but also through the integration of various databases such as patient records and treatment summaries.

Before AI models reach the market, it is crucial that they undergo validation. This can be done in various ways. Commonly, studies compare them with previously unseen data to investigate whether their performance allows for generalizability across new data and different populations.

To perform validation of an AI model, access to ground truth or a reference standard, also known as a gold standard, is essential. This ground truth or gold standard represents the most reliable and accurate information about what the AI model is trying to predict or identify.

In the case of medical image analysis, such as MRI prostate diagnostics, the gold standard could be an expert assessment by a radiologist. This expert evaluation is considered the "truth" against which the model is compared during validation.

Certification

Software that may impact patient outcomes is considered a medical device and needs to conform to certain safety standards. The CE mark indicates conformity to those standards and allows the sale and clinical use of the product within Europe. There are different classes from low risk (class I) to high risk (class III), i.e. the same classes as for other medical devices, e.g. embolisation materials. Class I can be obtained through self-certifications whereas class II requires an external audit by a notified body. Since May 2021 the MDR have come into effect and have replaced the former Medical Devices Directive (MDD). Products marked under the former MDD may be sold until May 2024, if not expired or major changes have been made to the product. Software for clinical use is classified by the FDA in a similar manner; most software for medical devices is class IIb according to the MDR and class II according to the FDA[136].

Leeuwen et al. have listed all commercially available software products for medical imaging in a database[136, 137]. For every software product, the scientific papers evaluating the algorithm are listed. Every paper is scored based on the Fryback and Thornbury Efficacy table (model of efficacy) [138]. A paper which is scored grade I demonstrates the technical efficacy, which basically demonstrates whether the software product does what it is supposed to do. The highest grade is 6 and is given to a paper that demonstrates that the software product has an impact on society with economic analysis. Papers given a score of 5 demonstrate the software's impact on patient outcomes (table 4).

Table 4
Hierarchical model of efficacy to assess the contribution of AI software to the diagnostic imaging process, adapted from Fryback and Thornbury (1991)[136, 138]

	Explanation	Typical measures
Level 1t	Technical efficacy	Reproducibility, inter software agreement, error rate
Level 1c	Potential clinical efficacy	Correlation to alternative methods, potential predictive value
Level 2	Diagnostic accuracy efficacy	Standalone sensitivity, specificity, AUC (ROC), Dice score
Level 3	Diagnostic thinking efficacy	Radiologist performance with/without AI, change in judgement
Level 4	Therapeutic efficacy	Effect on treatment or follow-up examinations
Level 5	Patient outcome efficacy	Effect on QoL, morbidity, or survival
Level 6	Societal efficacy	Effect on costs and quality-adjusted life years.

To date, six AI software products for prostate MRI have been CE marked and three are FDA-approved. No software product has been subject to published peer-reviewed papers showing a level of efficacy more than grade 4 (Table 5). In 2021, the level of efficacy for 239 peer-reviewed publications for the 100 CE marked AI software products of the entire field of radiology only found four papers showing efficacy level 6 and nine publications of level 5. The latter were all conducted on the same software for cardiac imaging. Less than half of the publications were made independent from the vendors and almost all were retrospective in study design. More than two-thirds of the publications were single-centre studies.

Table 5
The six current CE- and FDA-approved AI software products for prostate MRI. The total number of peer-reviewed papers for each software product and their level of efficacy[137]. (*) Refers to paper IV in this thesis.

Vendor	CE (MDR)	FDA	Peer-reviewed papers	Efficacy (evidence) level 1 t/c	2	3	4	5	6
Deephealth (Saige prostate)	IIb	II	4		1	2	1		
JLK Inc (JPC-01K)	I (MDD)	-	0						
Lucida Medical (Prostate Intelligence)	IIb	-	0						
Mediaire (medprostate)	IIb	-	0						
Quibim (QP-Prostate)	IIb	II	1		1				
Siemens Healthineers (AI-Rad companion prostate)	IIb	II	3		1	2*			

Material and methods

Statistical methods used in the papers.

Chi-2 test and Fisher's exact test

The chi-square test or Fisher's exact test can be used to determine whether there is a significant association between categorical variables. The latter is particularly useful when the sample size is small and the assumptions required for the chi-square test are not met (e.g., expected cell frequencies are less than five). In paper II, Fisher's exact test was used for evaluating whether recanalisation occurred or not for the two different spheres[139].

T-test

A t-test is used to determine if there is a significant difference between the means of two groups. The data should be normally distributed, especially for a small sample size, with fewer than 30 observations per group. An independent samples t-test is used to determine if the means of two independent groups differ from each other, for example, to find if the weight loss is different in two groups that had different treatments. A paired samples t-test is used on one group tested twice. For example, if there is weight loss before and after a treatment. The t-test provides a p-value. If the p-value is less than a chosen significance level (commonly 0.05), then the null hypothesis is rejected, suggesting that there is a significant difference between the groups. Independent and paired T-tests are used in paper II to evaluate the differences between the groups. A paired t-test was used in paper IV to compare the mean differences between measurements made by experienced and inexperienced radiologists.

Spearman's rank correlation coefficient

Spearman's rank correlation coefficient (denoted by ρ or r_s) quantifies the strength of association between two variables. The Spearman correlation is utilised for nonparametric variables that may not vary linearly with each other, whereas a similar test, Pearson correlation, is used for two continuous variables that vary linearly with each other. Spearman, which employs a ranking of variables, is thus

less sensitive to outliers. Spearman is more suitable for ordinal data (i.e., ordinal variables like Gleason Score or PI-RADS). The coefficient is reported between -1 and 1, where -1 and 1 indicate perfect correlation, while 0 signifies a completely random distribution with no correlation between variables. Negative values indicate an inverse correlation. In paper 3, this method was employed to assess the correlation between ISUP grading groups and ADC metrics.

ICC

The Intraclass Correlation Coefficient (ICC) is a statistical metric utilised to evaluate the consistency or reliability of measurements taken by multiple raters. It assesses the level of agreement among different raters or between repeated measurements by the same rater. ICC proves particularly valuable when dealing with continuous or ordinal data. Its values range from 0 to 1, with higher values indicating stronger agreement or reliability among raters. Interpretation of ICC values can vary depending on the study's context; however, typically, values above 0.75 are deemed excellent, values falling between 0.40 and 0.75 denote fair to good agreement, and values below 0.40 suggest poor agreement (Koo, 2016). ICC serves for assessing interrater reliability, which represents the variation between two or more raters conducting the same measurements. Moreover, different types of ICC exist, such as test-retest reliability and intra-rater reliability. There are approximately ten different methods to compute ICC, contingent upon the type of data and the number of raters involved.

In summary, ICC is employed to evaluate interrater reliability (ranging from 0 to 1) and should not be confused with Spearman's Rank Correlation Coefficient (for nonparametric variables) and Pearson's Correlation Coefficient (for parametric variables), both of which quantify the association between variables (-1 to +1). In paper 3, ICC was used to assess interrater reliability for ADC values, while in paper 4, it was employed for evaluating prostate volume using the ellipsoid formula.

Bland-Altman plot

A Bland-Altman plot, like ICC, is used to assess the agreement between two measurements or methods. While ICC gives a value for the agreement, Bland-Altman gives a graphical visualisation of the agreement (figure 24). It is a graphical method that plots the difference between the two measurements against their mean value. A central line represents the mean of the differences between the two measurements and thus indicates if there is any systematic error (bias) between them. If the line lies close to or on zero, it indicates that there is little to no systematic difference between the measurements. Often, 95% limits of agreement (average difference ± 1.95 standard deviations of the difference) are provided as upper and lower horizontal lines. These are also referred to as lines of critical difference.

A symmetrical spread near the central line suggests good agreement, while values far from the central line indicate poorer agreement. Values that tend to deviate more from the central line as they increase suggest that measurement error increases with larger values.

In papers 3 and 4, Bland-Altman plots are utilised to visualise measurements of ADC and prostate volume between readers or methods.

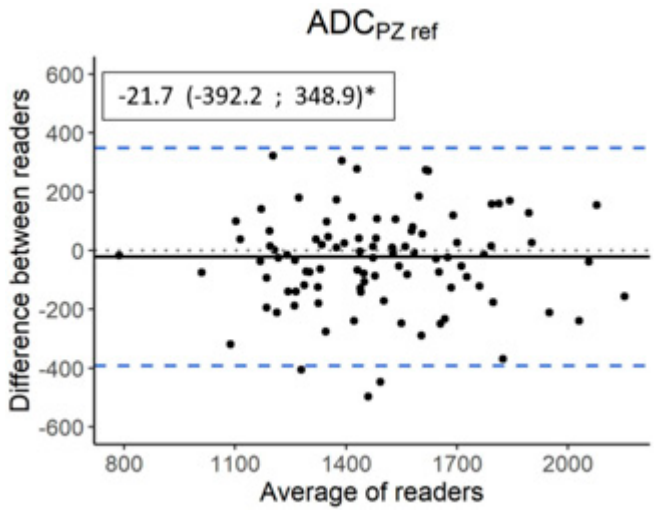

Figure 24.
Bland-Altman plot. The black horizontal line is the mean of differences (central line) which is close to the zero line (black dotted line), hence there is no systematic error. Measurements between the blue lines are within 98% CI. The values of the three lines are noted in the square. Source: Author.

Receiver operating characteristic curves

A receiver operating characteristic (ROC) curve is a graphical plot illustrating the diagnostic ability of a binary classification system as its discrimination threshold is varied. It is commonly used in binary classification to evaluate the performance of a classifier by plotting the true positive rate (sensitivity) against the false positive rate (1 – specificity) at different threshold values (figure 25).

Put simply, the ROC curve shows how well a test can determine whether a patient has a disease (e.g., clinically significant prostate cancer) or not. A perfect test would have an ROC curve passing through the upper left corner, indicating high sensitivity (true positive rate) and a low false positive rate across all threshold values. Conversely, a test with no ability to distinguish between diseased and healthy individuals would have an ROC curve resembling the diagonal line (45-degree line), indicating random guessing.

The area under the ROC curve (AUC) is often used as a summary measure of a test's performance, where values closer to 1 indicate better performance and values around 0.5 indicate performance no better than random guessing (figure 25).

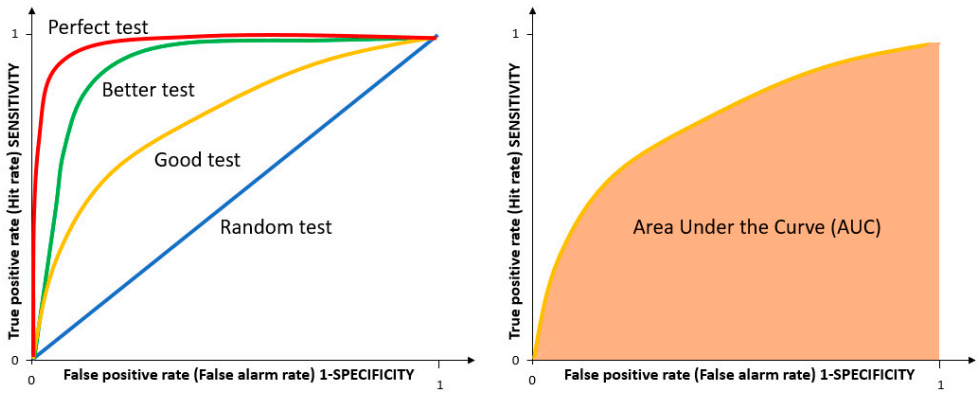

Figure. 25.
Example of a receiver operating characteristic (ROC) curve. The curve plots the true positive rate against the false positive rate at each threshold setting. The area under the curve (AUC) is a measure of test performance. A value closer to 1 indicates better performance and a value around 0.5 indicates performance no better than chance. Source: Author.

ROC curves were used in paper 3 to evaluate how well ADC metrics performed in distinguishing between clinically significant and insignificant prostate cancer.

Cohorts and study design

Paper I

The study was a feasibility study. Seven adult Texel female sheep were used. The ewes were aged five to six years, and all had previous pregnancies. They were housed under strict conditions according to regulations for animals in research.

Unilateral embolisation of the uterine artery was performed, and a follow-up angiography was done at different time intervals (0-65 hours later) for each animal followed by euthanisation. The degree of occlusion and recanalisation was assigned a number between 0-4 according to an adapted Emboscore (table 6).

Paper II

The study was a blinded randomised controlled trial (RCT). Twenty-two Texel female sheep were used. They were aged 4-6 years and had a history of pregnancies. Body weight was 54 to 82 kg. They were divided into a study group and a control group. They were housed under conditions regulated by the authorities and had a free supply of food and water. The experimental animals were under the supervision of laboratory animal caretakers and a veterinarian. Between the two interventions they returned to the nearby pen. Before the radiological interventions started, the ewes were artificially cycled. On day -15, 20 mg flugestone acetate (Chronogest®) sponge was inserted into the vagina. The animals were transferred to the laboratory on day -3. On day -1, 500 IE gonadotropin (Folligon®) was administered with an intramuscular injection.

All radiological procedures were performed under general anaesthesia.

On day 0 angiography followed by unilateral embolisation of the uterus was performed. None of the interventionists or other present staff knew if the study sphere or control sphere had been used. The two different spheres had the same macroscopic appearance. On day 14 another angiography was performed, and the degree of recanalisation was assessed by Emboscore. Thereafter, the animals were euthanised and different organs were collected and fixed in formalin for macroscopic and histopathological analyses which were performed by a pathologist, certified by the European College of Veterinary Pathology. The euthanasia was performed while the animals were still under anaesthesia with an overdose of iv pentobarbital.

Papers III and IV

Both studies were retrospective multicentre studies. The cohort consisted of men that underwent Robot-Assisted Laparoscopic Prostatectomy (RALP) in Malmö, Sweden, in 2018 with an MRI of the prostate within one year prior to the surgery (figure 26).

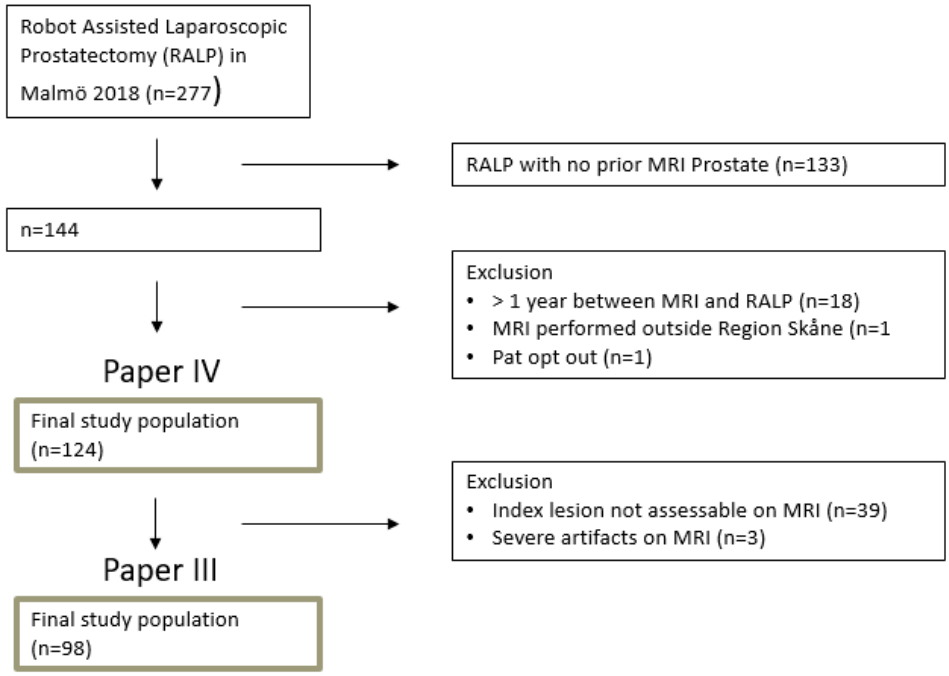

Figure 26.
Cohorts for papers III and IV. Source: Author.

In paper III the largest tumour per patient was selected and designated as the index tumour. ADC measurements were performed of the index tumour, of the corresponding contralateral region, of the normal PZ, and of the urine by two experienced radiologists independently (figure 27).

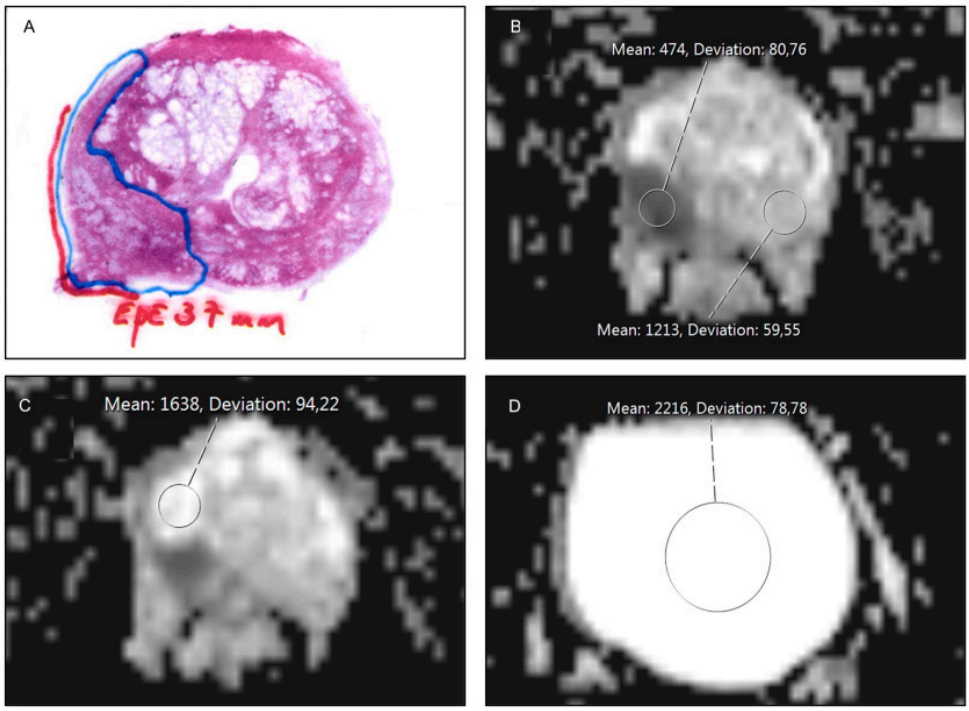

Figure 27
Tumour map from a pathology specimen and placement of ROIs in the ADC map from Paper III. **(A)** Tumour map with a large tumour in the right peripheral zone (blue border) with a 37 mm extraprostatic extension (red line). **(B)**, Circular ROI in the tumour and in contralateral non-tumorous tissue. **(C)**, Circular ROI drawn in non-tumorous PZ and **(D)**, circular ROI in the urinary bladder. Source. Author[125]

In paper IV the volume of the prostate was measured with eight different methods, of which two were used as reference standards: manual planimetry by an experienced radiologist on MRI (MPE) and weight volume of the surgically removed specimen (SW). The other six methods used were ellipsoid formula performed by two radiologists on MRI (EF1, EF2) and by a urologist on TRUS (TRUS), by inexperienced radiologist MRI planimetry (MPU), by ellipsoid formula on the surgically removed specimen (SD) and finally by an AI model on MRI (DL). The AI model was a proprietary available product (AI-Rad Companion Prostate MR VVA20A_HF02, Siemens Healthcare AG). The algorithm had not previously been exposed on the dataset.

Ethics

Approvals

Papers 1 and 2

The experiments were approved by the Animal Ethics Committee in Lund/Malmö with reference number M339-12.

The study was conducted in compliance with the principles of Good Laboratory Practice Standards as outlined in the OECD Principles of Good Laboratory Practice (as revised in 1997), ENV/MC/CHEM(1998)17 (OECD 1998). This study complied with all applicable sections of the Act and the associated Codes of Practice for the Housing and Care of Animals used in Scientific Procedures and the Humane Killing of Animals under Schedule 1 of the Act, issued under section 21 of the Act[140].

The number of animals used was the minimum consistent with scientific integrity and regulatory acceptability. Consideration was given to the welfare of individual animals in terms of the number and extent of procedures carried out on each animal.

The rationale for using sheep as a research animal is twofold. Firstly, the vascular anatomy of the uterus is similar to that in humans[53]. Secondly, the blood level of α-amylase, which degrades the degradable starch microsphere (DSM), is similar to that in humans. Additionally, the sheep uterus is bicornuate, meaning that its contralateral side is not affected by the embolisation and can therefore be used as a reference.

Papers 3 and 4

The local ethics review committee at Lund University approved the studies in Papers I-III (entry no. 2014-886). The Swedish Ethical Review Authority approved an addendum for Papers I-III (entry no. 2019-03674) and also approved the study in Paper IV (2020-03923 and 2021-06647-02).

Research on animals

In Sweden, animal experiments are primarily regulated by the Animal Welfare Act (Djurskyddslagen) and the Animal Welfare Ordinance (Djurskyddsförordningen)[141]. These laws establish guidelines for the use of animals in research and experiments to ensure their welfare and minimise suffering. In addition, there are ethical principles and guidelines that researchers must follow when applying for permits to conduct animal experiments.

3R

The 3R concept was introduced by William Russell and Rex Burch in 1957[142]. Today, the 3R principles are embodied in both Swedish and European legislation for using animals in research. Consequently, anyone who uses animals for scientific purposes must implement the 3Rs in their work. The 3R stands for Replace, Reduce, and Refine.

Replace refers to experiments that can replace live animals with alternative methods that do not involve using live animals, such as computer modelling, artificial organs, or cell cultures.

Reduce refers to experiments where the same knowledge and quality of data can be achieved by using fewer research animals than before. It can also mean obtaining more information from the same animal without increasing their suffering.

Refine means ensuring laboratory animals experience as little pain, suffering, discomfort, and anxiety as possible compared to previous similar studies. Refine also implies improving animal welfare and providing laboratory animals with a better quality of life through measures such as enriched environment and larger spaces.

Ethical aspects of the studies

In papers I and II we applied all three 3R aspects. Alternatives to animal studies were considered, however, no other way to answer the endpoints was found. The number of animals needed for achieving a useful result was also taken into consideration; a smaller number would likely have led to non-significant results. A larger number would have been unnecessary for the stated endpoints. As far as we could see, the animals did not suffer during the trial and all interventions were performed to minimise suffering. It is however an undeniable fact that the trial was performed at the cost of the life of the sheep. Unfortunately, as far as we know, the development of this sphere did not proceed beyond our two studies. This might be considered as a failure and as indicating potentially unnecessary use and suffering of the animals. However, the knowledge gained from the studies will contribute to the research field.

Both papers III and IV were retrospective cohort studies. Participants were offered the opportunity of opting out, which one man did. All patient data were protected and anonymised during the whole process and no individual data was pointed out, nor did we find any incidental findings or other concerning findings in the images.

AI in general and in medical imaging in particular requires several ethical considerations. The complexity of AI models, such as deep learning networks, often hinders the interpretability of their decision-making processes. This lack of transparency poses challenges for both patients and clinicians in understanding how

the AI arrives at a particular diagnosis or treatment recommendation. Establishing methods to make AI systems more interpretable and providing transparent explanations for their outputs is crucial to gain trust and acceptance from the medical community. Privacy and data security also raise ethical dilemmas in the context of AI in prostate MRI. Patient data used for training AI algorithms must be anonymised and adequately protected to maintain confidentiality. Additionally, obtaining informed consent from patients for the use of their data is essential. Furthermore, the impact of AI on the role of healthcare professionals requires careful consideration. While AI can assist radiologists in detecting abnormalities and making accurate diagnoses, there is concern about the potential displacement of radiologists' expertise and the loss of the human touch in patient care. Ensuring that AI is used as a supportive tool, augmenting healthcare professionals' skills rather than replacing them, is important. The impact of the AI-delivered output on the radiologist is not negligible, this is called automation bias and must be taken into consideration when developing a workflow which combines machine learning with manual assessment. By proactively addressing these issues, we can harness the potential of AI to improve diagnostic accuracy and patient outcomes while upholding ethical principles and standards in healthcare.

In the context of using AI algorithms for objective data analysis, such as segmentation for volume assessment, the downsides are negligible, and the time saved for the radiologist is of great value.

Results

Paper I

Seven sheep were included in the study. However, the first sheep died during the introduction of anaesthesia, and the second could not undergo embolisation due to an intimal dissection of the uterine artery. The remaining five ewes successfully underwent embolisation with DSM 500-700µm and achieved a post-embolisation Emboscore of 3, which was in line with the intended intervention (figure 28A, B).

Table 6.
Emboscore, adapted from Stampfl et al.[143]

Emboscore	Description
0	No angiographically visible signs of occlusion
1	Reduction of parenchymal staining of the dependent territory
2	Reduction of parenchymal staining and occlusion of the supplying artery
3	Reduction of parenchymal staining and occlusion of the supplying artery and occlusion of the feeding artery downstream of the catheter-tip
4	Overembolization (embolization of the adjacent branches)

During the observation period, no signs of malaise or discomfort were noted. Follow-up angiography (figure 28C) was performed at 19, 20, 28, 49, and 65 hours. Partial recanalisation was noted in three of the animals. Spheres were found at the intended locations along with vasculitis and inflammation and necrosis of the target organs (figure 29B). The DSM showed different stages of degradation (figure 29A), but no conclusion could be made regarding degradation time in vivo.

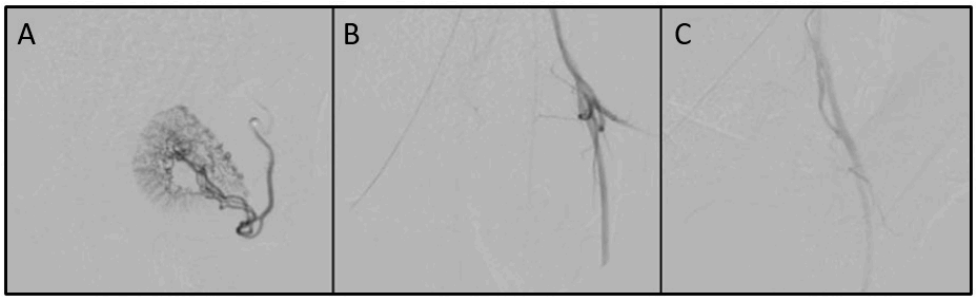

Figure 28
Angiogram before **(A)**, immediately after embolisation **(B)** and at follow-up **(C)**. Emboscore 3, hence no recanalisation. Source: Author. Reprinted with permission from Acta Radiologica, Sage Publications Inc[10].

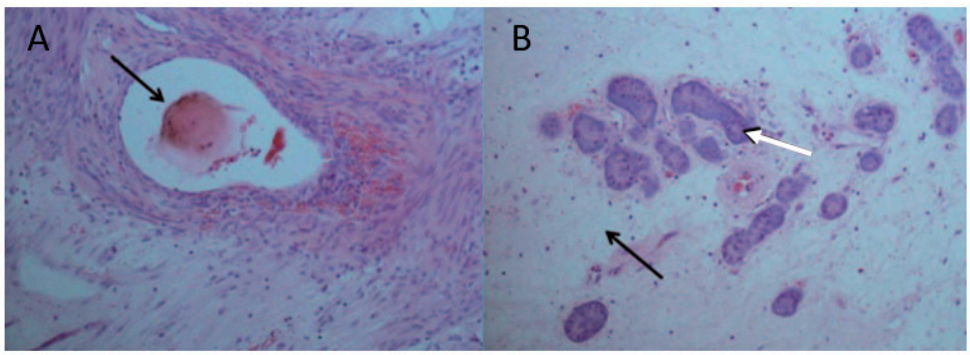

Figure 29.
Histopathological specimen, haematoxylin and eosin stain. **(A)** shows a partly degraded DSM (degradable starch microsphere) (arrow) in the artery lumen. Surrounding necrotising inflammation with presence of neutrophils. **(B)** Endometrium of the embolised side 65 hours post-intervention. Severe oedema in the interstitial tissue (black arrow) and the uterine glands are necrotic (white arrow). Source: Author. Reprinted with permission from Acta Radiologica, Sage Publications Inc[10].

No histological changes were found in other examined organs (ovaries, liver kidney, spleen, and skeletal muscle). However, PAS-positive material was found in the Kupffer cells of the liver and macrophages in the red pulp of the spleen in all animals, except for the one that could not be embolised.

Macroscopic evaluation revealed swelling and discolouration on the embolised side, but not on the contralateral side (fig 30). The ovaries were not affected on either side. A small battery of blood samples was collected before and after embolisation, as well as before follow-up. A significant rise in aspartate aminotransferase levels was noted, with a somewhat less pronounced increase in alanine aminotransferase.

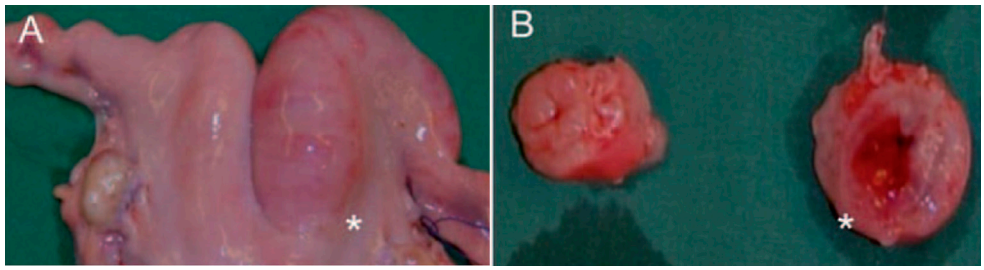

Figure 30.
Macroscopic photo of the uterus **(A)**; note that the embolised side (*) is swollen and reddish. **(B)** Transverse pieces of the right and left uterine horn of the same uterus show bleeding in the lumen and swelling of the tissue. Source: Author. Reprinted with permission from Acta Radiologica, Sage Publications Inc[10].

Conclusion

The study proves that embolisation can be performed with the new DSM and that degradation occurs *in vivo*. This allows for recanalisation and possible restoration of blood flow to the target organ.

Paper II

Eleven ewes were successfully embolised with the study sphere (DSM) and 11 with the control sphere (TGMS) until complete stasis was achieved, in keeping with Emboscore 3. No difference in procedure time, volume of spheres, or adverse events between the groups was noted. Follow-up angiography after two weeks was successful in all animals and showed recanalisation in nine of 11 animals in the DSM group and in two of 11 in the TGMS group (figure 31).

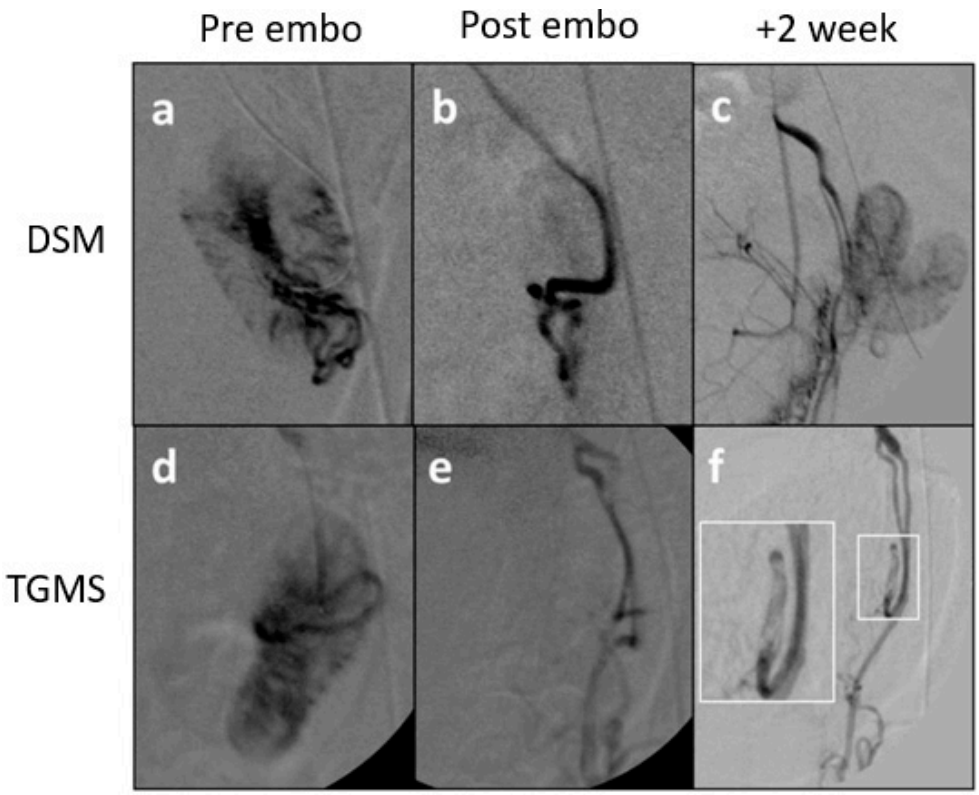

Figure 31.
Digital subtraction angiography of one sheep in each group with evidence of recanalisation in the degradable starch microsphere (DSM) specimen **(c)** but not in the trisacryl gelatine microspheres (TGMS) **(f)** at follow-up. Source: Author. Reprinted with permission from Acta Radiologica, Sage Publications Inc[144].

On postmortem palpation during surgical removal of organs, the uterine arteries were hard and enlarged on the embolised side in the TGMS group (figure 32 a,b). In contrast, they were smooth and had a similar appearance compared to the contralateral side in 10 of 11 animals in the DSM group (figure 32 c,d).

Histopathological examination revealed degraded spheres in two out of 11 animals in the DSM group, while intact spheres were found in all animals in the TGMS group. Peripheral vascular changes were more pronounced in the TGMS group but were also present in both groups. In the TGMS group, the changes were characterised by chronic, foreign body type inflammation centred around the spheres, resulting in complete obstruction of the lumen. In the DSM group, the inflammation was mild to moderate, and sub-intimal loose connective tissue caused a mild narrowing of the lumen.

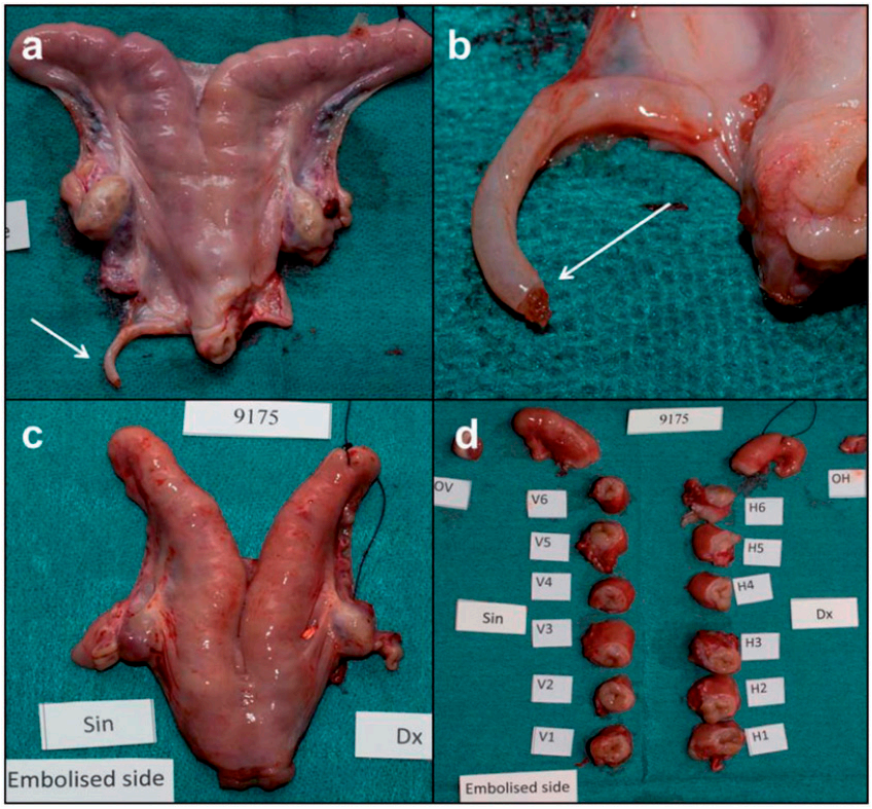

Figure 32.
(a, b). Uterus from ewe in the trisacryl gelatine microspheres group and **(c, d)** from the degradable starch microsphere group. No macroscopical differences were noted between the two. However, the uterine arteries were indurated in the TGMS group and spheres were visible. Source: Author. Reprinted with permission from Acta Radiologica, Sage Publications Inc[144].

The reactions in the endometrium were similar in both groups with fibrosis and endometrial atrophy, which were not found on the non-embolised side.

A large battery of blood samples was collected, and only AST and ALT showed changes 24 hours after embolisation. However, there was no difference between the groups. At follow-up, all tests were back to normal. It is worth mentioning that the mean weight loss in the DSM group was 2.9 kg, compared to 1.5 kg in the TGMS group during the two-week period. However, this difference was not significant. No signs of discomfort were noted apart from this.

Statistics

The statistics reported in the original paper were limited and some additional analyses follow.

The number of recanalised objects in the two different groups (two of 11 in the TGMS group and nine of 11 in the DSM group) were analysed with Fisher´s exact test. There was a significant difference between the groups ($p<0.01$).

The weight loss in the DSM group of 2.9 kg was statistically significant ($p<0.05$) but not the weight loss of 1.5 kg in the TGMS group. The mean weight loss between the groups was not statistically significant. These analyses were performed with t-tests.

There was no difference in the volume of spheres needed to achieve complete statis of the uterine arteries between the groups. Nor were there any differences in the clinical chemistry blood samples.

The number of research objects needed to get significant power was estimated to be ten in each group. There was one spare object in each group in case of a failed intervention. A smaller number, for example six objects in each group, would have been too small to find a significant difference between the two groups if one object differed from the other five in the group. Hence the estimation of 22 animals was reasonable.

Conclusion

Embolisation with DSM achieved similar tissue effects as TGMS in the target organ; however, it resulted in less vascular inflammation and a higher degree of recanalisation. There was no difference in adverse events.

Paper III

The cohort consisted of 98 men who had undergone RALP with an MRI of the prostate one year prior to the surgery. All men had PCa, ISUP 2 or higher. The agreement in the ADC measurements between the two radiologists was nearly perfect, with an ICC of 0.8 for the tumour, 0.82 for the contralateral region, 0.96 for urine, and substantial for the normal PZ, ICC = 0.75. The measurements were visualised in a Bland-Altman plot, and no systematic errors were detected.

The majority (69.4%) of the index tumours were located in the PZ, while the remaining (30.6%) were in the TZ. 61.2% of the patients were examined using a 3T scanner, and the remaining 38.8% were examined using a 1.5T scanner. A total of eight different scanners were utilised.

The mean value of ADC for malignancy was significantly lower than that for healthy prostate tissue. However, no correlation was observed between absolute ADC values or different ADC ratios (ADC of tumour relative to healthy contralateral area, healthy PZ, or urine) in relation to ISUP grade. Additionally, no correlation was found based on localisation in the PZ or TZ, or examination at 1.5T or 3T. This is visualised in a box-and-whisker plot, Fig 33. In an ROC curve, an AUC close to 0.5 was noted for the method's ability to distinguish ISUP 2 from ISUP 3-5, suggesting it is no better than chance.

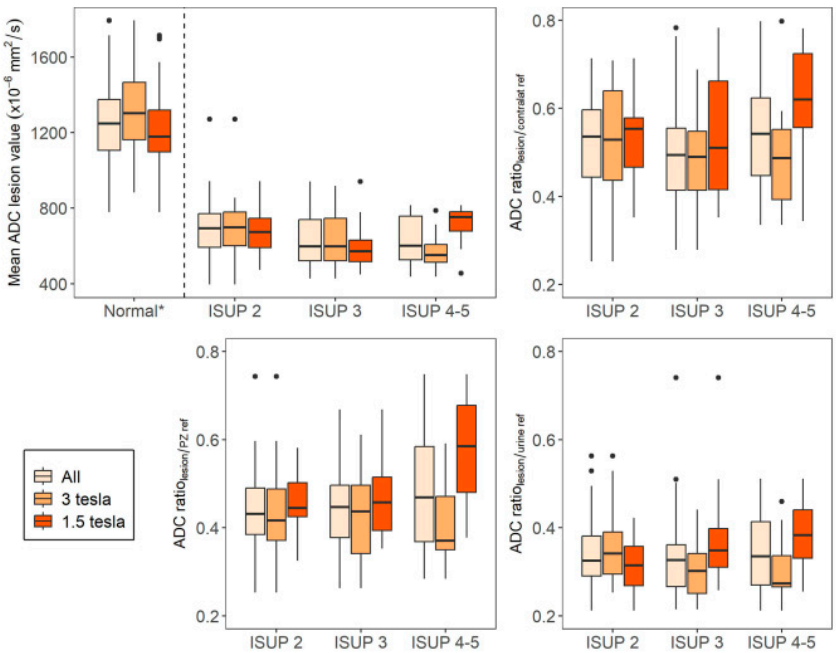

Figure 33
Box-and-whisker plots of apparent diffusion coefficient (ADC) metrics for tumours stratified by ISUP grade. (*) Normal represents the absolute ADC value of the normal-appearing tissue in the contralateral position of the index lesion. Source: Author[125]

Conclusion

In contrast to previous research in the field, we found no correlation between ADC metrics and ISUP grade in this multicentre, multi-scanner retrospective study. However, the agreement between readers regarding ADC values was good to excellent.

Paper IV

The initial cohort was the same as in paper 3. However, due to other requirements, the number of excluded patients was smaller (figure 26) The final cohort consisted of 124 patients who had undergone RALP with an MRI of the prostate within one year prior to the surgery. The same eight scanners described in paper III were used. Compared to SW as the reference standard, the mean difference and limits of agreement were lower for DL than for EF1 and EF2, indicating higher accuracy for DL (figure 34). There was a tendency for DL and EF to underestimate the volume of large prostate volumes (figure 34). The ICC between the EF1 and EF2 was excellent (0.95).

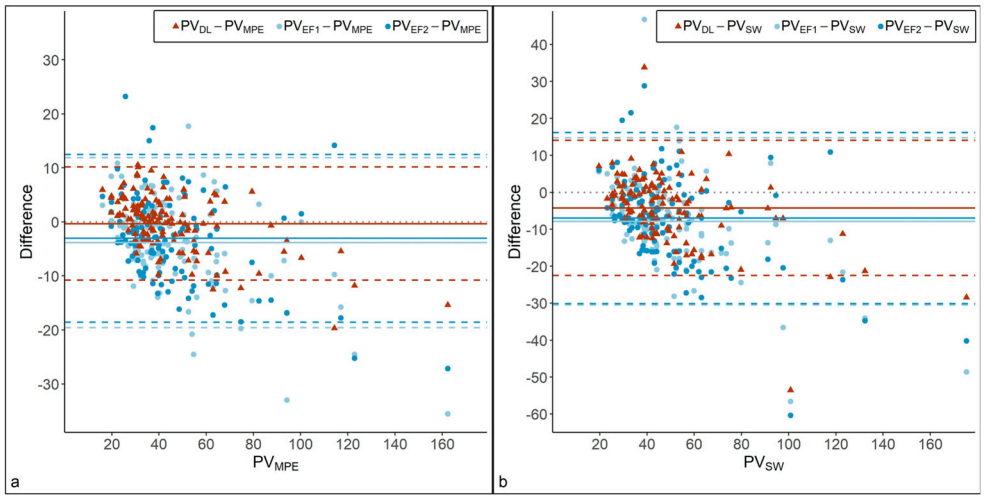

Figure 34.
Bland-Altman plots comparing **(a)** expert manual planimetry (MPE) as reference standard with Deep learning (DL) and MRI Ellipsoid formula (EF1 and EF2). In **(b)** the volume based on specimen weight (SW) serves as a reference standard and is compared to the same methods as in (a), DL, EF1 and EF2. The dotted blue line is the zero line, and the solid lines show the mean difference for each pair. The dashed lines represent the limits of agreement, mean difference ± 1.96DS. The closer the solid lines are to the zero line the more accurate the method, and the smaller the distance between the upper and lower dashed lines the more consistent the measurements. Source: Author[131].

Conclusion

A deep learning algorithm is at least as good as manual methods based on images for assessing prostate volume.

Discussion

Papers I and II

The purpose of the first two papers was to evaluate whether the new DSM could be used for embolisation and, if so, how well it performed compared to the market-leading sphere, TGMS. The main endpoints were of radiological and histopathological character. Secondary endpoints were toxicological, product safety, and usability and have not been included in the papers.

Smaller DSM (50 μm) from the same supplier has been commercially available for many years; hence, the material itself has been tested and approved for toxicology. Nevertheless, the new size of the spheres and the new intended indications require new documentation and trials for medical device registration.

Our conclusions were that the spheres caused an ischaemic effect and that degradation *in vivo* occurred. However, the exact time for restoration of blood flow is unknown and could not be estimated more accurately than between three days and two weeks. We do not know which degradation time is optimal, and it is probably different for different purposes. To get a more exact estimation of the degradation time a much larger set of research animals would be needed, which would be euthanised at different time intervals from embolisation. Another method would be repeated angiographies or contrast-enhanced MRI.

Similar studies on degradable spheres have been performed. The intended degradation time varies from less than an hour up to six months. There is no proof that degradable materials entail any benefits. However, several possible advantages have been proposed by us and other authors[12, 18, 145]. The most common statement is that once the goal of embolisation has been reached, the material is no longer needed. We also know that a few hours of ischaemia are enough to irreversibly harm most tissues. This is the most often used theoretical rationale for why degradable materials should be as good as permanent materials. Maclean evaluated the UFE results of six different embolisation materials, for example TGMS, PVA and a new gelatine-based bioresorbable calibrated sphere (Gel-Bead) which degrades in 12 weeks. Gel-Bead had similar outcomes in terms of fibroid infarction[146].

Foreign materials cause tissue reactions, often chronic. Some materials are more inert, like stents and replaced joints, and cause less inflammation, while others cause more aggressive inflammation.

Another advantage of degradable material is that it minimises the expression of VEGF which is induced by ischaemia. Elevated VEGF in plasma has been shown to persist for up to one month after prolonged ischaemia following embolisation. A rise was noted even with fast degrading microspheres but at lower levels than with permanent material[147]. Up-regulation of VEGF plasma levels after TACE has been shown to be a negative prognostic factor, not only for tumour response rate but also for progression-free survival, being associated with a higher incidence of local tumour recurrence and distant metastases[148]. Furthermore, it may be responsible for a more aggressive HCC behaviour leading to infiltrative or metastatic change and for the development of collateral tumour feeders, inducing TACE resistance[149].

In PAE, repeated interventions are less likely to be performed, and such patients are less likely to express concern about a permanent material. When it comes to young women who might consider embolisation for their uterine fibroid, the psychological aspect of having a permanent material injected might be a reason to choose alternative treatments. We know from research that pregnancy-associated complications occur more frequently in women who get pregnant post-UFE. One reason that has been proposed is impaired vascular regulation because of the bilateral occluded uterine arteries. The recruited anastomotic vessels do not have the same ability to adapt to the new higher demand for blood flow required during pregnancy. Therefore, a degradable biocompatible, calibrated sphere could be the perfect device of choice in these cases; however, this is yet to be proved[146]. So far, though, it has not been shown that there is a correlation between occluded or impaired uterine arteries and fertility issues.

Strengths and weaknesses of the studies

The design of these two studies demonstrates suitability for the intended endpoints, although certain enhancements could have been implemented. The statistical analysis presented in the papers is limited, with a more comprehensive statistical report available in the non-public Preclinical report. Supplementary statistical data for Paper II has been included within the results chapter of this thesis. It should be noted that the Emboscore, as a qualitative variable, lacks objectivity, thus an objective quantification of blood flow would be preferable. In Paper II, conducting an additional angiography within the two-week interval would have provided a more accurate estimate of degradation time and restoration of blood flow. Furthermore, including a larger number of study subjects would yield insights into the acute and chronic development of inflammation and perfusion, along with the ability to investigate the effects of using spheres of different sizes. The use of repeated contrast-enhanced MRI could also be considered to assess the progression of ischaemia and restoration of blood flow. Unfortunately, an animal model enabling embolisation under pathological conditions is currently unavailable. However, with the results from the conducted studies, in conjunction with prior toxicology and

safety studies, the subsequent step should involve human studies, preferably employing blinded randomised controlled trials combined with MRI.

Several strengths of these studies should be acknowledged. Despite the seemingly simplistic design of the initial study (paper I), it yielded significant knowledge and successfully addressed the stated endpoints. The occurrence of an unintended failed embolisation in one sheep provided an ideal control subject. The design of the second study was notably well-constructed in various aspects. All individuals involved in the study groups were blinded until the completion of all analyses. The interventions and associated analyses exhibited a high success rate. The animals did not appear to experience significant suffering. The stated endpoints were adequately addressed. Moreover, the findings of these studies offer opportunities for future advancements and research of the DSM.

Paper III

In clinical routines, radiologists use ADC values with different cut-offs. A commonly used argument for this is that they consider themselves calibrated to their specific scanner. Another commonly used application is to perform a cognitive calibration of a specific scanner or study by drawing a region of interest for ADC in the urine or muscular tissue, and with the help of this value, correcting the value of the tumour.

Möller et al. evaluated the variability of ADC measurements across different vendors and MRI protocols on a phantom and found no clinically relevant differences[126]. This is not in line with our results. A stratified analysis of the ADC values of the urine in our dataset varied from $1200 – 3300 \times 10^{-6}$ mm^2/s. Prostate and tumour tissue had a smaller, but considerable variation as well.

Since most previous studies were conducted under relatively uniform conditions, we wanted to perform a study with patient data from various hospitals, examined with different scanners and sequences, hence under heterogeneous and realistic conditions.

Our results indicate that the method is entirely random with an AUC close to 0.5 for distinguishing ISUP (1-)2 from ISUP 3-5. The truth likely lies somewhere between our results and others. Some methodological weaknesses in our material should be mentioned. The number of subjects was relatively small, so some stratifications contained only a few patients and could not be analysed separately. In addition, the material did not include patients with ISUP 1, which would have added extra weight to the ISUP 1-2 group in the statistics. ISUP 1 is usually defined as low-grade tumours and the patients are usually treated with active surveillance, according to most treatment guidelines[88], did not undergo RALP.

In the compilation of scanning parameters, it emerged that several scanners used b-values that were incorrect and resulted in incorrect ADC values. Using the ratio technique is considered by many as a way for erroneous variables to cancel each other out, but this is unlikely to be the case. Earlier in the thesis, it is described that errors are rather increased, adding further noise to the data, resulting in even more uncertain values. There is a mathematical relationship that describes how errors increase when making a ratio between two measurements. This concept is often referred to as error propagation or uncertainty propagation and can be approximated by using a formula. For example, if both measurements have an error of 50%, the uncertainty in the resulting ratio will be around 70% of the ratio's value[150, 151]. This is probably the main rationale for why the application of the ratio or normalising ADC does not work.

Despite this, the use of the ADC ratio has been shown to be useful by some authors[152-155], while others did not see any additional value in it[127, 156].

Krauss et al. were able to show that completely different variables such as PI-RADS and PSA/PSAD could predict the risk of csPCa with an AUC of 0.80 – 0.82, and no additional value in adding radiomics-based information ADC information[157].

Our conclusion is that ADC values should be used with caution in the assessment of prostate cancer and that the ADC ratio does not add any value.

Paper IV

Previous studies have evaluated the assessment of prostate volume using experimental deep learning algorithms against various reference standards, yielding results consistent with our studies[130, 131, 158-163]. Strengths of our study were its distinct approach, where we evaluated a commercially available AI model on diversified multicentre MRI data without pre-adjustment, and that all 124 prostates could be assessed by the software.

Previous studies have used various statistical methods for correlation[130, 159] and overlay measures[158, 160]. We emphasised Bland-Altman plots because we believe that the method comparison was better visualised with this measure by showing all data points. Despite our attempts to mimic a real clinical situation, our dataset has its limitations, as there was a dominant manufacturer in our health region and some of the participating centres were numerically dominant in terms of the number of prostate MRIs performed.

It is well established that there is variation between different readers, and we highlight this from several perspectives. We demonstrated slightly lower agreement between experienced and inexperienced radiologists performing manual planimetry, but the precision remained good. We showed good agreement between two

experienced radiologists using the ellipsoid formula measure, in line with previous studies[164, 165].

An important but time-consuming step in the assessment of prostate MRI is volume calculation, which is the basis for PSAD, which in turn forms the basis for further workup and treatment. Our results can contribute to better understanding of how AI models can be integrated into the workflow for efficient patient selection and better utilisation of radiology resources. We feel that we are confident in using the volume tools in our daily workflow.

Conclusions

In conclusion, our study showcases the efficacy of embolisation using the new DSM, offering potential for recanalisation and improved blood flow restoration. Moreover, embolisation with DSM demonstrates comparable tissue effects to TGMS, with fewer vascular inflammations and enhanced recanalisation. Our findings also challenge previous assumptions by revealing no correlation between ADC metrics and ISUP grade, while affirming the reliability of deep learning algorithms for prostate volume assessment. These insights underscore the evolving landscape of interventional procedures and imaging techniques which will shape future clinical practices.

Future perspectives

The development of embolisation materials continues at an unabated pace. Since we commenced our trials with DSM, numerous calibrated spheres have emerged in the market. Further advancements have been made towards the creation of the ideal sphere, with many studies focusing on the smaller variant of our sphere, now also produced as drug-eluting beads for HCC treatment. For many indications, I believe that bioabsorbable spheres will dominate in the future, especially in oncological conditions where the ischaemic effect needs to be combined with the effect of local cytostatic drug. I also hope to see studies on uterine embolisation using bioabsorbable spheres, assessing if they will result in fewer adverse effects on future pregnancies compared to permanent materials. Presumably, PAE for benign prostatic hyperplasia will continue to be performed using permanent spheres. At our institution, we are setting up a trial for comparing degradable with permanent spheres in DEB-TACE for HCC.

Local treatment of prostate cancer now includes cryotherapy and HIFU, both of which will soon be available at Skåne University Hospital. Initially, treatment will be conducted within the framework of studies, with MRI being central to radiological follow-up. Some studies have been published regarding the treatment of prostate cancer using drug-eluting beads for PAE, generating interest at our institution in initiating a similar study. Progress is also being made in prostate cancer diagnosis using MRI, with new machine-learning applications emerging at a high rate. It is evident that assistance with contouring for volumetric determination works well and can already be used clinically. Several software suites also make diagnostic assessments with high sensitivity. However, specificity remains generally low, and improvements are needed, specifically in prostate diagnostics.

There is a wealth of hidden information in our MRI images, and valuable information can be extracted. Significant progress is likely to be made soon, and I am pleased that our clinic has an AI department to enable our participation and to benefit from developments in this field. Our colleagues in the MRI Physics Group at the Department of Medical Radiation Physics of Lund University are running several studies. One project focuses on functional MRI diagnostics and histopathology. Other projects utilise advanced diffusion methods that incorporate, for example, IVIM for the assessment of perfusion and hypoxia. Another novel method is diffusional variance decomposition (DIVIDE) which employs non-

conventional diffusion encoding to provide considerably more information about the examined tissue than simply measuring ADC[166].

The diagnostic accuracy of new imaging techniques requires validation, preferably by histopathological verification. In collaboration with Sandgren et al[167] we are setting up a study in which the fresh surgical prostate specimen will be placed in a tailor-made mold for *ex vivo* MRI which will enable perfect matching with the subsequent histology and the preoperative *in vivo* MRI and hence allowing us to evaluate the accuracy of new MRI sequences.

In conclusion, there is a substantial amount of information to be obtained from MRI technology beyond what is currently utilised in clinical routine. With the assistance of these projects, we can move a step closer to MRI-based biomarkers and non-invasive MRI-based histology. With continued enhancements in diagnostic accuracy, we anticipate further decrease in unnecessary biopsies and overdiagnosis, coupled with better early detection and treatment of aggressive prostate cancer.

I am grateful for the opportunity to be involved in this exciting development.

Acknowledgements

Jag vill uttrycka min tacksamhet till alla er som hjälpt mig på vägen under mina doktorandstudier, både professionellt och personligt.

Min huvudhandledare, *Pia Sundgren* som under många år tålmodigt stöttat mig och alltid lyssnat på mig. Tack för att du ställt lagom mycket krav, du har fingertoppskänsla. Det tog sina år, men nu är det snart gjort.

Sophia Zackrisson, min bihandledare som anslöt när min forskning ändrade inriktning. Tack, du har verkligen en stor del i det här till slut gick vägen. Tänk att du till och med hälsade på mig i Sydney!

Inger Keussen, min vän och handledare under första halvan av det här arbetet. Jag vet hur mycket tid och engagemang du gav mig. Vilken tur att den där stolpen i Tokyo var vadderad!

Min rumskompis och handledare, *Erik Baubeta-Fridh*. Tack för att du anslöt till mitt team, din snabba hjärna och dina kreativa tankar har varit till stor hjälp. Jag ser fram emot fortsatt forskning tillsammans.

Despina Flondell-Sité, urolog och handledare. Din energi och entusiasm är underbar. Tack för hjälp med alla kliniska data och goda idéer.

Wojciech Cwikiel, du förtjänar ett av de största tacken för genomförandet av första halvan av avhandlingen. Din erfarenhet, känsla och engagemang kan inte överskattas. Tack för att du fick mig intresserad av intervention och gav mig chansen att börja forska. Våra äventyr med sfärerna är oförglömliga.

Magdalena Häggström, min gamla rumskompis och bästa kollega. Principfast som få och alltid med en åsikt. Du sätter färg på tillvaron. Det är inte kul att du är så långt borta.

Mina nuvarande och tidigare chefer på Bild och Funktion som genom åren varit flexibla och gett mig utrymme att forska. Tack till *Sophia Zachrisson*, *Carin Cronberg*, *Daisy Lee* och *Peter Hochbergs*.

Tack till *Annika Törling-Ring*, *Ulrika Andersson* och *Kajsa Trens* forskningsadministratörer, för att ni haft koll på all formalia. Och jag är ledsen för att ni behövt påminna mig så många gånger.

Erik Thimansson, vän och medförfattare. Tillsammans sätter vi Skåne på MR prostatakartan. Vi har så mycket på gång.

Carina Bursjöö och *Mårten Forssén* för ovärderlig hjälp med fåren.

Eric Sandrup, *Eddie Thordarson*, *Peter Fyhr* och övriga på Magle Life Sciences. Det var ett nöja att lära känna er.

Karl Thulin och *Anders Forslid* på BMC, in vivo lab, som bidrog med professionell hjälp med fåren.

Dolores Gavier-Widén och *Erika Karlstam* på Statens Veterinärmedicinska Anstalt i Uppsala. Vilken tur att vi fann varandra. Det har varit ett sant nöje att arbeta med er! Det hade inte blivit något utan er insats.

Anita Brinck och *Kristina Olausson*, röntgensjuksköterskor på interventionslab. Tack för all hjälp med kontrast, katetrar och ledare.

Jacob Engellau för goda råd och bra samtal.

MR-fysiker *Jimmy Lätt* för hjälp med b-värden och ADC.

MR-fysiker *Filip Szczepankiewicz* för allt du lärt mig om diffusion och för att du läst och gett mig feed-back. Jag ser verkligen fram emot våra kommande projekt.

Anders Bjartell, Thomas Jiborn, Ymir Saemundsson, Max Alterbeck, Jacob Ingvar. Det är alltid ett nöje att arbeta med Urologer!

Tack till *Anna-Carin Börjedahl.* koordinator för OPT, *Anetta Bolekjo*, forskningssjuksköterska i OPT-teamet och *Anna Holst*, sekreterare på Malmö Cancer Center.

Wiveka Rosenqvist för att du skötte alla fakturor och transaktioner i samband med försöken i studie 1 och 2.

Kevin Sandeman, ett ankare på patologen med ett aldrig sinande driv, du är positiv till allt. Jag hoppas vi kommer samarbeta mycket framöver.

Jakob Swanberg, Hans Lindgren och *Mateusz Krasun*, interventionsradiologer som så generöst delat med sig av sina erfarenheter om embolisering.

Hanna Sartor, min one-stop-shop! Du är alltid lika energisk och sarkastisk, det älskar jag.

Sam Eriksson, kollega på gastro. Tack för att jag fick vara med på dina lever-ADC. Du är en stjärna, en vän och ett ankare på röntgen.

Kristin Johnson, stugkompis och kollega som kommer lämna ett stort tomrum efter sig men som kommer tillbaka ännu starkare och bättre. Lycka till i Belgien.

Anni Gålne, kollega, padelpartner och cykelsällskap. Det är alltid bra samtal med dig. Oavsett vad det gäller.

Anna Kahn, som jag kamperat ihop med så många år. Jag hoppas vi kommer göra det igen någon gång.

Gustav Sundström som generöst hjälpt mig med designen av framsidan.

Kjartan Thorarinsson som steppat in som prostataankare och *Johanna Berg* som ser till att MR-standarden på SUS håller världsklass. *Jonatan Engman*, medförfattare och mycket erfaren uroradiolog. *Sonja Pudaric* och *Nils-Olof Wallengren* som introducerade mig till MR Prostata.

Nuvarande och före detta kolleger på röntgen i Lund och Malmö, som har arbetat så jag kunnat forska. Ni är otroligt viktiga för mig.

Röntgensjuksköterskor och undersköterskor på röntgen i Lund. Ni gör att fantastiskt arbete.

Alla kolleger och vänner på TMC för att ni gjorde äventyren i Australien så bra. Ett extra tack till *Hans Billing*, *Eva Bornell*, *Aleksandra Garbacz*, *Fausto Labruto*, *Daniel Gierhake-Stahlhoven*, *Cathrine Lefort*, *Odd och Lisa Runeborg*, *Ida och Niklas Wingenfeldt*. Ida, vad skulle jag göra utan dig?

Alla kolleger och vänner på DDA/Teleconsult. Ni är så många som varit viktiga och som gjorde året på Bali så bra. *Karl Isacsson*, du var livsviktig. *Jonas Nilsson* och *Emma Ulfsdottir*, *Krister och Helene Askaner*, *Daisy Lee med Alvaro*, *Mansour Grand*, *Istvan Herzfeldt*, *Katarina* och *Johan Degerman*, *Axel Tjörnstrand*, *Signe Norgren* och *Olof Huldt*, *Siri Bårdskär*, *Hala Mehrez*, *Gitte Leger* och *Martin Leger*, *Genta Banushi* och *Agus Dharsana*.

Karin Åstrand, *Mattias och Mia Hjort*, *Jakob Svensson*, *Tobias och Ingrid Schölin*, *Jonas och Katrin Lindhe-Persson*, *Dariusz Slusarczyk*. Gamla kompisgänget, *Jesper*, *Fredrik*, *Thomas*, *Pär* och *Olof*. Hit räknas även *Jenny* som kommit med goda språkliga tips. Ni är alla vänner och kolleger från förr och nu som inte kategoriserats någon annanstans men som är och har varit ytterst viktiga för mig, alla på sitt sätt.

Mina föräldrar, *Lena Wargren* och *Kalle Bengtsson*. Mina systrar, *Emma Bengtsson* och *Matilda Hedén* med familjer. *Sara Elvermåhr* och *Ulla-Britt Elversson*.

Sist, och viktigast av alla, min älskade fru *Jessica Elversson* och våra fina barn. *Ella*, *Ludvig* och *Märta*. Ni är verkligen bäst. Jag älskar er!

References

1. Lindbom A. Arteriosclerosis and arterial thrombosis in the lower limb; a roentgenological study. Acta radiologica Supplementum. 1950;80:1-80.
2. Seldinger S. Catheter replacement of the needle in percutaneous arteriography; a new technique. Acta Radiologica. 1953:368-76.
3. Dotter CT, Judkins MP. Transluminal Treatment of Arteriosclerotic Obstruction. Circulation. 1964;30(5):654-70.
4. Bollinger, Schlumpf. Andreas Grüntzigs Ballon-Katheter zur Angioplastie von peripheren Arterien (PTA) ist 25 Jahre alt. Vasa. 1999;28(1):58-64.
5. Grüntzig A, Hopff H. Perkutane Rekanalisation chronischer arterieller Verschlüsse mit einem neuen Dilatationskatheter. DMW-Deutsche Medizinische Wochenschrift. 1974;99(49):2502-5.
6. Rösch J, Dotter CT, Brown MJ. Selective arterial embolization: a new method for control of acute gastrointestinal bleeding. Radiology. 1972;102(2):303-6.
7. Kumar A, Ouriel K. Handbook of Endovascular interventions: Springer Science & Business Media; 2012.
8. Sheth RA, Sabir S, Krishnamurthy S, Avery RK, Zhang YS, Khademhosseini A, Oklu R. Endovascular Embolization by Transcatheter Delivery of Particles: Past, Present, and Future. J Funct Biomater. 2017;8(2).
9. Lewandowski RJ, Sato KT, Atassi B, Ryu RK, Nemcek AA, Kulik L, et al. Radioembolization with 90 Y microspheres: angiographic and technical considerations. Cardiovascular and interventional radiology. 2007;30:571-92.
10. Bengtsson J, Cwikiel W, Sundgren PC, Karlstam E, Gavier-Widen D, Keussen I. The effects of uterine artery embolization with a new degradable microsphere in an experimental study. Acta Radiol. 2017;58(11):1334-41.
11. Doucet J, Kiri L, O'Connell K, Kehoe S, Lewandowski RJ, Liu DM, et al. Advances in degradable embolic microspheres: a state of the art review. Journal of functional biomaterials. 2018;9(1):14.
12. Laurent A. Microspheres and nonspherical particles for embolization. Tech Vasc Interv Radiol. 2007;10(4):248-56.
13. Davidson GS, Terbrugge KG. Histologic long-term follow-up after embolization with polyvinyl alcohol particles. American journal of neuroradiology. 1995;16(4):843-6.
14. Laurent A, Wassef M, Namur J, Martal J, Labarre D, Pelage JP. Recanalization and particle exclusion after embolization of uterine arteries in sheep: a long-term study. Fertil Steril. 2009;91(3):884-92.

15. Carli D, Sluzewski M, Beute G, Van Rooij W. Complications of particle embolization of meningiomas: frequency, risk factors, and outcome. American journal of neuroradiology. 2010;31(1):152-4.
16. Duvnjak S, Ravn P, Green A, Andersen PE. Uterine fibroid embolization with acrylamido polyvinyl microspheres: prospective 12-month clinical and MRI follow-up study. Acta Radiol. 2017;58(8):952-8.
17. Spies JB, Allison S, Flick P, Cramp M, Bruno J, Jha RC, Ascher SA. Spherical polyvinyl alcohol versus tris-acryl gelatin microspheres for uterine artery embolization for leiomyomas: results of a limited randomized comparative study. Journal of Vascular and Interventional Radiology. 2005;16(11):1431-7.
18. Owen RJ, Nation PN, Polakowski R, Biliske JA, Tiege PB, Griffith IJ. A preclinical study of the safety and efficacy of Occlusin 500 Artificial Embolization Device in sheep. Cardiovasc Intervent Radiol. 2012;35(3):636-44.
19. Lee S, Ghosh A, Xiao N, Gordon AC, Heidarpour N, Funaki B, Lewandowski RJ, editors. Embolic Agents: Particles. Seminars in Interventional Radiology; 2023: Thieme Medical Publishers, Inc. 333 Seventh Avenue, 18th Floor, New York, NY ….
20. Wang CY, Hu J, Sheth RA, Oklu R. Emerging embolic agents in endovascular embolization: an overview. Progress in Biomedical Engineering. 2020;2(1):012003.
21. Medsinge A, Zajko A, Orons P, Amesur N, Santos E. A case-based approach to common embolization agents used in vascular interventional radiology. American Journal of Roentgenology. 2014;203(4):699-708.
22. Jordan O, Doelker E, Rufenacht DA. Biomaterials used in injectable implants (liquid embolics) for percutaneous filling of vascular spaces. Cardiovasc Intervent Radiol. 2005;28(5):561-9.
23. Fan XD, Su LX, Zheng JW, Zheng LZ, Zhang ZY. Ethanol embolization of arteriovenous malformations of the mandible. AJNR Am J Neuroradiol. 2009;30(6):1178-83.
24. Maxwell NJ, Saleem Amer N, Rogers E, Kiely D, Sweeney P, Brady AP. Renal artery embolisation in the palliative treatment of renal carcinoma. Br J Radiol. 2007;80(950):96-102.
25. Maeda N, Verret V, Moine L, Bedouet L, Louguet S, Servais E, et al. Targeting and recanalization after embolization with calibrated resorbable microspheres versus hand-cut gelatin sponge particles in a porcine kidney model. J Vasc Interv Radiol. 2013;24(9):1391-8.
26. Costa C, Incio J, Soares R. Angiogenesis and chronic inflammation: cause or consequence? Angiogenesis. 2007;10(3):149-66.
27. Malhotra K, Liebeskind DS. Collaterals in ischemic stroke. Brain Hemorrhages. 2020;1(1):6-12.
28. Dong H, Yang D, Hu Y, Song X. Recent advances in smart nanoplatforms for tumor non-interventional embolization therapy. J Nanobiotechnology. 2022;20(1):337.
29. Seiler C. The human coronary collateral circulation. Heart. 2003;89(11):1352-7.

30. Mr H. Smooth muscle neoplasms. Surgical pathology of the uterine corpus. 1980:468-529.
31. Baird DD, Dunson DB, Hill MC, Cousins D, Schectman JM. High cumulative incidence of uterine leiomyoma in black and white women: ultrasound evidence. Am J Obstet Gynecol. 2003;188(1):100-7.
32. Baird D, Schectman J, Dixon D, Sandler D, Hill M, editors. African Americans at higher risk than whites for uterine fibroids: Ultrasound evidence. American journal of epidemiology; 1998: JOHNS HOPKINS UNIV SCHOOL HYGIENE PUB HEALTH 111 MARKET PLACE, STE 840 ….
33. Borgfeldt C, Aandolf E. Transvaginal ultrasonographic findings in the uterus and the endometrium: low prevalence of leiomyoma in a random sample of women age 25-40 years. Acta obstetricia et gynecologica Scandinavica. 2000;79(3):202-7.
34. Marshall LM, Spiegelman D, Barbieri RL, Goldman MB, Manson JE, Colditz GA, et al. Variation in the incidence of uterine leiomyoma among premenopausal women by age and race. Obstetrics & Gynecology. 1997;90(6):967-73.
35. Chavez NF, Stewart EA. Medical treatment of uterine fibroids. Clinical Obstetrics and Gynecology. 2001;44(2):372-84.
36. Vilos GA, Allaire C, Laberge PY, Leyland N, Special C. The management of uterine leiomyomas. J Obstet Gynaecol Can. 2015;37(2):157-78.
37. Cardozo ER, Clark AD, Banks NK, Henne MB, Stegmann BJ, Segars JH. The estimated annual cost of uterine leiomyomata in the United States. American journal of obstetrics and gynecology. 2012;206(3):211. e1-. e9.
38. Metwally M, Li T-C. Modern Management of Uterine Fibroids: Cambridge University Press; 2020.
39. Yang Q, Ciebiera M, Bariani MV, Ali M, Elkafas H, Boyer TG, Al-Hendy A. Comprehensive Review of Uterine Fibroids: Developmental Origin, Pathogenesis, and Treatment. Endocr Rev. 2022;43(4):678-719.
40. Cook H, Ezzati M, Segars JH, McCarthy D. The impact of uterine leiomyomas on reproductive outcomes. Minerva ginecologica. 2010;62(3):225.
41. Laughlin SK, Stewart EA. Uterine leiomyomas: individualizing the approach to a heterogeneous condition. Obstetrics and gynecology. 2011;117(2 Pt 1):396.
42. Carranza-Mamane B, Havelock J, Hemmings R, Reproductive E, Infertility C, Special C. The management of uterine fibroids in women with otherwise unexplained infertility. J Obstet Gynaecol Can. 2015;37(3):277-85.
43. Pritts EA, Parker WH, Olive DL. Fibroids and infertility: an updated systematic review of the evidence. Fertility and sterility. 2009;91(4):1215-23.
44. Borah BJ, Yao X, Laughlin-Tommaso SK, Heien HC, Stewart EA. Comparative Effectiveness of Uterine Leiomyoma Procedures Using a Large Insurance Claims Database. Obstet Gynecol. 2017;130(5):1047-56.
45. Sizzi O, Rossetti A, Malzoni M, Minelli L, La Grotta F, Soranna L, et al. Italian multicenter study on complications of laparoscopic myomectomy. J Minim Invasive Gynecol. 2007;14(4):453-62.

46. Patel N, Chaudhari K, Patel D, Joshi J. High-Intensity Focused Ultrasound Ablation of Uterine Fibroids: A Review. Cureus. 2023;15(9):e44680.
47. Capezzuoli T, Aslan B, Vannuccini S, Orlandi G, La Torre F, Sorbi F, et al. Recurrence of Uterine Fibroids After Conservative Surgery or Radiological Procedures: a Narrative Review. Reprod Sci. 2023.
48. Liu L, Wang T, Lei B. High-intensity focused ultrasound (HIFU) ablation versus surgical interventions for the treatment of symptomatic uterine fibroids: a meta-analysis. Eur Radiol. 2022;32(2):1195-204.
49. Spies JB, Roth AR, Jha RC, Gomez-Jorge J, Levy EB, Chang TC, Ascher SA. Leiomyomata treated with uterine artery embolization: factors associated with successful symptom and imaging outcome. Radiology. 2002;222(1):45-52.
50. Andrews RT, Spies JB, Sacks D, Worthington-Kirsch RL, Niedzwiecki GA, Marx MV, et al. Patient care and uterine artery embolization for leiomyomata. Journal of vascular and interventional radiology: JVIR. 2004;15(2 Pt 1):115-20.
51. Bulman JC, Ascher SM, Spies JB. Current concepts in uterine fibroid embolization. Radiographics. 2012;32(6):1735-50.
52. Pelage J-P, Cazejust J, Pluot E, Dref OL, Laurent A, Spies JB, et al. Uterine fibroid vascularization and clinical relevance to uterine fibroid embolization. Radiographics. 2005;25(suppl_1):S99-S117.
53. Pelage J-P, Le Dref O, Soyer P, Jacob D, Kardache M, Dahan H, et al. Arterial anatomy of the female genital tract: variations and relevance to transcatheter embolization of the uterus. AJR American journal of roentgenology. 1999;172(4):989-94.
54. Razavi MK, Wolanske KA, Hwang GL, Sze DY, Kee ST, Dake MD. Angiographic classification of ovarian artery–to–uterine artery anastomoses: initial observations in uterine fibroid embolization. Radiology. 2002;224(3):707-12.
55. Pelage J-P, Guaou NG, Jha RC, Ascher SM, Spies JB. Uterine fibroid tumors: long-term MR imaging outcome after embolization. Radiology. 2004;230(3):803-9.
56. Expert Panel on Interventional R, Knuttinen MG, Stark G, Hohenwalter EJ, Bradley LD, Braun AR, et al. ACR Appropriateness Criteria((R)) Radiologic Management of Uterine Leiomyomas. J Am Coll Radiol. 2018;15(5S):S160-S70.
57. Badiani B, Chiumente M, Messori A. Ulipristal acetate for pre-operative management of uterine fibroids: Modeling outcomes and costs. Eur J Obstet Gynecol Reprod Biol. 2018;222:84-8.
58. Fonseca MCM, Castro R, Machado M, Conte T, Girao M. Uterine Artery Embolization and Surgical Methods for the Treatment of Symptomatic Uterine Leiomyomas: A Systemic Review and Meta-analysis Followed by Indirect Treatment Comparison. Clin Ther. 2017;39(7):1438-55 e2.
59. Donnez J, Dolmans MM. Uterine fibroid management: from the present to the future. Hum Reprod Update. 2016;22(6):665-86.
60. Jiang W, Shen Z, Luo H, Hu X, Zhu X. Comparison of polyvinyl alcohol and tris-acryl gelatin microsphere materials in embolization for symptomatic leiomyomas: a systematic review. Minim Invasive Ther Allied Technol. 2016;25(6):289-300.

61. Falkenberg M DM. Endovaskulär intervention : en praktisk vägledning. 1. uppl. ed: Studentlitteratur; 2014.
62. Kandarpa K M. Handbook of interventional radiologic procedures. 5. ed: Wolters Kluwer; 2016.
63. Ganguli S, Faintuch S, Salazar GM, Rabkin DJ. Postembolization syndrome: changes in white blood cell counts immediately after uterine artery embolization. Journal of Vascular and Interventional Radiology. 2008;19(3):443-5.
64. Investigators R. Uterine-artery embolization versus surgery for symptomatic uterine fibroids. New England Journal of Medicine. 2007;356(4):360-70.
65. Mara M, Maskova J, Fucikova Z, Kuzel D, Belsan T, Sosna O. Midterm clinical and first reproductive results of a randomized controlled trial comparing uterine fibroid embolization and myomectomy. Cardiovascular and interventional radiology. 2008;31:73-85.
66. Sandhu JS, Bixler BR, Dahm P, Goueli R, Kirkby E, Stoffel JT, Wilt TJ. Management of lower urinary tract symptoms attributed to benign prostatic hyperplasia (BPH): AUA guideline amendment 2023. The Journal of Urology. 2024;211(1):11-9.
67. Patel ND, Parsons JK. Epidemiology and etiology of benign prostatic hyperplasia and bladder outlet obstruction. Indian J Urol. 2014;30(2):170-6.
68. Stranne J, Damber JE, Fall M, Hammarsten J, Knutson T, Peeker R. One-third of the Swedish male population over 50 years of age suffers from lower urinary tract symptoms. Scand J Urol Nephrol. 2009;43(3):199-205.
69. Page T, Veeratterapillay R, Keltie K, Burn J, Sims A. Prostatic urethral lift (UroLift): a real-world analysis of outcomes using hospital episodes statistics. BMC Urol. 2021;21(1):55.
70. Miller LE, Chughtai B, McVary K, Gonzalez RR, Rojanasarot S, DeRouen K, Bhattacharyya S. Water vapor thermal therapy for lower urinary tract symptoms secondary to benign prostatic hyperplasia: Systematic review and meta-analysis. Medicine (Baltimore). 2020;99(30):e21365.
71. Naidu SG, Narayanan H, Saini G, Segaran N, Alzubaidi SJ, Patel IJ, Oklu R. Prostate Artery Embolization-Review of Indications, Patient Selection, Techniques and Results. J Clin Med. 2021;10(21).
72. Mitchell ME, Waltman AC, Athanasoulis CA, Kerr Jr WS, Dretler SP. Control of massive prostatic bleeding with angiographic techniques. The Journal of Urology. 1976;115(6):692-5.
73. DeMeritt JS, Elmasri FF, Esposito MP, Rosenberg GS. Relief of benign prostatic hyperplasia-related bladder outlet obstruction after transarterial polyvinyl alcohol prostate embolization. J Vasc Interv Radiol. 2000;11(6):767-70.
74. Carnevale FC, Antunes AA, da Motta Leal Filho JM, de Oliveira Cerri LM, Baroni RH, Marcelino AS, et al. Prostatic artery embolization as a primary treatment for benign prostatic hyperplasia: preliminary results in two patients. Cardiovasc Intervent Radiol. 2010;33(2):355-61.

75. Pisco JM, Pinheiro LC, Bilhim T, Duarte M, Mendes JR, Oliveira AG. Prostatic arterial embolization to treat benign prostatic hyperplasia. J Vasc Interv Radiol. 2011;22(1):11-9; quiz 20.
76. Carnevale FC, Iscaife A, Yoshinaga EM, Moreira AM, Antunes AA, Srougi M. Transurethral Resection of the Prostate (TURP) Versus Original and PErFecTED Prostate Artery Embolization (PAE) Due to Benign Prostatic Hyperplasia (BPH): Preliminary Results of a Single Center, Prospective, Urodynamic-Controlled Analysis. Cardiovasc Intervent Radiol. 2016;39(1):44-52.
77. Jung JH, McCutcheon KA, Borofsky M, Young S, Golzarian J, Kim MH, et al. Prostatic arterial embolization for the treatment of lower urinary tract symptoms in men with benign prostatic hyperplasia. Cochrane Database Syst Rev. 2022;3(3):CD012867.
78. Ray AF, Powell J, Speakman MJ, Longford NT, DasGupta R, Bryant T, et al. Efficacy and safety of prostate artery embolization for benign prostatic hyperplasia: an observational study and propensity-matched comparison with transurethral resection of the prostate (the UK-ROPE study). BJU Int. 2018;122(2):270-82.
79. Dias US, Jr., de Moura MRL, Viana PCC, de Assis AM, Marcelino ASZ, Moreira AM, et al. Prostatic Artery Embolization: Indications, Preparation, Techniques, Imaging Evaluation, Reporting, and Complications. Radiographics. 2021;41(5):1509-30.
80. Chung E. Penile Glans Necrosis Following Prostatic Artery Embolization for Benign Prostatic Hyperplasia: Case Series and Review of Current Literature. World J Mens Health. 2023;41(2):396-402.
81. Clift AK, Thomas R, Frilling A. Developments in interventional management of hepatic metastases from neuroendocrine tumours. Best Pract Res Clin Endocrinol Metab. 2023;37(5):101798.
82. Ayyub J, Dabhi KN, Gohil NV, Tanveer N, Hussein S, Pingili S, et al. Evaluation of the Safety and Efficacy of Conventional Transarterial Chemoembolization (cTACE) and Drug-Eluting Bead (DEB)-TACE in the Management of Unresectable Hepatocellular Carcinoma: A Systematic Review. Cureus. 2023;15(7):e41943.
83. Leigh N, Sanford DE. Colorectal liver metastases: Resect, ablate, or embolize. Seminars in Colon and Rectal Surgery. 2023;34(3).
84. Burkhardt O, Abt D, Engeler D, Schmid HP, Mullhaupt G, Zumstein V. Prostatic Artery Embolization in Patients with Prostate Cancer: A Systematic Review. Eur Urol Focus. 2023.
85. Guan Y, Wang W, Zhang T, Liao L, Chen J, Zhang Z, et al. Epirubicin-loaded beads transarterial prostatic arterial chemoembolization is a promising treatment for advanced prostate cancer with lower urinary tract obstruction or hematuria-a case series report. Transl Androl Urol. 2022;11(4):480-94.
86. Vilanova JC, Catalá V, Algaba F, Laucirica O. Atlas of Multiparametric Prostate MRI. Springer. 2018;10:978-3.
87. Cancer IAfRo. Global cancer observatory Lyon, France: International Agency for Research on Cancer; [cited 2024].

88. Regionala cancercentrum i samverkan. Prostatacancer: Nationellt vårdprogram [Internet]. Stockholm: Regionala cancercentrum i samverkan; 2023 [cited 2024 Feb 6]. Available from: https://kunskapsbanken.cancercentrum.se/globalassets/cancerdiagnoser/prostatacancer/vardprogram/nvp-prostatacancer2.pdf.
89. Engholm G, Ferlay J, Christensen N, Bray F, Gjerstorff ML, Klint Å, et al. NORDCAN–a Nordic tool for cancer information, planning, quality control and research. Acta oncologica. 2010;49(5):725-36.
90. Engholm G, Storm H, Ferlay J, Christensen N, Johannesen T, Klint Å, et al. NORDCAN: cancer incidence, mortality, prevalence and survival in the Nordic countries. 2012.
91. Häggström C, Stocks T, Ulmert D, Bjørge T, Ulmer H, Hallmans G, et al. Prospective study on metabolic factors and risk of prostate cancer. Cancer. 2012;118(24):6199-206.
92. Mandair D, Rossi RE, Pericleous M, Whyand T, Caplin ME. Prostate cancer and the influence of dietary factors and supplements: a systematic review. Nutrition & metabolism. 2014;11(1):1-11.
93. Moreira DM, Aronson WJ, Terris MK, Kane CJ, Amling CL, Cooperberg MR, et al. Cigarette smoking is associated with an increased risk of biochemical disease recurrence, metastasis, castration-resistant prostate cancer, and mortality after radical prostatectomy: results from the SEARCH database. Cancer. 2014;120(2):197-204.
94. Alanee SR, Glogowski EA, Schrader KA, Eastham JA, Offit K. Clinical features and management of BRCA1 and BRCA2-associated prostate cancer. Front Biosci (Elite Ed). 2014;6:15-30.
95. Akbari MR, Wallis CJ, Toi A, Trachtenberg J, Sun P, Narod SA, Nam RK. The impact of a BRCA2 mutation on mortality from screen-detected prostate cancer. Br J Cancer. 2014;111(6):1238-40.
96. Theodorsson E, Berggren Söderlund M. Laurells Klinisk kemi i praktisk medicin: Studentlitteratur AB; 2018.
97. Wang M, Valenzuela L, Murphy G, Chu T. Purification of a human prostate specific antigen. Investigative urology. 1979;17(2):159-63.
98. Benson MC, Whang IS, Pantuck A, Ring K, Kaplan SA, Olsson CA, Cooner WH. Prostate specific antigen density: a means of distinguishing benign prostatic hypertrophy and prostate cancer. The Journal of urology. 1992;147(3):815-6.
99. Vickers AJ, Savage C, O'Brien MF, Lilja H. Systematic review of pretreatment prostate-specific antigen velocity and doubling time as predictors for prostate cancer. Journal of Clinical Oncology. 2009;27(3):398.
100. Nordström T, Akre O, Aly M, Grönberg H, Eklund M. Prostate-specific antigen (PSA) density in the diagnostic algorithm of prostate cancer. Prostate cancer and prostatic diseases. 2018;21(1):57-63.
101. Naji L, Randhawa H, Sohani Z, Dennis B, Lautenbach D, Kavanagh O, et al. Digital rectal examination for prostate cancer screening in primary care: a systematic review and meta-analysis. The Annals of Family Medicine. 2018;16(2):149-54.

102. Kasivisvanathan V, Dufour R, Moore CM, Ahmed HU, Abd-Alazeez M, Charman SC, et al. Transperineal magnetic resonance image targeted prostate biopsy versus transperineal template prostate biopsy in the detection of clinically significant prostate cancer. The Journal of urology. 2013;189(3):860-6.
103. Gleason DF. Classification of prostatic carcinomas. Cancer Chemother Rep. 1966;50:125-8.
104. Egevad L, Algaba F, Berney D, Boccon-Gibod L, Griffiths D, Lopez-Beltran A, et al. Handling and reporting of radical prostatectomy specimens in Europe: a web-based survey by the European Network of Uropathology (ENUP). Histopathology. 2008;53(3):333-9.
105. Persson J, Wilderäng U, Jiborn T, Wiklund PN, Damber J-E, Hugosson J, et al. Interobserver variability in the pathological assessment of radical prostatectomy specimens: findings of the Laparoscopic Prostatectomy Robot Open (LAPPRO) study. Scandinavian journal of urology. 2014;48(2):160-7.
106. Egevad L, Ahmad AS, Algaba F, Berney DM, Boccon-Gibod L, Compérat E, et al. Standardization of Gleason grading among 337 European pathologists. Histopathology. 2013;62(2):247-56.
107. Epstein JI, Egevad L, Amin MB, Delahunt B, Srigley JR, Humphrey PA, Committee G. The 2014 International Society of Urological Pathology (ISUP) consensus conference on Gleason grading of prostatic carcinoma: definition of grading patterns and proposal for a new grading system. The American journal of surgical pathology. 2016;40(2):244-52.
108. Steyn JH, Smith FW. Nuclear magnetic resonance imaging of the prostate. Br J Urol. 1982;54(6):726-8.
109. Engelbrecht MR, Jager GJ, Laheij RJ, Verbeek AL, van Lier HJ, Barentsz JO. Local staging of prostate cancer using magnetic resonance imaging: a meta-analysis. Eur Radiol. 2002;12(9):2294-302.
110. Verma S, Rajesh A, Futterer JJ, Turkbey B, Scheenen TW, Pang Y, et al. Prostate MRI and 3D MR spectroscopy: how we do it. AJR Am J Roentgenol. 2010;194(6):1414-26.
111. Turkbey B, Rosenkrantz AB, Haider MA, Padhani AR, Villeirs G, Macura KJ, et al. Prostate imaging reporting and data system version 2.1: 2019 update of prostate imaging reporting and data system version 2. European urology. 2019;76(3):340-51.
112. Einstein A. Über die von der molekularkinetischen Theorie der Wärme geforderte Bewegung von in ruhenden Flüssigkeiten suspendierten Teilchen. Annalen der physik. 1905;4.
113. Renn J. Einstein's invention of Brownian motion. Annalen der Physik. 2005;517:23-37.
114. Le Bihan D. Apparent diffusion coefficient and beyond: what diffusion MR imaging can tell us about tissue structure. Radiological Society of North America, Inc.; 2013. p. 318-22.
115. Szczepankiewicz F, editor Workshop on Diffusion MRI: From Research to Clinic. Sequence Design & Contrast Mechanisms. ISMRM; 2022; Amsterdam, Netherlands.
116. Le Bihan D. What can we see with IVIM MRI? Neuroimage. 2019;187:56-67.

117. Gronberg H, Adolfsson J, Aly M, Nordstrom T, Wiklund P, Brandberg Y, et al. Prostate cancer screening in men aged 50-69 years (STHLM3): a prospective population-based diagnostic study. Lancet Oncol. 2015;16(16):1667-76.
118. Kasivisvanathan V, Rannikko AS, Borghi M, Panebianco V, Mynderse LA, Vaarala MH, et al. MRI-Targeted or Standard Biopsy for Prostate-Cancer Diagnosis. New England Journal of Medicine. 2018;378(19):1767-77.
119. Drost FH, Osses DF, Nieboer D, Steyerberg EW, Bangma CH, Roobol MJ, Schoots IG. Prostate MRI, with or without MRI-targeted biopsy, and systematic biopsy for detecting prostate cancer. Cochrane Database Syst Rev. 2019;4(4):CD012663.
120. Mottet N, Van den Bergh R, Briers E, Cornford P, De Santis M, Fanti S, et al. Eau-Eanm-Estro-Esur-Siog Guidelines On Prostate Cancer. Eur Assoc Urol. 2020:1-182.
121. Cui Y, Zhang X-P, Sun Y-S, Tang L, Shen L. Apparent diffusion coefficient: potential imaging biomarker for prediction and early detection of response to chemotherapy in hepatic metastases. Radiology. 2008;248(3):894-900.
122. Donati F, Boraschi P, Pacciardi F, Cervelli R, Castagna M, Urbani L, et al. 3T diffusion-weighted MRI in the response assessment of colorectal liver metastases after chemotherapy: Correlation between ADC value and histological tumour regression grading. European journal of radiology. 2017;91:57-65.
123. Eriksson S, Bengtsson J, Torén W, Lätt J, Andersson R, Sturesson C. Changes in apparent diffusion coefficient and pathological response in colorectal liver metastases after preoperative chemotherapy. Acta Radiologica. 2023;64(1):51-7.
124. Meyer H-J, Wienke A, Surov A. Discrimination between clinical significant and insignificant prostate cancer with apparent diffusion coefficient–a systematic review and meta analysis. BMC cancer. 2020;20:1-11.
125. Bengtsson J, Thimansson E, Baubeta E, Zackrisson S, Sundgren PC, Bjartell A, Flondell-Site D. Correlation between ADC, ADC ratio, and Gleason Grade group in prostate cancer patients undergoing radical prostatectomy: Retrospective multicenter study with different MRI scanners. Front Oncol. 2023;13:1079040.
126. Moller JM, Boesen L, Hansen AE, Kettles K, Logager V. Quantification of cross-vendor variation in ADC measurements in vendor-specific prostate MRI-protocols. Eur J Radiol. 2023;165:110942.
127. Woo S, Kim SY, Cho JY, Kim SH. Preoperative Evaluation of Prostate Cancer Aggressiveness: Using ADC and ADC Ratio in Determining Gleason Score. AJR Am J Roentgenol. 2016;207(1):114-20.
128. De Cobelli F, Ravelli S, Esposito A, Giganti F, Gallina A, Montorsi F, Del Maschio A. Apparent diffusion coefficient value and ratio as noninvasive potential biomarkers to predict prostate cancer grading: comparison with prostate biopsy and radical prostatectomy specimen. AJR Am J Roentgenol. 2015;204(3):550-7.
129. Schoots IG, Padhani AR. Risk-adapted biopsy decision based on prostate magnetic resonance imaging and prostate-specific antigen density for enhanced biopsy avoidance in first prostate cancer diagnostic evaluation. BJU international. 2021;127(2):175.
130. Turkbey B, Haider MA. Deep learning-based artificial intelligence applications in prostate MRI: brief summary. Br J Radiol. 2022;95(1131):20210563.

131. Thimansson E, Bengtsson J, Baubeta E, Engman J, Flondell-Site D, Bjartell A, Zackrisson S. Deep learning algorithm performs similarly to radiologists in the assessment of prostate volume on MRI. Eur Radiol. 2023;33(4):2519-28.
132. Zhang Z, Sejdic E. Radiological images and machine learning: Trends, perspectives, and prospects. Comput Biol Med. 2019;108:354-70.
133. Najjar R. Redefining Radiology: A Review of Artificial Intelligence Integration in Medical Imaging. Diagnostics (Basel). 2023;13(17).
134. Winkel DJ, Grimm R, Benkert T, Kiefer B, Boll DT. A Fully Automated, End-to-End Prostate MRI Workflow Solution Incorporating Dot, Ultrashort Biparametric Imaging and Deep-Learning-based Detection, Classification, and Reporting. Magnetom Flash. 2020:78-83.
135. Wolterink JM, Mukhopadhyay A, Leiner T, Vogl TJ, Bucher AM, Isgum I. Generative Adversarial Networks: A Primer for Radiologists. Radiographics. 2021;41(3):840-57.
136. van Leeuwen KG, Schalekamp S, Rutten M, van Ginneken B, de Rooij M. Artificial intelligence in radiology: 100 commercially available products and their scientific evidence. Eur Radiol. 2021;31(6):3797-804.
137. van Leeuwen KG, Romeijn S. HealthAIregister Utrecht, The Netherlands: Romion Health; [cited 2024 Feb 28]. Available from: www.HealthAIregister.com.
138. Fryback DG, Thornbury JR. The efficacy of diagnostic imaging. Medical decision making. 1991;11(2):88-94.
139. Björk J. Praktisk statistik för medicin och hälsa: Liber; 2011.
140. Commission E. Directive 2010/63/EU of the European Parliament and of the Council of 22 September 2010 on the protection of animals used for scientific purposes. Off J Eur Union. 2010;50:33-79.
141. Djurskyddslag (2018:1192) Stockholm: Landsbygds- och infrastrukturdepartementet RSL; [cited 2024 Feb 6]. Available from: https://www.riksdagen.se/sv/dokument-och-lagar/dokument/svensk-forfattningssamling/djurskyddslag-20181192_sfs-2018-1192/.
142. Russell WMS, Burch RL. The principles of humane experimental technique: Methuen; 1959.
143. Stampfl S, Stampfl U, Rehnitz C, Schnabel P, Satzl S, Christoph P, et al. Experimental evaluation of early and long-term effects of microparticle embolization in two different mini-pig models. Part I: kidney. Cardiovasc Intervent Radiol. 2007;30(2):257-67.
144. Keussen I, Bengtsson J, Gavier-Widen D, Karlstam E. Uterine artery embolization in a sheep model: biodegradable versus non-degradable microspheres. Acta Radiol. 2018;59(10):1210-7.
145. Verret V, Pelage JP, Wassef M, Louguet S, Servais E, Bedouet L, et al. A novel resorbable embolization microsphere for transient uterine artery occlusion: a comparative study with trisacryl-gelatin microspheres in the sheep model. J Vasc Interv Radiol. 2014;25(11):1759-66.

146. Maclean D, Vigneswaran G, Bryant T, Modi S, Hacking N. A retrospective cohort study comparing a novel, spherical, resorbable particle against five established embolic agents for uterine fibroid embolisation. Clin Radiol. 2021;76(6):452-7.
147. Rozzanigo U, Gatti F, Luppi G, Costa L, Petralia B, Pravadelli C, et al. Chemoembolization with Degradable Starch Microspheres (DSM-TACE): expanding indications in HCC multidisciplinary tumor board. Hepatoma Research. 2023;9.
148. Sergio A, Cristofori C, Cardin R, Pivetta G, Ragazzi R, Baldan A, et al. Transcatheter arterial chemoembolization (TACE) in hepatocellular carcinoma (HCC): the role of angiogenesis and invasiveness. Official journal of the American College of Gastroenterology| ACG. 2008;103(4):914-21.
149. Chegai F, Orlacchio A, Merolla S, Monti S, Mannelli L. Intermediate hepatocellular carcinoma: the role of transarterial therapy. Hepatic oncology. 2015;2(4):399-408.
150. Taylor JR, Thompson W. An introduction to error analysis: the study of uncertainties in physical measurements: Springer; 1982.
151. Glen S. StatisicsHowTo.com [Internet]. Jacksonville [cited 2024]. Available from: https://www.statisticshowto.com/statistics-basics/error-propagation/#multiplication.
152. Barrett T, Priest AN, Lawrence EM, Goldman DA, Warren AY, Gnanapragasam VJ, et al. Ratio of Tumor to Normal Prostate Tissue Apparent Diffusion Coefficient as a Method for Quantifying DWI of the Prostate. AJR Am J Roentgenol. 2015;205(6):W585-93.
153. Boesen L, Chabanova E, Logager V, Balslev I, Thomsen HS. Apparent diffusion coefficient ratio correlates significantly with prostate cancer gleason score at final pathology. J Magn Reson Imaging. 2015;42(2):446-53.
154. Lebovici A, Sfrangeu SA, Feier D, Caraiani C, Lucan C, Suciu M, et al. Evaluation of the normal-to-diseased apparent diffusion coefficient ratio as an indicator of prostate cancer aggressiveness. BMC medical imaging. 2014;14(1):1-7.
155. Litjens GJ, Hambrock T, Hulsbergen–van de Kaa C, Barentsz JO, Huisman HJ. Interpatient variation in normal peripheral zone apparent diffusion coefficient: effect on the prediction of prostate cancer aggressiveness. Radiology. 2012;265(1):260-6.
156. Rosenkrantz AB, Kopec M, Kong X, Melamed J, Dakwar G, Babb JS, Taouli B. Prostate cancer vs. post-biopsy hemorrhage: diagnosis with T2- and diffusion-weighted imaging. J Magn Reson Imaging. 2010;31(6):1387-94.
157. Krauss W, Frey J, Heydorn Lagerlof J, Liden M, Thunberg P. Radiomics from multisite MRI and clinical data to predict clinically significant prostate cancer. Acta Radiol. 2023:2841851231216555.
158. Lee DK, Sung DJ, Kim CS, Heo Y, Lee JY, Park BJ, Kim MJ. Three-Dimensional Convolutional Neural Network for Prostate MRI Segmentation and Comparison of Prostate Volume Measurements by Use of Artificial Neural Network and Ellipsoid Formula. AJR Am J Roentgenol. 2020;214(6):1229-38.
159. Bulman JC, Toth R, Patel AD, Bloch BN, McMahon CJ, Ngo L, et al. Automated computer-derived prostate volumes from MR imaging data: comparison with radiologist-derived MR imaging and pathologic specimen volumes. Radiology. 2012;262(1):144-51.

160. Cuocolo R, Cipullo MB, Stanzione A, Ugga L, Romeo V, Radice L, et al. Machine learning applications in prostate cancer magnetic resonance imaging. Eur Radiol Exp. 2019;3(1):35.
161. Mazaheri Y, Goldman DA, Di Paolo PL, Akin O, Hricak H. Comparison of prostate volume measured by endorectal coil MRI to prostate specimen volume and mass after radical prostatectomy. Academic radiology. 2015;22(5):556-62.
162. Salvaggio G, Comelli A, Portoghese M, Cutaia G, Cannella R, Vernuccio F, et al. Deep learning network for segmentation of the prostate gland with median lobe enlargement in T2-weighted MR images: comparison with manual segmentation method. Current problems in diagnostic radiology. 2022;51(3):328-33.
163. Lee DK, Sung DJ, Kim C-S, Heo Y, Lee JY, Park BJ, Kim MJ. Three-dimensional convolutional neural network for prostate MRI segmentation and comparison of prostate volume measurements by use of artificial neural network and ellipsoid formula. American Journal of Roentgenology. 2020;214(6):1229-38.
164. Bezinque A, Moriarity A, Farrell C, Peabody H, Noyes SL, Lane BR. Determination of prostate volume: a comparison of contemporary methods. Academic radiology. 2018;25(12):1582-7.
165. Ghafoor S, Becker AS, Woo S, Andrieu PIC, Stocker D, Gangai N, et al. Comparison of PI-RADS versions 2.0 and 2.1 for MRI-based calculation of the prostate volume. Academic Radiology. 2021;28(11):1548-56.
166. Szczepankiewicz F, van Westen D, Englund E, Westin CF, Stahlberg F, Latt J, et al. The link between diffusion MRI and tumor heterogeneity: Mapping cell eccentricity and density by diffusional variance decomposition (DIVIDE). Neuroimage. 2016;142:522-32.
167. Sandgren K, Nilsson E, Keeratijarut Lindberg A, Strandberg S, Blomqvist L, Bergh A, et al. Registration of histopathology to magnetic resonance imaging of prostate cancer. Phys Imaging Radiat Oncol. 2021;18:19-25.

Printed by Media-Tryck, Lund 2024 NORDIC SWAN ECOLABEL 3041 0903

About the author

JOHAN BENGTSSON, M.D., is a consultant radiologist currently affiliated with Skåne University Hospital, Sweden. Johan began his journey into specialised medicine with interventional radiology during the early years of his career, coinciding with the inception of this thesis. Over time, Johan shifted his focus to diagnostic radiology, refining his expertise in abdominal, urological, and gynecological imaging utilising cutting-edge CT and MRI technologies. The culmination of his experiences in these distinct branches sub-specialties is portrayed in this thesis, reflecting his commitment to advancing the field.

LUND UNIVERSITY

FACULTY OF MEDICINE

Diagnostic Radiology
Department of Clinical Sciences, Lund

Lund University, Faculty of Medicine
Doctoral Dissertation Series 2024:82
ISBN 978-91-8021-577-0
ISSN 1652-8220